Characterization on the structure and dynamics of protein-protein complexes between cytochrome P450 and its redox partners

by

Meng Zhang

A dissertation submitted in partial fulfillment
of the requirements for the degree of
Doctor of Philosophy
(Chemistry)
in the University of Michigan
2016

Doctoral Committee:

Professor Ayyalusamy Ramamoorthy, Chair
Professor Zhan Chen
Associate Professor Kenichi Kuroda
Professor Michael Morris

Acknowledgements

I would like to first thank my advisor Dr. Ayyalusamy Ramamoorthy for his constant support and encouragement throughout my PhD. I would like to thank him for his guidance and valuable advice, for his patience and confidence in me, for inspiring me to take the challenges and overcome the difficulties in this work, and for training me into an independent researcher. He has set an example of excellence as a scientific researcher, a mentor and a role model.

I would also like to thank my committee members – Dr. Michael Morris, Dr. Zhan Chen and Dr. Kenichi Kuroda. Thank you very much for your insights and suggestions on my PhD projects, which are very helpful and precious to me.

I would like to thank Dr. Lucy Waskell, who has been helping me like a second advisor to me. Thank you so much for your instructions, your critical thinking, your suggestions for reading, writing and giving seminar talks, your encouragement are very helpful and will affect me further into my future career.

My sincere thanks also goes to Dr. Stéphanie Valérie Le Clair, Dr. Rui Huang, Dr. Subramanian Vivekanandan and Dr. Sangchoul Im for teaching me so much about NMR, protein science and training me to think logically through my research projects. Thank you for being both an instructor and a great friend to me.

A great many thanks to the Rams lab members: Katie, Elke, Thiru, Rongchun, Kyle, Amit, Kian, Sarah, Josh, Sam, Kazu, Patrick, Kamal, Nicole, Neil, Soma and Pratima. Thank you for so many useful discussions on our research projects, for providing such a comfortable working environment, for making our work full of fun, and for being a family.

Special thanks goes to my parents, my love Haoshi Yang and my friend Huiqing Zhou. Thank you for being there for me through the ups and downs, for encouraging me, understanding me and taking care of me. I would not have achieved my PhD without you. Thank you!

Table of Contents

List of Tables

List of Figures

ABSTRACT

Cytochrome P450s are a ubiquitous superfamily of monooxygenases responsible for the metabolism of thousands of compounds, including steroids, hormones, vitamins, and over 70% of the pharmaceuticals on the current market. They have been found to be related to human diseases including breast cancer and brain cancer. Therefore, it is of great importance to better understand the mechanism of how these enzymes function. In order for cytochrome P450s to complete the catalytic cycle, two electrons are required to be sequentially delivered to cytochrome P450 from its redox partners – cytochrome P450 reductase and cytochrome b_5. Mammalian cytochrome P450s and redox partners are membrane bound proteins mostly found on the cytoplasmic side of the endoplasmic reticulum membrane. In order to provide insights into these essential electron-transfer steps, it is important to better understand complex formation between cytochrome P450 and its redox partners. In this thesis, complex formation between cytochrome P450 and cytochrome b_5 is investigated under the effect of substrates and membrane. It is found that lipid bilayers provide stronger and more specific interactions between cytochrome P450 and cytochrome b_5 than a non-membrane and a detergent micelle environment. Interactions are found to be weak and widely dispersive all over cytochrome b_5 structure in the latter environments. Detergents have also been found to be destructive for cytochrome P450 secondary structure integrity and its functionality. These results emphasize on the important role that lipid bilayers play in facilitating cytochrome P450-cytochrome b_5 complex formation. It has also been found that the interaction between the hydrophobic portion of the globular domain of cytochrome P450 and the lipid bilayer could play a role in posing the protein into certain orientations that favor its interaction with cytochrome b_5 for more efficient electron transfer to occur. Better membrane mimetics – peptide-based nanodiscs – are developed in order to provide more physiologically relevant environment for future study on the cytochrome P450 system. The complex of cytochrome P450-cytochrome b_5 have been successfully reconstituted into the nanodiscs with proper orientations with respect to each other for productive interactions to occur, which is proved by NMR techniques. Both each individual proteins and their complexes are more stable at room temperature in the nanodiscs for longer period of time, rendering it possible for higher dimensional NMR experiments to be performed for more valuable information. Substrates have been found to facilitate stronger interactions between cytochrome P450 and cytochrome b_5. It is found that the substrate-bound complexes compose a larger population of stereospecific complexes while the substrate-free complexes are rich in

encounter complexes. Therefore, substrates likely promote short-range specific interactions including hydrophobic interactions, hydrogen bonds *etc*. between the two proteins due to structure rearrangement of cytochrome P450 for accommodation of the substrate. Residues most likely involved in stereospecific interactions are found to be D65, V66, T70, D71 and A72 on cytochrome b_5. The interaction between the FMN binding domain of cytochrome P450 reductase and cytochrome P450 is also investigated. Both the binding interface and dynamics of the FMN binding domain have been studied using solution NMR techniques. Sequential backbone assignment for the FMN binding domain on a two-dimensional $^{1}H/^{15}N$ correlated NMR spectrum is achieved through a series of standard triple-resonance three-dimensional NMR experiments. It is found that the FMN binding domain mainly interacts with cytochrome P450 in the solvent exposed edge surrounding the FMN cofactor, which facilitates more efficient electron transfer between the two proteins. A protein-protein complex structure is simulated using a docking program HADDOCK for the FMN binding domain of cytochrome P450 reductase and cytochrome P450. An electron transfer pathway is predicted based on this complex structure, which involves residue Met132 and R133 of cytochrome P450. This study provides better understanding on the interaction, binding interface and electron transfer process between the FMN binding domain of cytochrome P450 reductase and cytochrome P450. Substrates are found not to perturb the interaction between these two proteins, but affect the interplay of the three proteins when all of them are present in the same system, unravelling a competitive binding mechanism between cytochrome P450 reductase and cytochrome b_5 for binding to cytochrome P450. This result provides structural explanation on the perplexing roles that cytochrome b5 plays in the cytochrome P450 activity and better understanding of substrate modulation on the tertiary protein complex system.

CHAPTER 1

Introduction*

1.1 Cytochrome P450

1.1.1 The physiological significance of the Cytochrome P450 monooxygenase enzyme system

The Cytochrome P450 (cyt P450) monooxygenases are a ubiquitous superfamily of enzymes found in all living kingdoms, including plants, animals, bacteria and fungi.[1,2] Sequence alignment of known cyt P450s indicate that they all have evolved from a single ancestral cyt P450 gene.[3] The name "cytochrome P450" was first proposed by Omura in 1962, where "P" stands for "pigment" and "450" indicates its unique absorption on a UV/Vis spectrum at 450 nm when cyt P450 is reduced and bound to carbon monoxide.[3] This optical characteristic of cyt P450 is widely used to determine cyt P450 concentration, and to distinguish between active cyt P450 (soret absorption at 450 nm) and inactive cyt P450 (soret absorption at 420 nm, termed cyt P420). To date, a total of 57 human genes have been identified to code for cyt P450s, which are found in most of the tissues and cell types.[4,5] Mammalian cyt P450s are membrane bound proteins mostly located on the endoplasmic reticulum (ER) membrane in liver cells and the inner membrane of mitochondia.[2] In contrast to the ER-associated cyt P450s, the N-terminus membrane-targeting sequence of the mitochondrial cyt P450s are found to be cleaved off once they are trans-located from the cytosol to the mitochondria.[6] The scope of this dissertation is focused on an ER-associated membrane-bound cyt P450 – cyt P450 2B4.

Together with its redox partners, cytochrome P450 reductase (CPR) and cytochrome b_5 (cyt b_5), ER-associated cyt P450s are capable of catalyzing the metabolism of a dazzling array of endogenous and exogenous substrates including sterols, vitamins, fatty acids, carcinogens, environmental pollutants and over 75% of the pharmaceuticals on the current market.[1,2,4,5,7,8] Cyt

* This thesis research was supported by funds from the National Institutes of Health (NIH to A.R.).

P450s are also involved in the biosynthesis of physiologically-relevant chemical compounds (e.g. vitamins A and D and bile acid).[9] The most well-known function of cyt P450s is to activate an inert C-H bond in a hydrophobic substrate by inserting an "activated" oxygen atom to form a hydroxyl group which makes the substrate more hydrophilic.[2] During the reaction, two electrons and two protons are required to be sequentially delivered to cyt P450 from water and its redox partners respectively to complete the catalytic cycle (Figure 1.1).[2,10] This monooxygenation reaction can either deactivate drugs and accelerate their clearance from the living system so that toxic side-effects caused by drug overdoses can be avoided, or activate inert compounds to their toxic form causing health problems. Therefore, it is of great clinical importance to study the cyt P450 enzyme system to develop better therapeutic drugs (*e.g.* antidepressants, antipsychotics, *etc*.).[7,11]

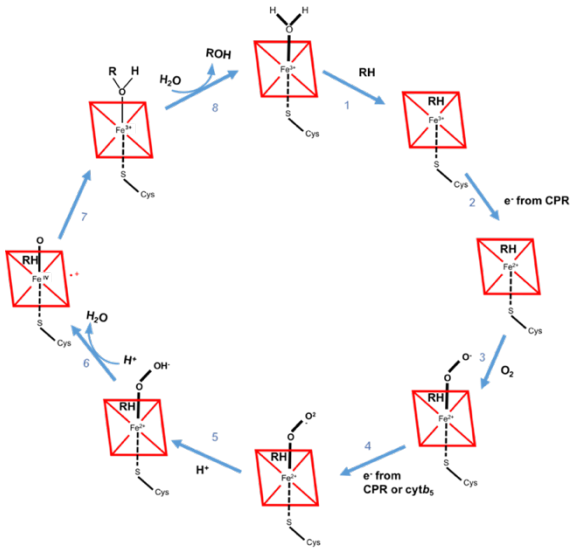

$$RH + O_2 + 2H^+ + 2e^- \rightarrow ROH + H_2O$$

Figure 1.1 The catalytic cycle of cytochrome P450. In the resting state, the heme iron is bound to a water molecule. (1) The substrate RH comes in and replaces the water molecule, but does not coordinate with the heme iron. The spin state of iron changes from low-spin state to high-spin state by most substrates. (2) The first electron is delivered from CPR, which shifts ferric iron to ferrous iron. (3) The ferrous iron binds to an oxygen molecule forming the oxyferrous P450. (4) The second electron is delivered to the oxyferrous P450 either from CPR or from cyt b_5, which leads to formation of the peroxo P450. (5) The peroxo P450 then obtains a H^+ from a water molecule and becomes the hydroperoxo P450. (6) The hydroperoxo P450 binds another H+ and releases a water molecule, which forms the oxyferryl P450. (7) The "activated" oxygen atom is inserted into the C-H bond of the substrate RH forming ROH. (8) A water molecule replaces the ROH completing the catalytic cycle and cyt P450 goes back to its resting state. The general process is summarized in the reaction below the cycle.

Cyt P450s are also related to the development/treatment of several health conditions: they are related to the pathogenesis and progression of cardiovascular diseases; they are found to be overexpressed in numerous human cancers (*e.g.* breast cancer, brain cancer, *etc.*); and they serve as novel anti-tuberculosis drug targets. All of these highlight the importance of understanding the structure and function of this protein family.[12–15]

1.1.2 Structure of cytochrome P450

Ever since the first discovery of cyt P450s as a mysterious "carbon monoxide binding pigment" in 1954 by Klingenberg,[3] researchers have been trying to elucidate the tertiary structure of member proteins in the cyt P450 superfamily. The first few crystal structures were obtained for cytochrome P450 camphor – a soluble bacterial cyt P450 – in the 1980s.[16,17] It was not until the year of 2000 when the first mammalian cyt P450 crystal structure was obtained by both N-terminus transmembrane (TM) domain cleavage and internal modifications.[18] Difficulties with ordered crystallization imposed by the bitopic nature of the mammalian cyt P450 structures have led researchers to follow the approach of N-terminus TM domain truncation for obtaining high resolution crystal structures. To date, nearly a thousand cyt P450 structures have been released by the Protein Data Bank, which reveal high conformational conservation, especially among the same subfamilies. For example, the cyt P450s in the CYP2 subfamily share 73% structure alignment, and up to 85% alignment when only closed structures are considered.[19] Cyt P450 2B4, a rabbit cyt P450, shares 78% sequence identity with human cyt P450 2B6 and has long been considered as a good model for understanding cyt P450 2B6.[20]

Cyt P450 2B4 is a 56 kDa membrane bound protein with 491 amino acids. The structure consists of a 53 kDa globular domain[20–30] and a transmembrane domain. The globular heme-containing domain is comprised of thirteen α-helices (A-L) and four β-sheets (1-4). (Figure 1.2) The type-b heme is buried deeply inside the globular domain, and the heme iron is coordinated via a thiolate ligand of Cys436, which is located between helices K and L on the proximal basic concave surface of cyt P450 2B4 where the heme is closest to. This surface has been reported to be involved in complex formation with CPR and cyt b_5 for electon transfer.[1,2,10,31,32] The globular domain of cyt P450 2B4 has been crystalized with and without various substrates. [20–30] These structures reveal drastic conformational rearrangements upon accommodation of different substrates, which leads to identification of five plastic regions (PR1-5) including the loop

preceding helix A (PR1), helix B' through C as well as the C/D loop (PR2), the C-terminus of helix E as well as the loop following it (PR3), the C-terminus of helix F through the N-terminus of helix I (PR4), and the β4 hairpin (PR5).[33] At the same time, half of the protein structure remain conserved over all the known crystal structures. The conserved regions mainly include the heme binding elements, *e.g.* C-terminus of helix I, helix J, K, L, *etc.*[33] The plastic and conserved regions coordinate with each other to re-shape the heme pocket for ligand binding while maintaining the overall fold of the protein. The transmembrane domain of cyt P450s have been found to be comprised of α-helical conformation either as a single α-helix[34] or a Z-type combination of two helices[35].

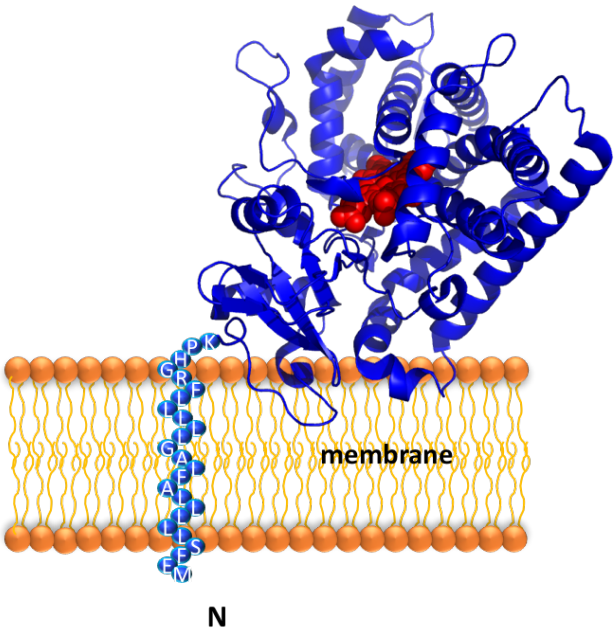

Figure 1.2Crystal structure of the globular domain of cyt P450 2B4 (1SUO). [21]

1.1.3 Membrane topology of cytochrome P450

Most mammalian cyt P450s are found on either the mitochondrial or ER membrane, with their hydrophobic TM domain spanning the lipid bilayer. While the TM domain serves as a membrane anchor of the entire protein, truncated cyt P450s are also able to bind with the membrane even in the absence of the TM domain.[36–41] Truncated CYP1A1, CYP2E1 and CYPc17 have been shown to be still membrane-bound even in solutions with high ionic strength, indicating the presence of membrane-associated regions other than the TM domain.[41–43] Similar situations

were found for other cyt P450s.[39,41,44–46] For cyt P450 2B4, it was found that the truncated form still retained 30% membrane localization but was not deeply embedded in the membrane.[39,47] It was also found by atomic force microscopy measurements that the height of cyt P450 2B4 above the membrane is about 3.5 nm.[48]

It has been proposed that several loop regions in the catalytic globular domain of cyt P450s also interact with the membrane, allowing a significant portion of the protein surface to be buried inside the membrane; this could serve in assisting the process in which the substrate enters the catalytic active site, and holding cyt P450 in an orientation that allows optimal contact with its redox partners for efficient electron transfer.[47,49–51] Understanding the binding between cyt P450s and membrane would therefore provide valuable information in the study of protein-substrate interaction and protein-protein interaction in the cyt P450 monooxygenase system.

1.2 Cytochrome b_5

1.2.1 Background

Cytochrome b_5, a heme containing amphipathic protein, is a philological redox partner of cyt P450. It can only transfer the second electron to cyt P450 (Figure 1.1) due to its high redox potential (~ 25 mV) as compared to that of ferric cyt P450 (~ -300 mV).[32,52] Cyt b_5 consists of 134 amino acids with a molecular weight of 17 kDa. It comprises three domains: a heme containing soluble domain, a hydrophobic transmembrane domain, and a 15-amino acid flexible linker connecting the aforementioned two domains. (Figure 1.3) The type b heme is coordinated with two histidines: His44 and His68. About 20% of cyt b_5 residues are glutamates and aspartates, rendering it mostly negatively charged, especially on the front face of cyt b_5 around the solvent exposed heme edge, which has been reported to be the binding interface with cyt P450.[1,53] (Figure 1.4) Due to the amphipathic nature of the protein, most crystal and NMR structures of cyt b_5 followed the approach of C-terminus truncation.[54–69] Therefore, the conformation of the TM domain and the flexible linker are not available in these structures. In 2013, the structure of the soluble domain and the flexible linker was determined by solution NMR using full-length cyt b_5 in a membrane mimetic environment, which took a step forward towards a more physiologically relevant high resolution structure.[1] (Figure 1.3, 1.4) In the same work, alanines in the TM domain, which are invisible on the solution NMR spectrum due to high total correlation time, were also

assigned with the application of Magic Angle Spinning solid state NMR technology and selective amino acid isotope labeling. The hydrophobic transmembrane domain anchors the entire protein to the cytoplasmic side of the ER membrane.[70] Both Circular Dichroism spectroscopy and Fourier IR studies imply a mostly helical structure of the transmembrane domain.[71–73] Solid state NMR study indicated that the TM domain comprises a single α-helix.[74] It has been reported that truncated cyt b_5, in which the TM domain is cleaved off, although still transfers electrons to bacterial soluble cyt P450s, it is not capable of transferring electrons to mammalian membrane-bound cyt P450s.[75–77] Besides cyt P450s, other proteins could also accept electrons from cyt b_5 including myoglobin, cytochrome c, *etc.*[75,78]

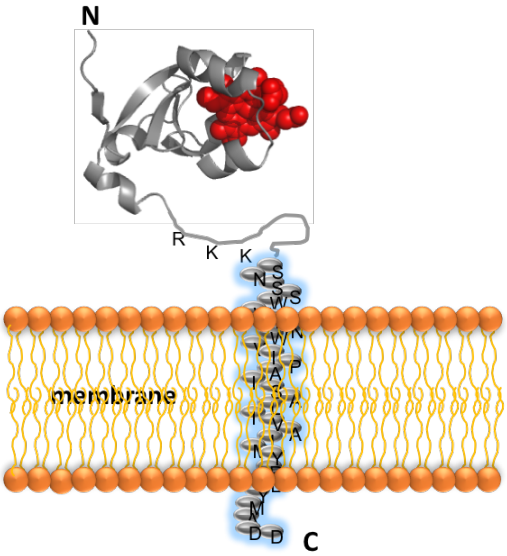

Figure 1.3NMR structure of the globular domain of cyt b5 (2M33). [1]

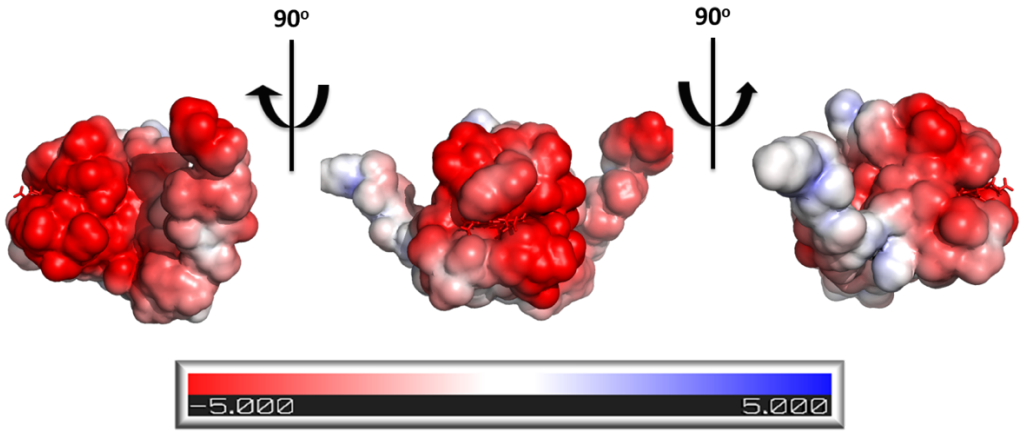

Figure 1.4Electrostatic surface potential of cyt b5 (2M33). [1]

1.2.2 Interaction between cyt b_5 and cyt P450

As mentioned above, cyt b_5 is able to donate an electron to the oxyferrous cyt P450. Kinetics studies on a reconstituted oxyferrous cyt P450 – ferrous cyt b_5 system reveal a very fast electron transfer rate of 2.5 s^{-1}, which can be affected by the presence of different substrates.[79,80]

Numerous studies have been carried out to investigate complex formation between cyt P450 and cyt b_5 on the structural basis. It has been postulated that complex formation between the two redox partners is driven by electrostatic interactions between the positively charged proximal surface of cyt P450 and the negatively charged surface of cyt b_5. Single site-directed mutagenesis studies indicate that mutations of E42(K) and E48(K) on rat cyt b_5 cause a decrease in cyt P450 17α and cyt P450 3A4 activity, while mutation of D65(A) does not alter cyt P450 activities, implying E42, E48 as important residues for binding cyt P450.[81] On the other hand, site-directed double mutant cycle studies indicate D65, V66 of rabbit cyt b_5 to be in contact with R122, R126, K433 of rabbit cyt P450 2B4.[82] Cross-linking studies on human cyt b_5 and cyt P450 2E1 found D58, E61 of cyt b_5 to be in ion pairs with M427, K433 of cyt P450 respectively.[83] Molecular modelling on cyt P450 2B4 with various cyt b_5 revealed the following residues pairs to be in contact: N417-E48, R422-E49, V89&I423-V50, R85-E53, K433-E61, R126-E64, R122-D65, L129-V66, R133-heme, R443-heme.[84] Although these studies show controversial results on the specific residues identified to be on the binding interface, they still point to the same general region of the two proteins which agree with the hypothesis that complex formation between cyt P450 and cyt b_5 is driven by charge pairing on their surfaces. In 2013, a complex structure model of cyt P450 - cyt b_5 was generated using a molecular docking program HADDOCK based on experimental restraints provided by mutagenesis studies and solution NMR experiments on both full-length proteins in membrane mimetics.[1] (Figure 1.5) This complex structure provided high resolution mapping of the interaction interface of both proteins, which revealed interactions mainly including hydrogen bonds between (cyt b_5 – cyt P450): N62 – E93 and K433, D65 – K433 and R122, H68 – R126, S69 – L129, D71 – D134, heme – R133; salt bridges between: E64 – R126, D65 – K433 and R122; van der Waals contacts between: F63 – R126, V66 – K433 and R125, G67 – R126, T70 – A130, D134 and G136, R73 – R126. In addition, an electron transfer pathway was predicted which involves both hemes and R125 on the helix C of cyt P450. R125 is highly conserved among cyt P450s and has been shown to be important for cyt P450 activity by mutagenesis studies.[85,86]

The role of cyt b_5 on cyt P450 activity is very perplexing, since it is able to stimulate, inhibit or not affect cyt P450 activities depending on the particular cyt P450 isoforms, or the substrates present in the system, or even experimental conditions.[10,87–89] A widely accepted hypothesis is that cyt b_5 and CPR compete for an overlapping but non-identical binding interface on cyt P450, which leads to inhibition of delivery of the first electron to cyt P450 from CPR, while presence of cyt b_5 stimulates the second electron transfer process, which in combination results in different "effect of cyt b_5" on cyt P450 activities. For cyt P450 2B4, it has been reported that cyt b_5 stimulates cyt P450 2B4 activity to different extents depending on the substrate involved: the activity increased by 8.5 fold for the substrate methoxyflurane and 1.3 fold for the substrate benzphetamine.[10] A lot of studies have been carried out which indicates a constant value for additional product formation and NADPH consumption resulting in different comparisons for different substrates.[10,90,91] However, an explanation on the structural basis remains lacking up till now.

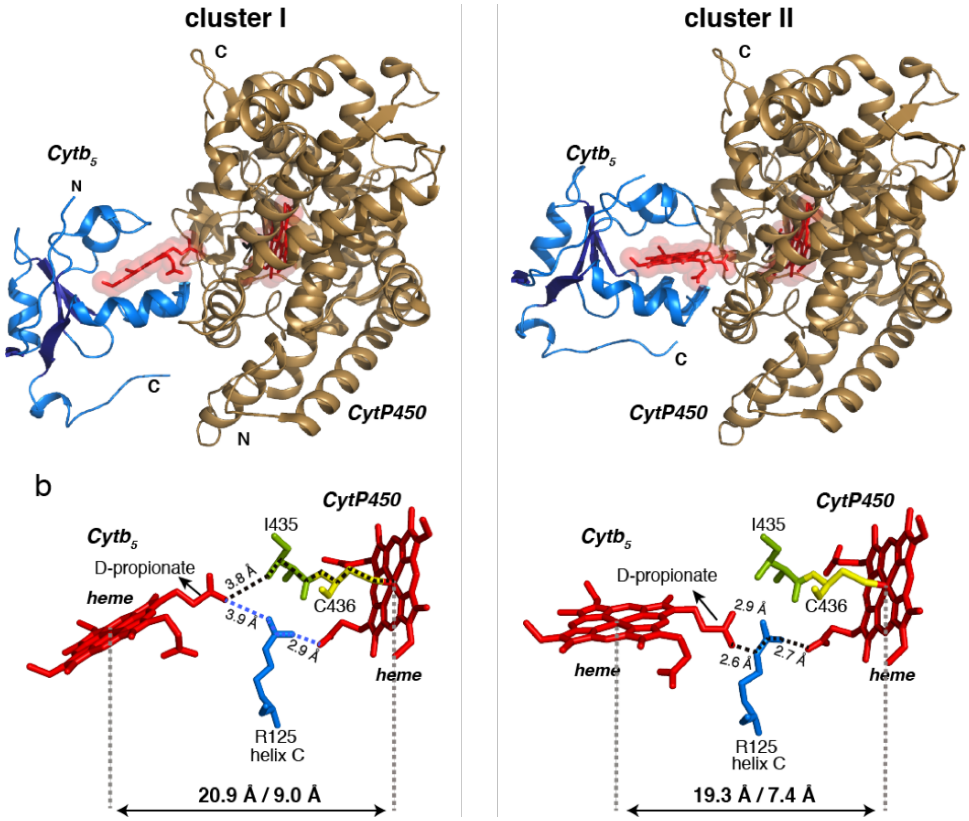

Figure 1.5 Structural model for cyt P450 2B4 – cyt b_5 complex. Reprinted with copyright permission from S. Ahuja, *et. al.* [1]

1.3 Cytochrome P450 Reductase (CPR)

1.3.1 Background

Cytochrome P450 reductase is capable of donating both the first electron and the second one to cyt P450, as compared to cyt b_5 which is only able to donate the second electron to cyt P450, which renders CPR essential for cyt P450 activities.[2,10] CPR consists of 678 amino acids with a molecular weight of 78 kDa. It comprises four major domains: an FAD/NADPH binding domain, an FMN binding domain, a connecting domain that links the aforementioned two domains together, and an N-terminus hydrophobic transmembrane domain. (Figure 1.6) During the catalytic cycle of cyt P450, electrons are shuttled from NADPH to cyt P450 via the following electron transfer pathway: NADPH first binds to the FAD binding domain of CPR and transfers electrons to FAD, then inter-domain electron transfer occurs between FAD and FMN, FMN then accepts the electron from FAD and transfers it to cyt P450. Therefore, the FMN binding domain is the direct electron transfer domain in CPR for donating electrons to cyt P450. The FMN binding domain adopts the typical α-β-α fold including five α-helices, five β-stands and several loop regions. The FMN cofactor binds to the protein at a dissociation constant of 2×10^8 M^{-1}.[92] It is held by four loops and buried deeply inside the closed structure of CPR.[93] It is hypothesized that CPR goes through a domain movement to let out the FMN cofactor in order to get in contact with cyt P450 for inter-protein electron transfer to occur. Similar to cyt b_5, CPR is mostly negatively charged on the solvent exposed surface. (Figure 1.7)

It is widely accepted that CPR is the result of evolution from two ancestral proteins: an FAD containing ferredoxin reductase and an FMN containing flavodoxin.[94,95] It is believed that during evolution the two ancestral proteins were brought together by a connecting domain due to gene fusion, which increases the electron transfer efficiency between the two proteins. [94,95] Theoretically, given the 4 Å distance between the two flavins in the crystal structure, the inter-flavin electron transfer rate could be as fast as 10^{10} s^{-1}.[93,96] Experimentally, the inter-flavin electron transfer rate is measured to be between 15 – 55 s^{-1}, suggesting a possible gating mechanism behind the electron transfer process.[97–99] One hypothesis of this gating mechanism refers back to domain motion, which possibly correlates inter-flavin electron transfer with inter-protein electron transfer. Direct evidence on this hypothesis or other possible mechanisms remains to be unraveled up till now.

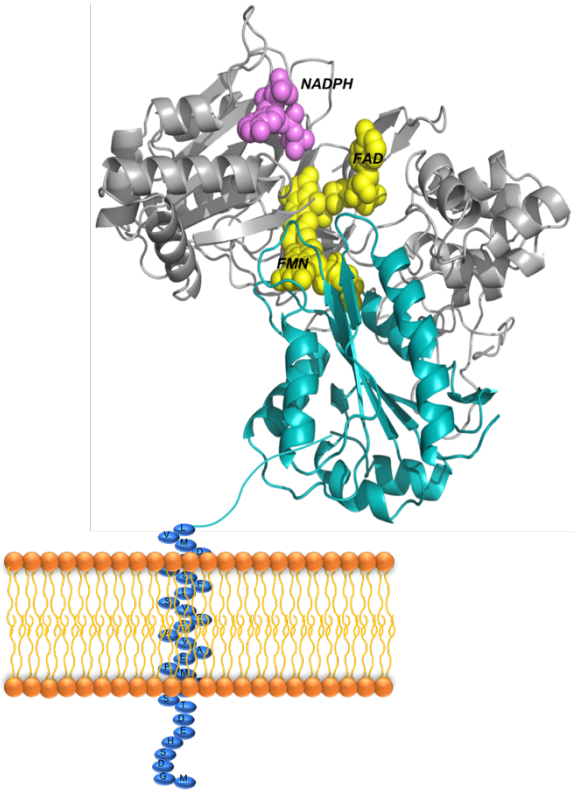

Figure 1.6 Crystal structure of cytochrome P450 reductase (1AMO). [93]

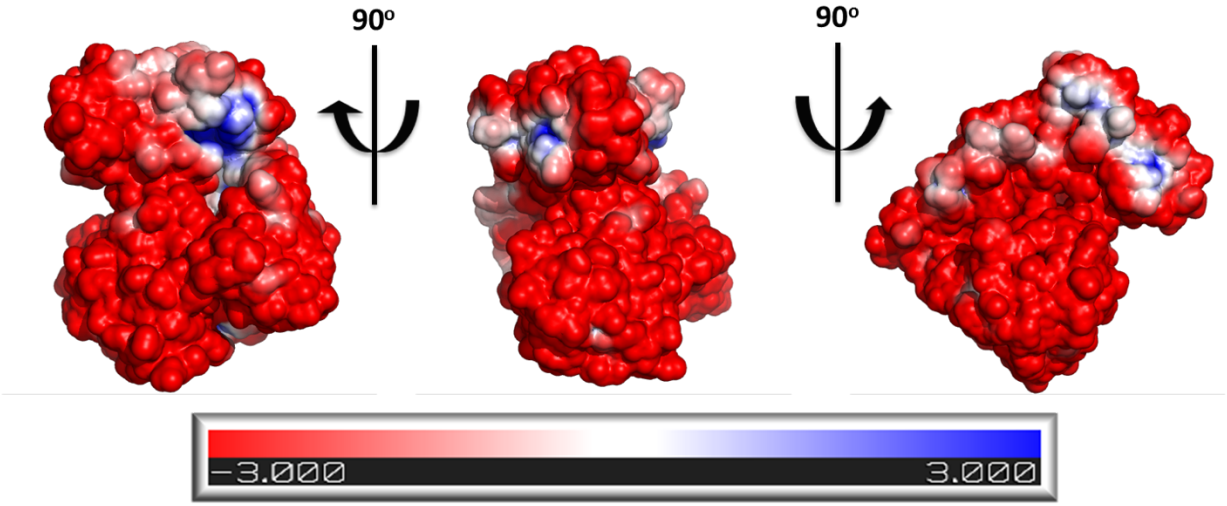

Figure 1.7 Electrostatic surface potential of cytochrome P450 reductase (1AMO). [93]

1.3.2 Interaction between CPR and cyt P450

As mentioned above, CPR is able to donate both the first electron to the ferric cyt P450 and the second electron to the oxyferrous cyt P450 through direct contact between cyt P450 and the FMN binding domain of CPR. A lot of studies have been performed to investigate the interaction between cyt P450 and CPR on the structural basis. Site-directed mutagenesis studies show drastic drop of binding affinity between the two proteins when the following residues of cyt P450 were mutated to alanine: Arg122, Arg126, Are133, Lys139, Arg422, Arg433 and Arg443.[82] Chemical modifications of lysine residues on cyt P450 also led to reduction in cyt P450 activity in a reconstituted system with CPR, implying importance of lysine residues in CPR – cyt P450 interactions.[100,101] Mutagenesis studies on CPR revealed residues Asp208, Asp113, Glu115 and Glu116 to be important for binding cyt P450.[102–104] These findings suggest that electrostatic interactions play an important role in complex formation between CPR and cyt P450. On the other hand, hydrophobic residues like Val267, Leu270 of cyt P450 2B4 and other cyt P450s have also been found to be involved in the interaction with CPR.[105,106] Although a lot of information on the potential binding interface of the CPR-cyt P450 complex is provided by the chemical modification and mutagenesis studies, which assume changes on the residues do no affect overall folding and the environment of the redox centers, a high resolution complex structure based on experimental results remains to be determined in order to get better insight into the mechanism of electron transfer between the two redox partners on the structural basis.

1.4 Goal of this research

In this dissertation, I aim to understand how different factors, including membrane (Chapter 2) and substrates (Chapter 4 and 5) affect the interaction between cyt b5 and cyt P450 through solution NMR techniques and other biological/biophysical assays. In order to provide a more physiological environment for future investigations on the cyt P450 enzyme system, a novel peptide-based nanodisc membrane mimetic will be developed and the productive complex of cyt b5 – cyt P450 2B4 is successfully reconstituted into these nanodiscs (Chapter 3). A complex structure will be generated for trFBD – cyt P450 2B4 based on a combination of NMR experimental results and previous mutagenesis study, which will aid in better understanding of the interaction between trFBD and cyt P450 2B4. The effect of substrates on the interaction between

trFBD and cyt P450 2B4 will be examined. A competitive binding mechanism will be unraveled for the trFBD – cyt P450 – cyt b5 tertiary protein system, which is proven to be regulated by different substrates. This work will provide insights into protein-protein interactions in the cyt P450 enzyme system on the structural basis.

1.5 Experimental methods

1.5.1 NMR techniques

Rapid development of the theory and experimental methodology of Nuclear Magnetic Resonance (NMR) spectroscopy have enabled an explosively increased application of NMR in elucidating the structure and dynamics of biomolecular systems including proteins, nucleic acids and their complexes at the atomic resolution under physiologically relevant conditions. Residue specific information, including structure or dynamics change in response to experimental condition change, binding a ligand or other biological macromolecules, redox state alteration, *etc.* could be obtained for proteins isotopically labeled with ^{13}C and/or ^{15}N using solid-/solution-state NMR techniques. Partial or full deuteration of proteins with a molecular weight of 30 kDa or more, in combination with proton back exchange for amide groups, could lead to drastic improvement in signal-to-noise ratio on the NMR spectrum. Residue-specific resonance assignment for $^{13}C\alpha$, $^{13}C\beta$, ^{15}N, $^{1}H_N$, ^{13}CO could be achieved through a set of standard three-dimensional solution NMR experiments including HNCACB, CBCA(CO)NH, HNCA, HNCO, HNCACO, HNCOCA, *etc*. On a two-dimensional heteronuclear $^{15}N/^{1}H$ HSQC spectrum, each resonance represents the amide group of each residue in the corresponding protein. The distribution of the resonances is determined by the unique structural and dynamic properties of the protein. Therefore, a heteronuclear $^{15}N/^{1}H$ HSQC spectrum is considered as the "fingerprint" of a protein. Perturbations in the position and/or line-width of the resonances reflect changes in the chemical environment and/or dynamics or the corresponding residues, providing information on the structure and motion of the protein under the specific condition at the atomic resolution.

1.5.1.1 Sequential assignment of amide backbone resonances by standard triple-resonance three *dimensional solution NMR techniques – HNCACB, CBCA(CO)NH, HNCA, HNCO, experiments*

Sequential resonance assignment for small proteins below 10 kDa could be achieved with homonuclear NMR experiments including TOCSY and NOESY based on through bond J-coupling and through space short range NOE effects. However, when the size of the protein increases to above 10 kDa and more, the homonuclear NMR spectrum is overwhelmed with the amount of peaks crowding the area, which necessitates high signal-to-noise ratio and resolution. As an alternative, three dimensional heteronuclear triple-resonance NMR experiments correlate backbone $^{13}C_{\alpha}$, $^{13}C_{\beta}$, ^{15}N, $^{1}H_{N}$, ^{13}CO resonances through J-scalar couplings, providing higher resolution even for proteins up to 30 kDa and enabling better assignment efficiency. For proteins above 30 kDa, partial deuteration is required to gain improvement in spectrum resolution. With a combination of isotope labeling strategy, *e.g.* selective amino acid labeling and/or selective ^{13}C methyl labeling, proteins with a molecular weight of up to 80 kDa could be assigned.[107,108]

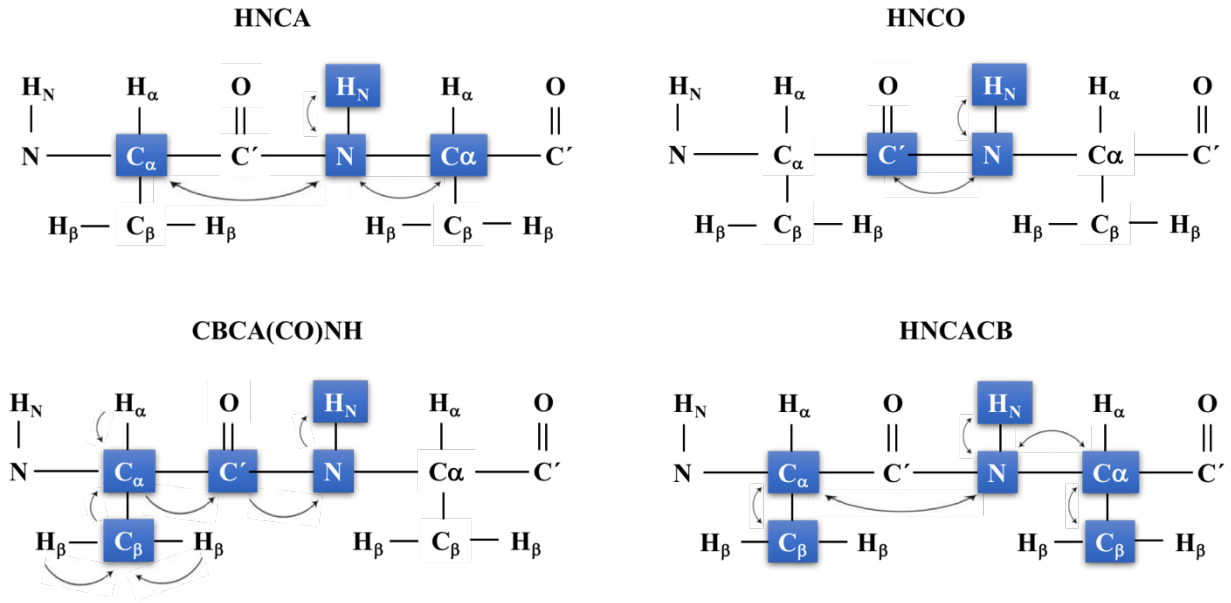

Figure 1.8 Triple-resonance NMR experiments for protein backbone resonance assignment.

The HNCA experiment correlates $^{1}H_{N}$ and ^{15}N with $^{13}C_{\alpha}$ of the current residue and that of the preceding residue through one-bond and two-bond scalar couplings respectively, which provides sequential connectivity for protein backbone sequential assignment.[109–111] (Fig. 1.8) The

intra-residue scalar coupling is usually stronger than the inter-residue scalar coupling. Therefore, the stronger peak is usually assigned to the current residue and the weaker to the preceding residue. Presented in Figure 1.9 is a simplified pulse sequence for the HNCA NMR experiments, which employs an "out-and-back" coherence transfer pathway where ^{1}H is initially excited and finally detected. After excitation, ^{1}H magnetization is transferred to ^{15}N during the INEPT sequence before t_1. Chemical shift evolution of ^{15}N is performed during t_1 period with decoupling from ^{1}H, $^{13}C_\alpha$ and ^{13}CO spins. Evolution due to ^{1}H-^{15}N coupling and ^{15}N-$^{13}C_\alpha$ coupling proceeds after t_1 and $^{13}C_\alpha$ chemical shift evolution takes place during t_2 with decoupling from ^{1}H, ^{15}N, and ^{13}CO spins. After t_2 period, spins evolve under scalar coupling and magnetization is transferred back to ^{1}H for detection.

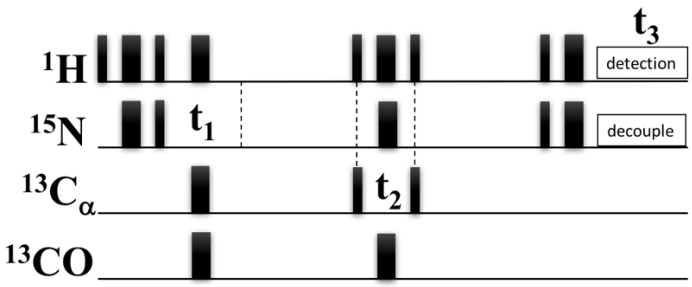

Figure 1.9 Pulse sequence of HNCA NMR experiment.

The HNCO experiment correlates $^{1}H_N$ and ^{15}N of the current residue with ^{13}CO of the preceding residue through one-bond ^{15}N-^{13}CO scalar couplings respectively, providing sequential connectivity for protein backbone sequential assignment. [109,111,112] (Fig. 1.8) Figure 1.10 gives the pulse sequence of HNCO NMR experiments, where magnetization is transferred from ^{1}H to ^{15}N, then to ^{13}CO and eventually back to ^{1}H for detection.

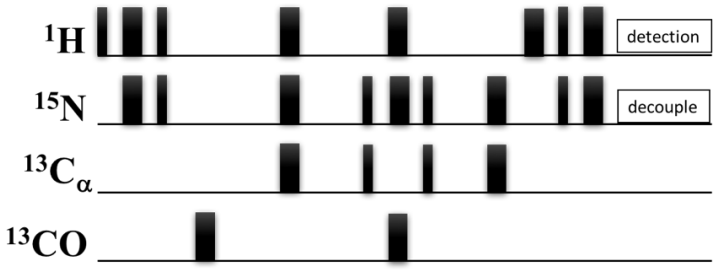

Figure 1.10 Pulse sequence of HNCO NMR experiment.

The CBCA(CO)NH experiment correlates $^{1}H_N$ and ^{15}N of the current residue with both $^{13}C_\alpha$ and $^{13}C_\beta$ of the preceding residue, which gives sequential connectivity.[113] The inter-residue coherence transfer is achieved by intervening the ^{13}CO spin. (Fig. 1.8) This experiment is usually utilized with HNCACB experiment for assignment of $^{13}C_\alpha$ and $^{13}C_\beta$ resonances. The $^{13}C_\alpha$ and $^{13}C_\beta$ chemical shift distribution provides information on the amino acid type of the preceding residue. In figure 1.11, the pulse sequence of the CBCA(CO)NH experiment is shown.

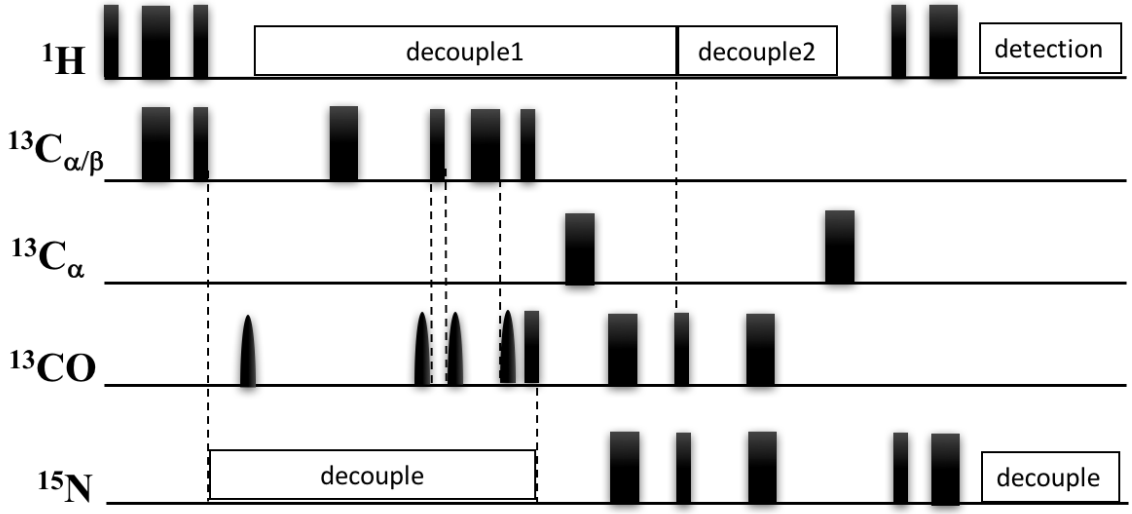

Figure 1.11 Pulse sequence of CBCA(CO)NH NMR experiment.

The HNCACB experiments correlates $^{1}H_N$ and ^{15}N with both $^{13}C_\alpha$ and $^{13}C_\beta$ of the current residue and those of the preceding residue, establishing inter-residue coherence transfer and sequential connectivity.[114] The pattern of $^{13}C_\alpha$ and $^{13}C_\beta$ chemical shift distribution helps in determination of the type of the amino acid of both the current and the previous residue. A pulse sequence of the HNCACB experiments is presented in figure 1.12, which is similar to the "out-and-back" HNCA pulse sequence.

With a combination of the above mentioned triple-resonance three-dimensional NMR experiments, which are complimentary to each other, sequential assignment of all residues but prolines of a protein could be unambiguously achieved.

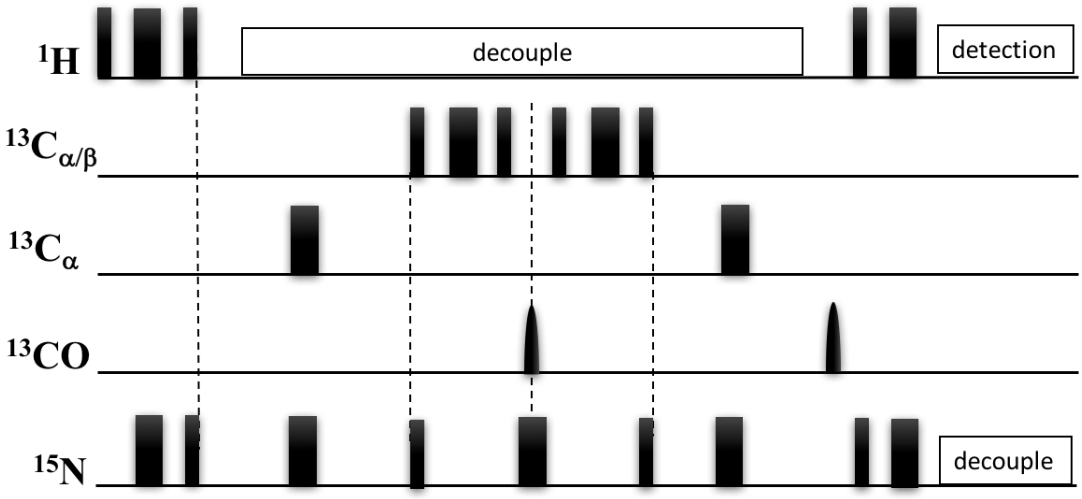

Figure 1.12 Pulse sequence of HNCACB NMR experiment.

1.5.1.2 Two dimensional ^{1}H-^{15}N TROSY HSQC experiments

The ^{1}H-^{15}N Heteronuclear Single Quantum Coherence (HSQC) NMR experiment is widely utilized in the study of biomolecular systems, especially proteins, since it provides residue specific information on the structure and dynamics of a ^{15}N labeled protein. It correlates $^{1}H_N$ with ^{15}N through one-bond scalar coupling, generating a specific distribution of resonances on the spectrum of a particular protein determined by its structural and dynamic properties. The position of a resonance, which is its chemical shift, on a NMR spectrum is determined by the magnetic shielding from the electron cloud from its own electron and its neighbors. The line-width of a resonance is dependent on the transverse relaxation rate of the spin, reflecting the dynamics of the corresponding residue. Therefore, analysis on chemical shift perturbation and differential line-broadening provides information on residue specific response to changes in its chemical environment and/or dynamics, which in turn gives information on protein-ligand binding, protein-protein interaction, *etc.* A simplified HSQC pulse sequence is presented in figure 1.13, in which the ^{1}H magnetization is initially excited and then transferred to ^{15}N during period A using the Insensitive Nuclei Enhanced by Polarization Transfer (INEPT) pulse sequence , the ^{15}N magnetization evolves under chemical shift during period B with decoupling from ^{1}H by the 180^{o} pulse in the ^{1}H channel, the magnetization is transferred back to ^{1}H and the anti-phase signals is converted back to in-phase signals during period C, detection in ^{1}H channel is performed during

period D with decoupling from ^{15}N. The two decoupling periods B and D collapse two doublets in each dimension – in total 4 peaks – into one peak eventually on the spectrum.

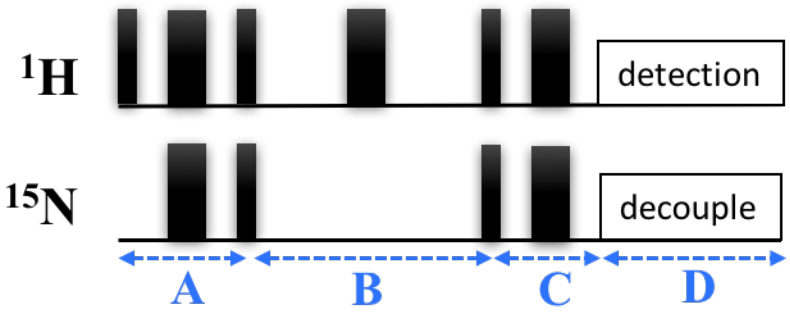

Figure 1.13 Pulse sequence of HSQC NMR experiment.

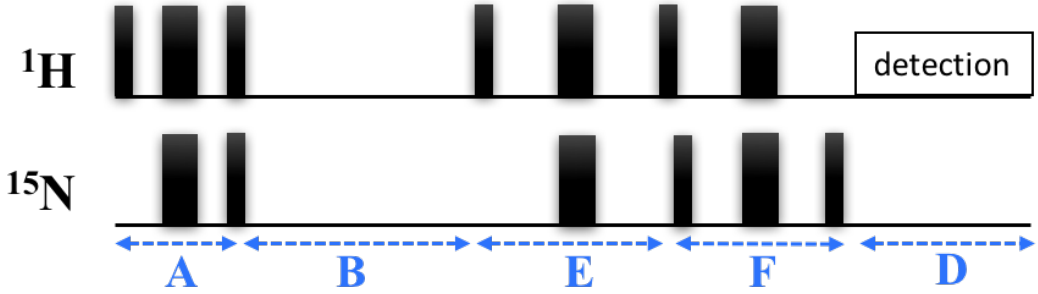

Figure 1.14 Pulse sequence of TROSY HSQC NMR experiment.

For proteins with larger molecular sizes, dipolar couplings become prominent and contribute to relaxation heavily leading to decreased signal-to-noise ratio and resolution. At higher magnetic field, the Chemical Shift Anisotropy (CSA) also becomes more and more significant, resulting in line-broadening of the resonances. The dipolar coupling and CSA could result in four distinct peaks on an HSQC spectrum in the absence of decoupling: one sharp peak where they constructively cancel each other out, two intermediate peaks where only one factor is causing line-broadening, and one peak broadened out due to destructive addition of both factors contributing to relaxation. In an HSQC spectrum, the aforementioned four peaks are collapsed into one peak resulting in an overall averaging of line-width, which gives low signal-to-noise ratio and poor resolution especially for large proteins at high magnetic field. The Transverse Relaxation Optimized SpectroscopY (TROSY) is then designed to selectively detect the sharpest peak of the

four instead of collapsing of all to one. A simplified TROSY HSQC pulse sequence is shown in figure 1.14, where the decoupling 180^{o} pulse in period B and that during period D are removed, and two selective pulse blocks are added (E and F). With this modification, the TROSY based HSQC experiment provides a 60% and 40% sensitivity increase in the ^{15}N and ^{1}H dimension respectively. Biomacromolecules up to the size of 50 kDa and more could be detected with the application of TROSY HSQC. The TROSY modification is also implemented into a number of three- and four-dimensional NMR experiments to gain sensitivity for large biomolecular systems.[115]

1.5.2 High Ambiguity Driven biomolecular DOCKing (HADDOCK)

The High Ambiguity Driven biomolecular DOCKing (HADDOCK) program predicts biomolecular complex structures based on known crystal or NMR structure of each component protein. The docking is driven by NMR and/or mutagenesis data, and take into account the side-chain flexibility of residues when biomacromolecules form a complex with one another. A number of protein-protein, protein-ligand, and protein-nucleic acid complex structures have been solved through HADDOCK with high accuracy. Most other docking programs calculate bimolecular complex structures solely based on surface complementarity, electrostatic interactions, van der Waals interactions, *etc.* by fixing one molecule in space and rotating its counterpart protein on its surface. These docking methods do not involve experimental data and usually result in multiple structures. HADDOCK, on the other hand, utilizes interaction interface information between partner biomolecules from NMR titration data and/or site-directed mutagenesis data as the ambiguous interaction restraints (AIRs) to drive the docking. The AIRs include active and passive residues. The active residues are those that show significant chemical shift perturbation, and/or differential line broadening by NMR data; or determined to be most likely involved in the binding interface by other studies, *e.g.* site-directed mutagenesis. They are also required to have over 50% of solvent accessibility as determined by the NACCESS program. The threshold for determination of residues significantly perturbed by binding its partner differs among different biomolecular systems. For the NMR studies in this thesis, residues with a chemical shift perturbation of more than one standard deviation above average, and/or a peak intensity of more than one standard deviation below average are considered to be most likely involved in direct contact with the partner protein for complex formation. The passive restraints are either less important residues, or residues

that are neighbors to the active residues. They are also required to possess a 50% or more solvent accessibility by NACCESS. Equation 1.1 defines AIR as an ambiguous distance d_{iAB} between any atom m of an active residue i of protein A and any atom n of either an active or a passive residue j of protein B

$$d_{iAB} = \left(\sum_{m_{iA}=1}^{N_{atoms}} \sum_{j=1}^{N_{resB}} \sum_{n_{jB}=1}^{N_{atoms}} \frac{1}{d_{m_{iA}n_{jB}}^{6}}\right)^{-\frac{1}{6}} \pi r^2 \qquad (1.1)$$

in which N_{atoms} represents all atoms of the corresponding residue, N_{res} represents all the residues of the corresponding protein.[116] The distance d_{iAB} must be within 3 Å for the two atoms m and n to be considered as in direct contact with each other. The HADDOCK docking program consists of three steps: the two proteins are first placed apart from each other and allowed random rotations in space, rigid-body energy minimization is meanwhile performed to determine the lowest energy state, usually 200 low energy structures are selected among the 1000 complex structures calculated in this step to proceed to the next one; the second step involves semirigid-body simulation annealing, which first considers the two proteins as rigid body for respective orientation optimization, then takes into consideration the dynamic properties of side-chains and backbone of the active and passive residues; the final step performs solvent refinement in which the complexes are placed in a shell of solvent molecules, typically water molecules. After the final cooling step, the resulting 50 lowest energy structures are analyzed and clustered based on their backbone RMSD.

1.6 References

1. Ahuja, S. *et al.* A model of the membrane-bound cytochrome b5-cytochrome P450 complex from NMR and mutagenesis data. *J. Biol. Chem.* **288,** 22080–95 (2013).
2. Dürr, U. H. N., Waskell, L. & Ramamoorthy, A. The cytochromes P450 and b5 and their reductases--promising targets for structural studies by advanced solid-state NMR spectroscopy. *Biochim. Biophys. Acta* **1768,** 3235–59 (2007).
3. OMURA, T. Recollection of the early years of the research on cytochrome P450. *Proc. Japan Acad. Ser. B* **87,** 617–640 (2011).

4. Nelson, D. R. Comparison of P450s from human and fugu: 420 million years of vertebrate P450 evolution. *Arch. Biochem. Biophys.* **409,** 18–24 (2003).
5. Guengerich, F. P., Wu, Z.-L. & Bartleson, C. J. Function of human cytochrome P450s: characterization of the orphans. *Biochem. Biophys. Res. Commun.* **338,** 465–9 (2005).
6. Black, S. Membrane topology of the mammalian P450 cytochromes. *FASEB J* **6,** 680–685 (1992).
7. Guengerich, F. P. Cytochrome P450s and other enzymes in drug metabolism and toxicity. *AAPS J.* **8,** E101–11 (2006).
8. Guengerich, F. P. Cytochromes P450, drugs, and diseases. *Mol. Interv.* **3,** 194–204 (2003).
9. Lorbek, G., Lewinska, M. & Rozman, D. Cytochrome P450s in the synthesis of cholesterol and bile acids--from mouse models to human diseases. *FEBS J.* **279,** 1516–33 (2012).
10. Im, S.-C. & Waskell, L. The interaction of microsomal cytochrome P450 2B4 with its redox partners, cytochrome P450 reductase and cytochrome b(5). *Arch. Biochem. Biophys.* **507,** 144–53 (2011).
11. Wang, J.-F., Zhang, C., Chou, K. & Wei, D. Structure of Cytochrome P450s and Personalized Drug. *Curr. Med. Chem.* **16,** 232–244 (2009).
12. Nebert, D. W. & Russell, D. W. Clinical importance of the cytochromes P450. *Lancet* **360,** 1155–62 (2002).
13. Fleming, I. Cytochrome P450-dependent eicosanoid production and crosstalk. *Curr. Opin. Lipidol.* **22,** 403–9 (2011).
14. Souter, A., McLean, K. J., Smith, W. E. & Munro, A. W. The genome sequence ofMycobacterium tuberculosis reveals cytochromes P450 as novel anti-TB drug targets. *J. Chem. Technol. Biotechnol.* **75,** 933–941 (2000).
15. Murray, G. I. *et al.* Tumor-specific Expression of Cytochrome P450 CYP1B1. *Cancer Res.* **57,** 3026–3031 (1997).
16. Poulos, T. L., Finzel, B. C. & Howard, A. J. High-resolution crystal structure of cytochrome P450cam. *J. Mol. Biol.* **195,** 687–700 (1987).
17. Raag, R. & Poulos, T. L. Crystal structure of the carbon monoxide-substrate-cytochrome P-450CAM ternary complex. *Biochemistry* **28,** 7586–92 (1989).
18. Williams, P. A., Cosme, J., Sridhar, V., Johnson, E. F. & McRee, D. E. Mammalian Microsomal Cytochrome P450 Monooxygenase. *Mol. Cell* **5,** 121–131 (2000).

19. Mestres, J. Structure conservation in cytochromes P450. *Proteins* **58,** 596–609 (2005).
20. Shah, M. B. *et al.* A structural snapshot of CYP2B4 in complex with paroxetine provides insights into ligand binding and clusters of conformational states. *J. Pharmacol. Exp. Ther.* **346,** 113–20 (2013).
21. Scott, E. E. *et al.* Structure of mammalian cytochrome P450 2B4 complexed with 4-(4-chlorophenyl)imidazole at 1.9-A resolution: insight into the range of P450 conformations and the coordination of redox partner binding. *J. Biol. Chem.* **279,** 27294–301 (2004).
22. Scott, E. E. *et al.* An open conformation of mammalian cytochrome P450 2B4 at 1.6-A resolution. *Proc. Natl. Acad. Sci. U. S. A.* **100,** 13196–201 (2003).
23. Zhao, Y. *et al.* Structure of microsomal cytochrome P450 2B4 complexed with the antifungal drug bifonazole: insight into P450 conformational plasticity and membrane interaction. *J. Biol. Chem.* **281,** 5973–81 (2006).
24. Zhao, Y. *et al.* Structural and thermodynamic consequences of 1-(4-chlorophenyl)imidazole binding to cytochrome P450 2B4. *Biochemistry* **46,** 11559–11567 (2007).
25. Gay, S. C., Sun, L., Maekawa, K., Halpert, J. R. & Stout, C. D. Crystal structures of cytochrome P450 2B4 in complex with the inhibitor 1-biphenyl-4-methyl-1H-imidazole: ligand-induced structural response through alpha-helical repositioning. *Biochemistry* **48,** 4762–71 (2009).
26. Gay, S. C. *et al.* Structures of cytochrome P450 2B4 complexed with the antiplatelet drugs ticlopidine and clopidogrel . *Biochemistry* **49,** 8709–20 (2010).
27. Wilderman, P. R. *et al.* Plasticity of cytochrome P450 2B4 as investigated by hydrogen-deuterium exchange mass spectrometry and X-ray crystallography. *J. Biol. Chem.* **285,** 38602–11 (2010).
28. Gay, S. C. *et al.* Structural Analysis of Mammalian Cytochrome P450 2B4 Covalently Bound to the Mechanism-Based Inactivator tert-Butylphenylacetylene: Insight into Partial Enzymatic Activity. *Biochemistry* **50,** 4903–4911 (2011).
29. Shah, M. B. *et al.* Conformational adaptation of human cytochrome P450 2B6 and rabbit cytochrome P450 2B4 revealed upon binding multiple amlodipine molecules. *Biochemistry* **51,** 7225–7238 (2012).
30. Zhang, H. *et al.* Potent mechanism-based inactivation of cytochrome P450 2B4 by 9-ethynylphenanthrene: implications for allosteric modulation of cytochrome P450 catalysis.

Biochemistry **52,** 355–64 (2013).

31. Shimada, T., Mernaugh, R. L. & Guengerich, F. P. Interactions of mammalian cytochrome P450, NADPH-cytochrome P450 reductase, and cytochrome b(5) enzymes. *Arch. Biochem. Biophys.* **435,** 207–16 (2005).
32. Zhang, H., Hamdane, D., Im, S.-C. & Waskell, L. Cytochrome b5 inhibits electron transfer from NADPH-cytochrome P450 reductase to ferric cytochrome P450 2B4. *J. Biol. Chem.* **283,** 5217–25 (2008).
33. Halpert, J. R. Structure and function of cytochromes P450 2B: from mechanism-based inactivators to X-ray crystal structures and back. *Drug Metab. Dispos.* **39,** 1113–21 (2011).
34. Yamamoto, K. *et al.* Probing the transmembrane structure and topology of microsomal cytochrome-p450 by solid-state NMR on temperature-resistant bicelles. *Sci. Rep.* **3,** 2556 (2013).
35. Monk, B. C. *et al.* Architecture of a single membrane spanning cytochrome P450 suggests constraints that orient the catalytic domain relative to a bilayer. *Proc. Natl. Acad. Sci. U. S. A.* **111,** 3865–70 (2014).
36. Clark, B. & Waterman, M. The hydrophobic amino-terminal sequence of bovine 17 alpha-hydroxylase is required for the expression of a functional hemoprotein in COS 1 cells. *J. Biol. Chem.* **266,** 5898–5904 (1991).
37. Larson, J., Coon, M. & Porter, T. Alcohol-inducible cytochrome P-450IIE1 lacking the hydrophobic NH2- terminal segment retains catalytic activity and is membrane-bound when expressed in Escherichia coli. *J. Biol. Chem.* **266,** 7321–7324 (1991).
38. Cullin, C. Two distinct sequences control the targeting and anchoring of the mouse P450 1A1 into the yeast endoplasmic reticulum membrane. *Biochem. Biophys. Res. Commun.* **184,** 1490–1495 (1992).
39. Pernecky, S. J., Larson, J. R., Philpot, R. M. & Coon, M. J. Expression of truncated forms of liver microsomal P450 cytochromes 2B4 and 2E1 in Escherichia coli: influence of NH2-terminal region on localization in cytosol and membranes. *Proc. Natl. Acad. Sci. U. S. A.* **90,** 2651–5 (1993).
40. Gillam, E. M., Baba, T., Kim, B. R., Ohmori, S. & Guengerich, F. P. Expression of modified human cytochrome P450 3A4 in Escherichia coli and purification and reconstitution of the enzyme. *Arch. Biochem. Biophys.* **305,** 123–31 (1993).

41. Sagara, Y., Barnes, H. J. & Waterman, M. R. Expression in Escherichia coli of functional cytochrome P450c17 lacking its hydrophobic amino-terminal signal anchor. *Arch. Biochem. Biophys.* **304,** 272–8 (1993).
42. Ohta, Y., Sakaki, T., Yabusaki, Y., Ohkawa, H. & Kawato, S. Rotation and membrane topology of genetically expressed methylcholanthrene-inducible cytochrome P-450IA1 lacking the N-terminal hydrophobic segment in yeast microsomes. *J. Biol. Chem.* **269,** 15597–15600 (1994).
43. Larson, J. R., Coon, M. J. & Porter, T. D. Purification and properties of a shortened form of cytochrome P-450 2E1: deletion of the NH2-terminal membrane-insertion signal peptide does not alter the catalytic activities. *Proc. Natl. Acad. Sci. U. S. A.* **88,** 9141–5 (1991).
44. Li, Y. C. & Chiang, J. Y. The expression of a catalytically active cholesterol 7 alpha-hydroxylase cytochrome P450 in Escherichia coli. *J. Biol. Chem.* **266,** 19186–19191 (1991).
45. Kempf, A. C., Zanger, U. M. & Meyer, U. A. Truncated human P450 2D6: expression in Escherichia coli, Ni(2+)-chelate affinity purification, and characterization of solubility and aggregation. *Arch. Biochem. Biophys.* **321,** 277–88 (1995).
46. Dong, M. S. *et al.* Identification of retained N-formylmethionine in bacterial recombinant mammalian cytochrome P450 proteins with the N-terminal sequence MALLLAVFL...: roles of residues 3-5 in retention and membrane topology. *Biochemistry* **35,** 10031–40 (1996).
47. Shank-Retzlaff, M. L., Raner, G. M., Coon, M. J. & Sligar, S. G. Membrane topology of cytochrome P450 2B4 in Langmuir-Blodgett monolayers. *Arch. Biochem. Biophys.* **359,** 82–8 (1998).
48. Bayburt, T. H. & Sligar, S. G. Single-molecule height measurements on microsomal cytochrome P450 in nanometer-scale phospholipid bilayer disks. *Proc. Natl. Acad. Sci. U. S. A.* **99,** 6725–30 (2002).
49. Kawato, S., Gut, J., Cherry, R. J., Winterhalter, K. H. & Richter, C. Rotation of cytochrome P-450. I. Investigations of protein-protein interactions of cytochrome P-450 in phospholipid vesicles and liver microsomes. *J. Biol. Chem.* **257,** 7023–7029 (1982).
50. Gut, J., Richter, C., Cherry, R. J., Winterhalter, K. H. & Kawato, S. Rotation of cytochrome P-450. Complex formation of cytochrome P-450 with NADPH-cytochrome P-450 reductase in liposomes demonstrated by combining protein rotation with antibody-induced cross-

linking. *J. Biol. Chem.* **258,** 8588–94 (1983).

51. Etter, H. U. *et al.* Rotation and interaction with epoxide hydrase of cytochrome P-450 in proteoliposomes. *J. Biol. Chem.* **266,** 18600–5 (1991).
52. Yang, Y. *et al.* Structural and functional characterization of a cytochrome P450 2B4 F429H mutant with an axial thiolate-histidine hydrogen bond. *Biochemistry* **53,** 5080–91 (2014).
53. Estrada, D. F., Laurence, J. S. & Scott, E. E. Substrate-modulated cytochrome P450 17A1 and cytochrome b5 interactions revealed by NMR. *J. Biol. Chem.* **288,** 17008–18 (2013).
54. Arnesano, F., Banci, L., Bertini, I. & Felli, I. C. The solution structure of oxidized rat microsomal cytochrome b5. *Biochemistry* **37,** 173–184 (1998).
55. Arnesano, F., Banci, L., Bertini, I., Felli, I. C. & Koulougliotis, D. Solution structure of the B form of oxidized rat microsomal cytochrome b5 and backbone dynamics via 15N rotating-frame NMR-relaxation measurements. Biological implications. *Eur J Biochem* **260,** 347–354 (1999).
56. Arnesano, F., Banci, L., Bertini, I. & Koulougliotis, D. Solution structure of oxidized rat microsomal cytochrome b5 in the presence of 2 M guanidinium chloride: monitoring the early steps in protein unfolding. *Biochemistry* **37,** 17082–17092 (1998).
57. Banci, L., Bertini, I., Rosato, A. & Scacchieri, S. Solution structure of oxidized microsomal rabbit cytochrome b5. Factors determining the heterogeneous binding of the heme. *Eur. J. Biochem.* **267,** 755–766 (2000).
58. Bhattacharya, S., Falzone, C. J. & Lecomte, J. T. Backbone dynamics of apocytochrome b5 in its native, partially folded state. *Biochemistry* **38,** 2577–2589 (1999).
59. Dangi, B., Blankman, J. I., Miller, C. J., Volkman, B. F. & Guiles, R. D. Contribution of backbone dynamics to entropy changes occurring on oxidation of cytochrome b5 . Can redox linked changes in hydrogen bond networks modulate reduction potentials? *J. Phys. Chem. B* **102,** 8201–8208 (1998).
60. Durley, R. C. E. & Mathews, F. S. Refinement and structural analysis of bovine cytochrome b5 at 1.5 angstrom resolution. *Acta Crystallogr. Sect. D-Biological Crystallogr.* **52,** 65–76 (1996).
61. Falzone, C. J. *et al.* Structural and dynamic perturbations induced by heme binding in cytochrome b5. *Biochemistry* **40,** 4879–4891 (2001).
62. Falzone, C. J., Mayer, M. R., Whiteman, E. L., Moore, C. D. & Lecomte, J. T. Design

challenges for hemoproteins: the solution structure of apocytochrome b5. *Biochemistry* **35,** 6519–6526 (1996).

63. Guiles, R. D., Altman, J., Kuntz, I. D., Waskell, L. & Lipka, J. J. Structural studies of cytochrome b5: complete sequence-specific resonance assignments for the trypsin-solubilized microsomal ferrocytochrome b5 obtained from pig and calf. *Biochemistry* **29,** 1276–1289 (1990).
64. Mathews, F. S., Levine, M. & Argos, P. Three-dimensional Fourier Synthesis of Calf Liver Cytochrome b5 at 2.8 A Resolution. *J. Mol. Biol.* **64,** 449–464 (1972).
65. Muskett, F. W., Kelly, G. P. & Whitford, D. The solution structure of bovine ferricytochrome b5 determined using heteronuclear NMR methods. *J. Mol. Biol.* **258,** 172–189 (1996).
66. Parthasarathy, S. *et al.* Accommodating a nonconservative internal mutation by water-mediated hydrogen bonding between β-sheet strands: a comparison of human and rat type B (mitochondrial) cytochrome b5. *Biochemistry* **50,** 5544–5554 (2011).
67. Wang, L., Cowley, A. B., Terzyan, S., Zhang, X. & Benson, D. R. Comparison of cytochromes b5 from insects and vertebrates. *Proteins* **67,** 293–304 (2007).
68. Wu, J. *et al.* Crystal structure of recombinant trypsin-solubilized fragment of cytochrome b5 and the structural comparison with Val61His mutant. *Proteins* **40,** 249–257 (2000).
69. Yokota, T. *et al.* Unique structure of Ascaris suum b5-type cytochrome: an additional alpha-helix and positively charged residues on the surface domain interact with redox partners. *Biochem. J.* **394,** 437–447 (2006).
70. Ito, A. & Sato, R. Proteolytic microdissection of smooth-surfaced vesicles of liver microsomes. *J. Cell Biol.* **40,** 179–189 (1969).
71. Dailey, H. A. & Strittmatter, P. Structural and functional properties of the membrane binding segment of cytochrome b5. *J. Biol. Chem.* **253,** 8203–8209 (1978).
72. Holloway, P. W. & Buchheit, C. Topography of the membrane-binding domain of cytochrome b5 in lipids by Fourier-transform infrared spectroscopy. *Biochemistry* **29,** 9631–9637 (1990).
73. Holloway, P. W. & Mantsch, H. H. Structure of cytochrome b5 in solution by Fourier-transform infrared spectroscopy. *Biochemistry* **28,** 931–5 (1989).
74. Dürr, U. H. N., Yamamoto, K., Im, S.-C., Waskell, L. & Ramamoorthy, A. Solid-state NMR

reveals structural and dynamical properties of a membrane-anchored electron-carrier protein, cytochrome b5. *J. Am. Chem. Soc.* **129,** 6670–1 (2007).

75. Stayton, P. S., Fisher, M. T. & Sligar, S. G. Determination of cytochrome b5 association reactions. Characterization of metmyoglobin and cytochrome P-450cam binding to genetically engineered cytochromeb5. *J. Biol. Chem.* **263,** 13544–8 (1988).
76. Chiang, J. Y. Interaction of purified microsomal cytochrome P-450 with cytochrome b5. *Arch. Biochem. Biophys.* **211,** 662–673 (1981).
77. Bendzko, P., Usanov, S. A., Pfeil, W. & Ruckpaul, K. Role of the hydrophobic tail of cytochrome b5 in the interaction with cytochrome P-450 LM2. *Acta Biol. Med. Ger.* **41,** K1–K8 (1982).
78. Volkov, A. N., Ferrari, D., Worrall, J. A. R., Bonvin, A. M. J. J. & Ubbink, M. The orientations of cytochrome c in the highly dynamic complex with cytochrome b5 visualized by NMR and docking using HADDOCK. *Protein Sci.* **14,** 799–811 (2005).
79. Pompon, D. & Coon, M. J. On the mechanism of action of cytochrome P-450. Oxidation and reduction of the ferrous dioxygen complex of liver microsomal cytochrome P-450 by cytochrome b5. *J. Biol. Chem.* **259,** 15377–15385 (1984).
80. Bonfils, C., Balny, C. & Maurel, P. Direct evidence for electron transfer from ferrous cytochrome b5 to the oxyferrous intermediate of liver microsomal cytochrome P-450 LM2. *J. Biol. Chem.* **256,** 9457–9465 (1981).
81. Chudaev, M. V, Gilep, A. A. & Usanov, S. A. Site-directed mutagenesis of cytochrome b5 for studies of its interaction with cytochrome P450. *Biochem.* **66,** 667–681 (2001).
82. Bridges, A. *et al.* Identification of the binding site on cytochrome P450 2B4 for cytochrome b5 and cytochrome P450 reductase. *J Biol Chem* **273,** 17036–17049 (1998).
83. Gao, Q. *et al.* Identification of the interactions between cytochrome P450 2E1 and cytochrome b5 by mass spectrometry and site-directed mutagenesis. *J Biol Chem* **281,** 20404–20417 (2006).
84. Lewis, D. F. *et al.* Molecular modelling of CYP2B6, the human CYP2B isoform, by homology with the substrate-bound CYP102 crystal structure: evaluation of CYP2B6 substrate characteristics, the cytochrome b5 binding site and comparisons with CYP2B1 and CYP2B4. *Xenobiotica.* **29,** 361–393 (1999).
85. Nakamura, K. *et al.* Significant contribution of arginine-112 and its positive charge of

Pseudomonas putida cytochrome P-450cam in the electron transport from putidaredoxin. *Biochim. Biophys. Acta* **1207,** 40–48 (1994).

86. Schlingmann, K. P. *et al.* CYP24A1 Mutations in Idiopathic Infantile Hypercalcemia. *N. Engl. J. Med.* **365,** 1741–1743 (2011).
87. Finn, R. D. *et al.* Defining the in Vivo Role for cytochrome b5 in cytochrome P450 function through the conditional hepatic deletion of microsomal cytochrome b5. *J. Biol. Chem.* **283,** 31385–93 (2008).
88. Zhang, H., Myshkin, E. & Waskell, L. Role of cytochrome b5 in catalysis by cytochrome P450 2B4. *Biochem. Biophys. Res. Commun.* **338,** 499–506 (2005).
89. McLaughlin, L. A., Ronseaux, S., Finn, R. D., Henderson, C. J. & Roland Wolf, C. Deletion of microsomal cytochrome b5 profoundly affects hepatic and extrahepatic drug metabolism. *Mol. Pharmacol.* **78,** 269–78 (2010).
90. Zhang, H., Im, S.-C. & Waskell, L. Cytochrome b5 increases the rate of product formation by cytochrome P450 2B4 and competes with cytochrome P450 reductase for a binding site on cytochrome P450 2B4. *J. Biol. Chem.* **282,** 29766–76 (2007).
91. Gruenke, L. D., Konopka, K., Cadieu, M. & Waskell, L. The stoichiometry of the cytochrome P-450-catalyzed metabolism of methoxyflurane and benzphetamine in the presence and absence of cytochrome b5. *J. Biol. Chem.* **270,** 24707–18 (1995).
92. Barsukov, I. *et al.* 1H, 15N and 13C NMR resonance assignment, secondary structure and global fold of the FMN-binding domain of human cytochrome P450. *J. Biomol. NMR* **10,** 63–75 (1997).
93. Wang, M. *et al.* Three-dimensional structure of NADPH-cytochrome P450 reductase: prototype for FMN- and FAD-containing enzymes. *Proc. Natl. Acad. Sci. U. S. A.* **94,** 8411–6 (1997).
94. Porter, T. D. & Kasper, C. B. NADPH-cytochrome P-450 oxidoreductase: flavin mononucleotide and flavin adenine dinucleotide domains evolved from different flavoproteins. *Biochemistry* **25,** 1682–1687 (1986).
95. Smith, G. C., Tew, D. G. & Wolf, C. R. Dissection of NADPH-cytochrome P450 oxidoreductase into distinct functional domains. *Proc. Natl. Acad. Sci. U. S. A.* **91,** 8710–4 (1994).
96. Page, C. C., Moser, C. C., Chen, X. & Dutton, P. L. Natural engineering principles of

electron tunnelling in biological oxidation-reduction. *Nature* **402,** 47–52 (1999).

97. Bhattacharyya, A. K., Lipka, J. J., Waskell, L. & Tollin, G. Laser flash photolysis studies of the reduction kinetics of NADPH:cytochrome P-450 reductase. *Biochemistry* **30,** 759–765 (1991).
98. Gutierrez, A. *et al.* Interflavin electron transfer in human cytochrome P450 reductase is enhanced by coenzyme binding. Relaxation kinetic studies with coenzyme analogues. *Eur. J. Biochem.* **270,** 2612–2621 (2003).
99. Gutierrez, A., Paine, M., Wolf, C. R., Scrutton, N. S. & Roberts, G. C. K. Relaxation kinetics of cytochrome P450 reductase: internal electron transfer is limited by conformational change and regulated by coenzyme binding. *Biochemistry* **41,** 4626–37 (2002).
100. Shen, S. & Strobel, H. W. Role of lysine and arginine residues of cytochrome P450 in the interaction between cytochrome P4502B1 and NADPH-cytochrome P450 reductase. *Arch. Biochem. Biophys.* **304,** 257–65 (1993).
101. Nikfarjam, L., Izumi, S., Yamazaki, T. & Kominami, S. The interaction of cytochrome P450 17alpha with NADPH-cytochrome P450 reductase, investigated using chemical modification and MALDI-TOF mass spectrometry. *Biochim. Biophys. Acta* **1764,** 1126–31 (2006).
102. Zhao, Q. *et al.* Crystal structure of the FMN-binding domain of human cytochrome P450 reductase at 1.93 A resolution. *Protein Sci.* **8,** 298–306 (1999).
103. Shen, A. L. & Kasper, C. B. Role of acidic residues in the interaction of NADPH-cytochrome P450 oxidoreductase with cytochrome P450 and cytochrome c. *J. Biol. Chem.* **270,** 27475–80 (1995).
104. Jang, H.-H. *et al.* Beta sheet 2-alpha helix C loop of cytochrome P450 reductase serves as a docking site for redox partners. *Biochim. Biophys. Acta* **1804,** 1285–93 (2010).
105. Kenaan, C., Zhang, H., Shea, E. V & Hollenberg, P. F. Uncovering the role of hydrophobic residues in cytochrome P450-cytochrome P450 reductase interactions. *Biochemistry* **50,** 3957–67 (2011).
106. Bridges, a *et al.* Identification of the binding site on cytochrome P450 2B4 for cytochrome b5 and cytochrome P450 reductase. *J. Biol. Chem.* **273,** 17036–49 (1998).
107. Tugarinov, V. & Kay, L. E. Ile, Leu, and Val methyl assignments of the 723-residue malate

synthase G using a new labeling strategy and novel NMR methods. *J. Am. Chem. Soc.* **125,** 13868–78 (2003).

108. Tugarinov, V., Muhandiram, R., Ayed, A. & Kay, L. E. Four-dimensional NMR spectroscopy of a 723-residue protein: chemical shift assignments and secondary structure of malate synthase g. *J. Am. Chem. Soc.* **124,** 10025–35 (2002).
109. Grzesiek, S. & Bax, A. Improved 3D triple-resonance NMR techniques applied to a 31 kDa protein. *J. Magn. Reson.* **96,** 432–440 (1992).
110. Farmer, B. T., Venters, R. A., Spicer, L. D., Wittekind, M. G. & Müller, L. A refocused and optimized HNCA: increased sensitivity and resolution in large macromolecules. *J. Biomol. NMR* **2,** 195–202 (1992).
111. Kay, L. E., Ikura, M., Tschudin, R. & Bax, A. Three-dimensional triple-resonance NMR spectroscopy of isotopically enriched proteins. *J. Magn. Reson.* **89,** 496–514 (1990).
112. Muhandiram, D. R. & Kay, L. E. Gradient-Enhanced Triple-Resonance Three-Dimensional NMR Experiments with Improved Sensitivity. *J. Magn. Reson. Ser. B* **103,** 203–216 (1994).
113. Grzesiek, S. & Bax, A. Amino acid type determination in the sequential assignment procedure of uniformly 13C/15N-enriched proteins. *J. Biomol. NMR* **3,** 185–204 (1993).
114. Wittekind, M. & Mueller, L. HNCACB, a High-Sensitivity 3D NMR Experiment to Correlate Amide-Proton and Nitrogen Resonances with the Alpha- and Beta-Carbon Resonances in Proteins. *J. Magn. Reson. Ser. B* **101,** 201–205 (1993).
115. Pervushin, K., Riek, R., Wider, G. & Wüthrich, K. Attenuated T2 relaxation by mutual cancellation of dipole-dipole coupling and chemical shift anisotropy indicates an avenue to NMR structures of very large biological macromolecules in solution. *Proc. Natl. Acad. Sci. U. S. A.* **94,** 12366–71 (1997).
116. Dominguez, C., Boelens, R. & Bonvin, A. M. HADDOCK: a protein-protein docking approach based on biochemical or biophysical information. *J Am Chem Soc* **125,** 1731–1737 (2003).

CHAPTER 2

Effects of Membrane Mimetics on Cytochrome P450 – Cytochrome b_5 Interactions Characterized by NMR Spectroscopy[*†]

2.1 Summery

Mammalian cytochrome P450 (P450) is a membrane-bound monooxygenase whose catalytic activities require two electrons to be sequentially delivered from its redox partners: cytochrome b_5 (cytb_5) and cytochrome P450 reductase, both of which are membrane proteins. Though P450 functional activities are known to be affected by lipids, experimental evidence to reveal the effect of membrane on P450-cytb_5 interactions is still lacking. Here, we present evidence for the influence of phospholipid bilayers on complex formation between rabbit P450 2B4 (CYP2B4) and rabbit cytb_5 at the atomic-level utilizing NMR techniques. General line-broadening and modest chemical shift perturbations of cytb_5 resonances characterize CYP2B4-cytb_5 interactions on the intermediate time scale. More significant intensity attenuation and a more specific protein-protein binding interface are observed in bicelles as compared to lipid-free solution, highlighting the importance of the lipid bilayer in stabilizing stronger and more specific interactions between CYP2B4 and cytb_5, which may lead to a more efficient electron transfer. Similar results observed for the interactions between CYP2B4 lacking the transmembrane domain (*tr*-CYP2B4) and cytb_5 imply interactions between *tr*-CYP2B4 and the membrane surface, which might assist in CYP2B4-cytb_5 complex formation by orienting *tr*-CYP2B4 for efficient contact

[*] This chapter is based on the published paper: Zhang, M., Huang, R., Im, S.-C., Waskell, L., and Ramamoorthy, A. (2015) Effects of membrane mimetics on cytochrome P450-cytochrome b_5 interactions characterized by NMR spectroscopy. *J. Biol. Chem.* **290**, 12705–12718

[†] This thesis research was supported by funds from the National Institutes of Health (NIH to A.R.).

with cytb_5. Furthermore, the observation of weak and non-specific interactions between CYP2B4 and cytb_5 in micelles suggests lipid bilayer structures and low curvature membrane surface being more preferable for CYP2B4-cytb_5 complex formation. Results presented in this study provide structural insights into the mechanism behind the important role that the lipid bilayer plays in the interactions between P450s and their redox partners.

2.2 Introduction

Cytochrome P450 (P450) monooxygenases are a ubiquitous superfamily of enzymes found in all living kingdoms, including plants, animals, bacteria and fungi[1]. Eukaryotic P450s are membrane-bound proteins, usually containing a large soluble domain and a single α-helical transmembrane (TM) domain[2]. A total of 57 human P450s have been discovered[3,4] and are responsible for the metabolism of a wide range of endogenous and exogenous substrates, including sterols, vitamins, fatty acids, environmental pollutants and over 50% of marketed drugs[1,3,5]. One of the most studied functions of P450s is the insertion of a single hydroxyl group into hydrophobic compounds, rendering them more hydrophilic for easier excretion from the kidneys[6]. Completion of the hydroxylation reaction requires two electrons to be sequentially delivered to P450, with the first one coming from cytochrome P450 reductase (CPR) and the second one from either CPR or cytochrome b_5 (cytb_5)[7–9].

Mammalian P450s and their redox partners (CPR and cytb_5) are membrane bound proteins primarily located on the cytoplasmic side of the endoplasmic reticulum (ER) of hepatic cells [10]. The structure of most mammalian P450s is composed of a large soluble domain and a single α-helical transmembrane (TM) domain; cytb_5 contains a soluble domain, a single α-helical TM domain, and a linker connecting the aforementioned two domains[1,11].It is well documented that the environment provided by the cell membrane, including phospholipids in the ER membrane, is closely tied to the functional activities of many membrane proteins[12]. Therefore, it is not surprising that phospholipids comprising the ER membrane have been demonstrated to be essential for optimal P450 activities[13–16]. It is widely believed that the TM domain of mammalian P450s is not the sole membrane binding segment, but a secondary binding site on the P450 lacking the N-terminal TM domain (*tr*-P450) exists. A number of different P450s have been reported to bind the membrane in the absence of the TM domain[17–22]. It has been proposed that several loop regions in the *tr*-P450s interact with the membrane, allowing for a significant portion of the protein surface

to be buried inside the membrane[23,24]; this interaction could further serve in assisting access of hydrophobic substrates to the catalytic active site, and holding P450 in an orientation that allows optimal contact with its redox partners for efficient electron transfer[23,25]. Furthermore, it is reported that substrate turn-over could be stimulated if phospholipids are present[16,26]. Extensive studies on the interaction and electron transfer between P450 and CPR in the presence and absence of phospholipids have been carried out and revealed stronger interactions between the two proteins and faster electron transfer from CPR to P450 in the presence of lipids or membrane-mimetics [27–30]. However, studies demonstrating the effect of phospholipid membrane on P450-cytb_5 interactions is still lacking in the literature.

Although cytb_5 is only capable of donating the second electron due to its high redox potential as compared to ferric P450, it plays a key role in the P450 enzyme system in the catalysis of a variety of compounds and significantly regulates the functional activities of P450s[31,32]. It is reported that cytb_5 could stimulate, inhibit or have no effect on P450 activities, depending on the P450 isozyme studied, the substrate involved, or the particular experimental conditions employed [33–36]. The mechanism underlying the differential effects of cytb_5 on P450 activities is not fully understood. A generally well-accepted explanation is that cytb_5 and CPR possess an overlapping but non-identical binding surface on P450, resulting in competitive binding between the two proteins.[37,38] When P450 predominantly binds cytb_5 due to a high cytb_5 concentration, the first electron to be delivered from CPR is inhibited[1,38]. To obtain an insight into the influence of cytb_5 on P450 activities, an in-depth understanding of P450-cytb_5 interaction is necessary. A recent study on the interaction between the truncated cytochrome P450 17A1 and the soluble domain of human cytb_5 in a lipid free environment revealed a binding interface located on the upper cleft of cytb_5 [37]. Since both proteins are naturally membrane-bound, our study aims to characterize the interactions of P450 and cytb_5 in a native-like membrane environment in order to obtain a more physiologically relevant view. Although the microsomes resemble the ER membrane most, it is a very complex system containing a variety of different types of lipids, cholesterol, carbohydrates, proteins, *etc.* [39,40] For mechanistic studies on the P450 system, a model membrane is needed that can both mimick the native membrane environment and be easily characterized and controlled. Among the most suitable membrane mimetics for NMR studies, detergent micelles and phospholipid/detergent isotropic bicelles have been most frequently and successfully applied to

the investigation of the structure and function of a number of different membrane proteins during the past few decades, as reviewed in [41,42].

In this study, we report an investigation of the interaction between full-length rabbit cytochrome P450 2B4 (CYP2B4) and full-length rabbit cytb_5 in different membrane mimetic environments – including lipid-free environment, isotropic bicelles and micelles – utilizing NMR techniques. Our study provides the first structural evidence on the importance of phospholipid bilayer in governing the interaction between these two proteins. The mechanism by which membrane affects CYP2B4-cytb_5 interaction is also explored. By comparing the effects of different membrane environments in assisting complex formation, we propose that phospholipid bilayers enhance both the affinity and specificity in the interaction between CYP2B4 and cytb_5.

2.3 Materials and Methods

2.3.1 Materials

1,2-dilauroyl-*sn*-glycero-3-phosphocholine (DLPC), 1,2-dihexanoyl-*sn*-glycero-3-phosphocholine (DHPC), n-dodecylphosphocholine (DPC) were purchased from Avanti Polar Lipids Inc. Potassium phosphate monobasic and dibasic, benzphetamine glycerol, and sodium dithionite were purchased from Sigma-Aldrich. Deuterium oxide was purchased from Cambridge Isotope Laboratories, Inc. The 5-mm symmetrical D_2O-matched Shigemi NMR Microtubes were purchased from Shigemi, Inc.

2.3.2 Protein expression and purification

Full-length wild-type rabbit CYP2B4 (*wt*-CYP2B4) and ^{15}N labeled full-length wild-type rabbit cytb_5 were expressed and purified individually as described previously [11,38,43,44]. Briefly, the pLW01 plasmid containing the gene for the *wt*-CYP2B4 was transformed to *E. Coli.* C41 cells and then plated on Luria Bertani (LB) agar plate with 0.24 mM carbenicillin overnight at 37 ^oC. Three colonies were selected from the plate and then incubated in 50 to 140 mL of LB medium/carbenicilline medium for 16 hours at 30 ^oC with shaking at 200 rpm. The overnighted culture was transferred to TB medium (100-fold dilution) supplemented with final concentrations of 500μM δ-aminolevulinic acid and 0.24mM carbenicillin. The cultures were incubated at 22-23 ^oC with shaking at 120 rpm. CYP2B4 expression was induced by IPTG when the cell density

reached A_{600} = 4 ~ 6. After induction, the cultures were grown at 22-23 ^{o}C with shaking at 120 rpm. The P450 and P420 content of the cultures were monitored. The cells were harvested between 76-110 hours after IPTG induction. The cells were lysed and solubilized by detergents, and then applied to DE52 column, Reactive Red agarose column, octyl Sepharose column and hydroxyl apatite column sequentially for purification of the protein[44]. The full-length rabbit ^{15}N-cytb_5 was expressed and purified similarly as wild-type CYP2B4 except that cells were grown in ^{15}N Celtone complete medium with additional supplements as detailed in [43]. The harvested cells were lysed and broken by sonication, and solubilized by detergents. The proteins went through two DEAE columns and one Size Exclusion column for purification.

Truncated rabbit CYP2B4 (*tr*-CYP2B4) was expressed and purified similarly with wild type CYP2B4, as described [45]. Amino acids at the N-terminus from 3 to 21 were truncated. In order to increase the solubility of *tr*-CYP2B4, which in turn increases the expression level, mutations of E2A, G22K, H23K, P24T, K25S, A26S, H27K and R29K were introduced, which made it possible to release the proteins from the membrane under high-salt conditions [45]. These mutations do not affect the binding affinity between *tr*-CYP2B4 and cytb_5, as indicated by the identical K_d values measured for wild-type *tr*-CYP2B4-cytb_5 and mutant *tr*-CYP2B4-cytb_5 (data not shown).

No affinity tags were used for the expression and purification of any of the three proteins.

2.3.3 Determination of the dissociation constant between cytb_5 and wt-CYP2B4

Measurements of the equilibrium dissociation constant of the *wt*-CYP2B4-cytb_5 complex were carried out as described in [38]. Briefly, *wt*-CYP2B4 (0.3 μM) was titrated by cytb_5 at the following concentrations: 0, 0.01, 0.05, 0.1, 0.3, 0.5, 0.8, 1.2 μM in the presence of 0.3 μM benzphetamine, in 100 mM potassium phosphate buffer containing 5%(w/v) glycerol at pH 7.4. The titrations were performed in the presence and absence of 30 μM DLPC respectively. The UV/Vis spectra were collected on a Cary 4000 spectrophotometer at 25 °C. The absorbance at 420 and 385 nm was recorded. The total change in absorbance ($\Delta A = \Delta A_{420} + \Delta A_{385}$) was plotted against the concentration of cytb_5 and fitted using a previously reported equation [38] to get the K_d values for the *wt*-CYP2B4-cytb_5 complex.

2.3.4 Preparation of protein samples incorporated in membrane mimetics

A DLPC/DHPC isotropic bicelle (q = [DLPC]/[DHPC] = 0.25) was prepared by mixing the appropriate amount of DLPC and DHPC in chloroform. The mixture was vortexed and dried under nitrogen to make a thin film, which was further dried under vacuum overnight. The film was then hydrated in 100 mM potassium phosphate buffer, containing 5% (w/v) glycerol, pH 7.4 (referred to as NMR buffer). A DPC micelle solution was prepared by dissolving DPC powder into NMR buffer followed by vortexing.

2.3.5 Carbon Monoxide (CO) assay

A solution containing 1 μM CYP2B4 in NMR buffer was added to a cuvette with 1 cm path length. The protein was then reduced by an excess of sodium dithionite, after which CO gas was allowed to flow over the solution for 1 min. UV/Vis absorption spectra were recorded from 400 nm to 600 nm on a Cary 4000 spectrophotometer before and after treatment of CO gas. This assay was performed in the presence of 10% (w/v) DLPC/DHPC isotropic bicelles and 2mM DPC micelles respectively to check the activity of CYP2B4.

2.3.6 Circular Dichroism (CD)

CD experiments were performed on a Jasco J-715 spectropolarimeter fitted with a 150-W xenon lamp at 25°C using a 1 mm cuvette. Spectra were recorded in the far UV region with 16 scans accumulated and averaged. DLPC/DHPC isotropic bicelles (q = 0.25) or DPC micelles were titrated into a solution containing 1 μM CYP2B4 in NMR buffer. The following final concentrations were achieved throughout the titrations: 0, 1, 2, 20, and 40 mM for bicelles and 0, 0.5, 0.8, 1.1 and 2 mM for DPC micelles. The CMC of DPC is 1.1 mM. Background (with everything present except CYP2B4) was subtracted for all experiments. Quantitative data analysis was performed by CDPro software package using Continll program [46,47].

2.3.7 NMR titration experiments and data analysis

NMR titration experiments were performed at 298 K on a Bruker Avance II 600 MHz Spectrometer equipped with a cryoprobe. For the titration experiments, spectra were first recorded with 0.2 mM free ^{15}N-cytb_5 either in NMR buffer or incorporated into 10% (w/v) membrane

mimetics in NMR buffer, followed by a titration of either *wt*-CYP2B4 or *tr*-CYP2B4 at molar ratios (cytb_5 : CYP2B4) of 1:0, 1:0.25, 1:0.5, 1:0.75 and 1:1. The CYP2B4 stock solutions used for titration were at low concentration (75 μM) in order to avoid any loss of CYP2B4 sample at high concentrations due to protein precipitation. After the spectrum of free ^{15}N-cytb_5 was acquired, a 0.25 molar equivalence of CYP2B4 stock solution was added to ^{15}N-cytb_5. Subsequently, the mixture was concentrated to 300 μL so that the final ^{15}N-cytb_5 concentration remained constant. The rest of the titration experiments were carried out identically. For the control experiments, ^{1}H/^{15}N-TROSY-HSQC spectra were collected from uniformly ^{15}N-labeled cytb$_5$ in complex with *wt*-CYP2B4 in DLPC/DHPC isotropic bicelles (q=0.25) at the following cytb$_5$ concentrations: 50, 80, and 100 μM. All the three experiments were performed at a cytb$_5$: *wt*-CYP2B4 molar ratio of 1:1.5 in NMR buffer.

All NMR experiments were recorded using two-dimensional (2D) ^{15}N/^{1}H TROSY HSQC spectra with 64 scans and 256 t1 increments. Data was processed using TopSpin 2.0 (Bruker) and analyzed using Sparky [48]. The backbone chemical shift assignments of the rabbit cytb_5 have been previously reported [11]. The weighted amide chemical shift perturbation ($\Delta\delta_{avg}$) was calculated using the equation below:

$$\Delta\delta_{avg} = \sqrt{(\Delta\delta N \times \frac{F_2\ SW}{F_1\ SW})^2 + \Delta\delta H^2}$$

where $\Delta\delta N$ and $\Delta\delta H$ are the changes in the amide's nitrogen and hydrogen chemical shifts respectively, while $F_1\ SW$ and $F_2\ SW$ represent the spectral width in the first and second dimension respectively, all parameters are in ppm [49,50].

2.4 Results

2.4.1 Characterization of the effect of lipids on the binding affinity between CYP2B4 and cytb$_5$

The K_d values between *wt*-CYP2B4 and cytb_5 were determined, based on the Type I spectral change (Fig. 2.1A) of CYP2B4 induced by cytb_5, to be 0.008 ± 0.015 μM and 0.14 ± 0.02 μM in the presence (Fig. 2.1B) and absence (Fig. 2.1C) of DLPC lipids respectively. This implies the ability of lipids in facilitating tighter binding between *wt*-CYP2B4 and cytb_5. Our results are

in agreement with the previous findings that phospholipids enhance the interactions between CYPs and the other redox partner – CPR. [27–30]

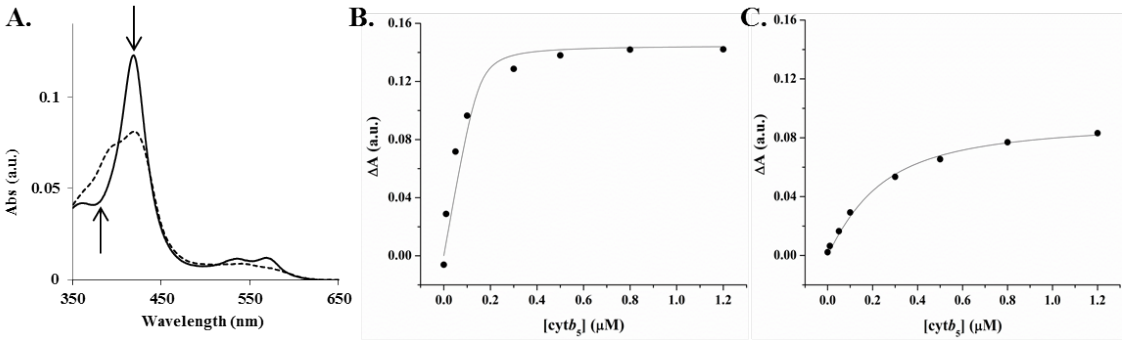

Figure 2.1 Determination of the dissociation constant Kd between cytb5 and wt-CYP2B4 in the presence (B) and absence (C) of DLPC lipid bilayers. (A) Illustration of Type I spectral shift of CYP2B4 induced by cytb_5: decrease at 420 nm and increase at 385 nm. The solid line represents CYP2B4, and the dashed line represents CYP2B4 bound with cytb_5 (the absolute cytb_5 spectrum is subtracted). (B&C) Titration of cytb_5 into 0.3 μM *wt*-CYP2B4 in the presence (B) and absence (C) of 30 μM DLPC lipid bilayers. Both titrations were performed in 100 mM potassium phosphate buffer, containing 5% (w/v) glycerol, 0.3 μM benzphetamine, pH 7.4. The *K*d values for *wt*-CYP2B4- cytb_5 were determined to be 0.008 ± 0.015 μM in DLPC lipid bilayers (B) and 0.14 ± 0.02 μM in the absence of DLPC lipid bilayers (C).

2.4.2 Interaction between cytb$_5$ and wt-CYP2B4

In order to investigate the influence of different membrane mimetic environments on CYP2B4-cytb_5 interaction, 2D ^{15}N/^{1}H TROSY HSQC NMR spectra were recorded to monitor the interaction between ^{15}N-labeled cytb_5 and unlabeled *wt*-CYP2B4 in lipid-free solution, DLPC/DHPC isotropic bicelles, and DPC micelles. In all three experiments, broadening of resonances and moderate chemical shift perturbations (CSP) ($\Delta\delta_{avg} \leq 0.1$ ppm) for amide nuclei of cytb_5 were observed upon interaction with *wt*-CYP2B4. A representative region of the 2D spectra of free cytb_5 and those in complex with *wt*-CYP2B4 in DLPC/DHPC isotropic bicelles are shown in Figure 2.2. In order to assess the effect of non-specific oligomerization/aggregation of CYP2B4 on the resonance intensities of cytb_5 upon titration, experiments were performed on a *wt*-CYP2B4-cytb_5 complex at the cytb_5 : CYP2B4 molar ratio of 1:1.5 in DLPC/DHPC bicelles at different protein concentrations. The average relative resonance intensities are 44.84%, 46.87% and 46.98% at the cytb_5 concentration of 50, 80 and 100 μM respectively. The small standard deviation (1.20%) between the three sets of average relative intensities reveal no significant difference between the

average relative intensities of cytb_5 at different protein concentrations, suggesting no (or negligible) interference of CYP2B4 oligemerization/aggregation on the interpretation of the observed resonance intensities of cytb_5 (Table 2.1).

Table 2.1 A comparison of the average relative intensities of the cytb5 resonances in complex with wt-CYP2B4 at different protein concentrations.

[cytb_5] (μM)	Average relative intensity of the cytb_5 resonances (%)
50	44.84
80	46.87
100	46.98
standard deviation	1.20

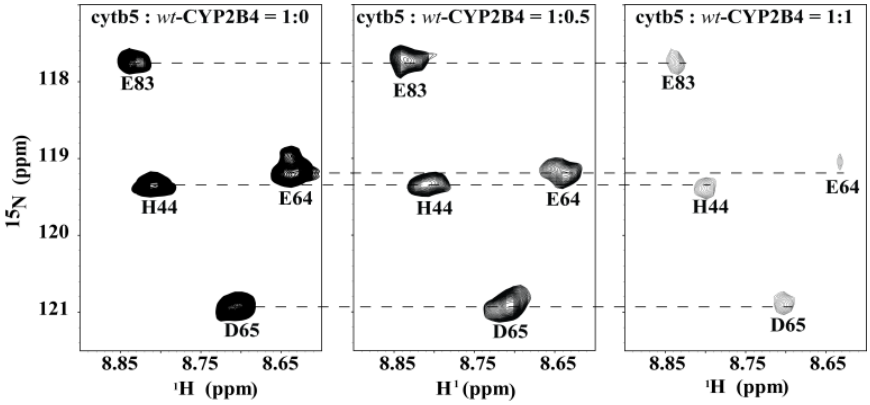

Figure 2.2 Representative 2D ^{15}N/^{1}H TROSY HSQC spectra for titration of unlabeled wt-CYP2B4 into ^{15}N-labeled cytb_5. The titration was performed in NMR buffer (100 mM potassium phosphate buffer, 5% glycerol, pH 7.4) containing 10 % (w/v) DLPC/DHPC isotropic bicelles. Interaction between *wt*-CYP2B4 and cytb_5 in isotropic bicelles causes a combination of moderate chemical shift perturbation and significant line-broadening of cytb_5 resonances, which is indicative of *wt*-CYP2B4-cytb_5 interaction on an intermediate exchange time scale.

The average chemical shift changes observed for lipid-free solution, bicelles and micelles are 0.009, 0.023 and 0.017 ppm, respectively. The small and wide-spread chemical shift perturbations could be occurring for two reasons: first, fast-to-intermediate chemical exchange between free- and bound-cytb_5, which would also explain the overall broadening of cytb_5 resonances [11,37]; second, the formation of an ensemble of dynamic "encounter complexes" causes the "averaging out" of the chemical shift changes, thus leading to small CSP values [51–55]. Due to

the small magnitude of the CSP values and the dispersive perturbation pattern of encounter complexes, residue specific CSPs only provide rough estimations of the binding interface and interaction strength between CYP2B4 and *cytb*$_5$.

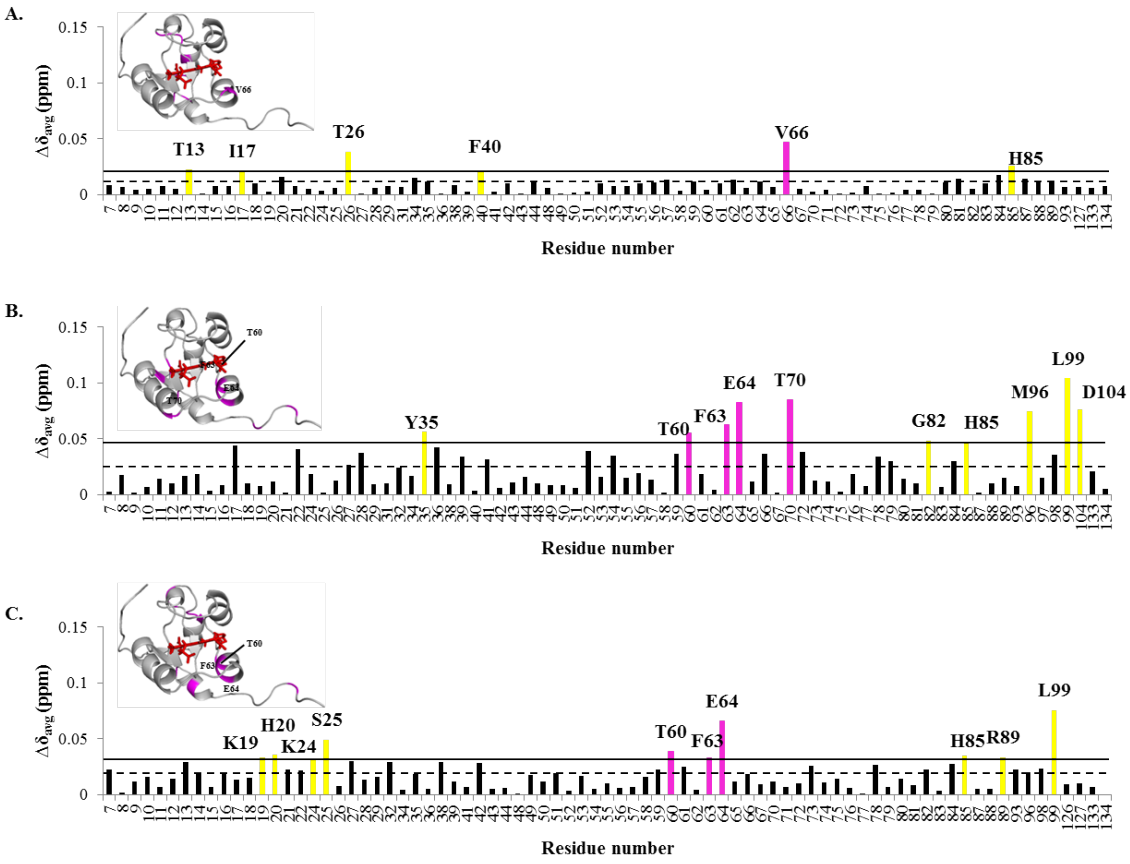

Figure 2.3 Chemical shift perturbation of cyt*b*$_5$ resonances upon complex formation with wt-CYP2B4. CSPs are characterized by the small magnitude and wide dispersion, rendering it impossible for accurate binding interface mapping but provide rough estimations of epitopes involved in *wt*-CYP2B4- cyt*b*$_5$ interactions. Weighted average of chemical shift differences ($\Delta\delta_{avg}$) for backbone amides of cyt*b*$_5$ upon interaction with molar equivalence of *wt*-CYP2B4 in a (A) lipid-free solution, (B) solution containing DLPC/DHPC isotropic bicelles and (C) solution containing DPC micelles are plotted against cyt*b*$_5$ residue number. The dashed line represents the mean chemical shift change among all residues, and the solid line represents the mean chemical shift change plus one standard deviation. Residues with $\Delta\delta_{avg}$ above the solid line are considered to be the most affected among all the cyt*b*$_5$ residues upon the addition of *wt*-CYP2B4. Residues most affected are highlighted in magenta for those located on the front face of cyt*b*$_5$ around the heme edge and yellow for those not in this area, both on the histogram and in the three-dimensional structures of cyt*b*$_5$ above each corresponding histogram. Since no residue in the TM domain of cyt*b*$_5$ is found to be perturbed, only the structure of the soluble domain of cyt*b*$_5$ is shown. The structure of cyt*b*$_5$ has been previously determined by our group [11].

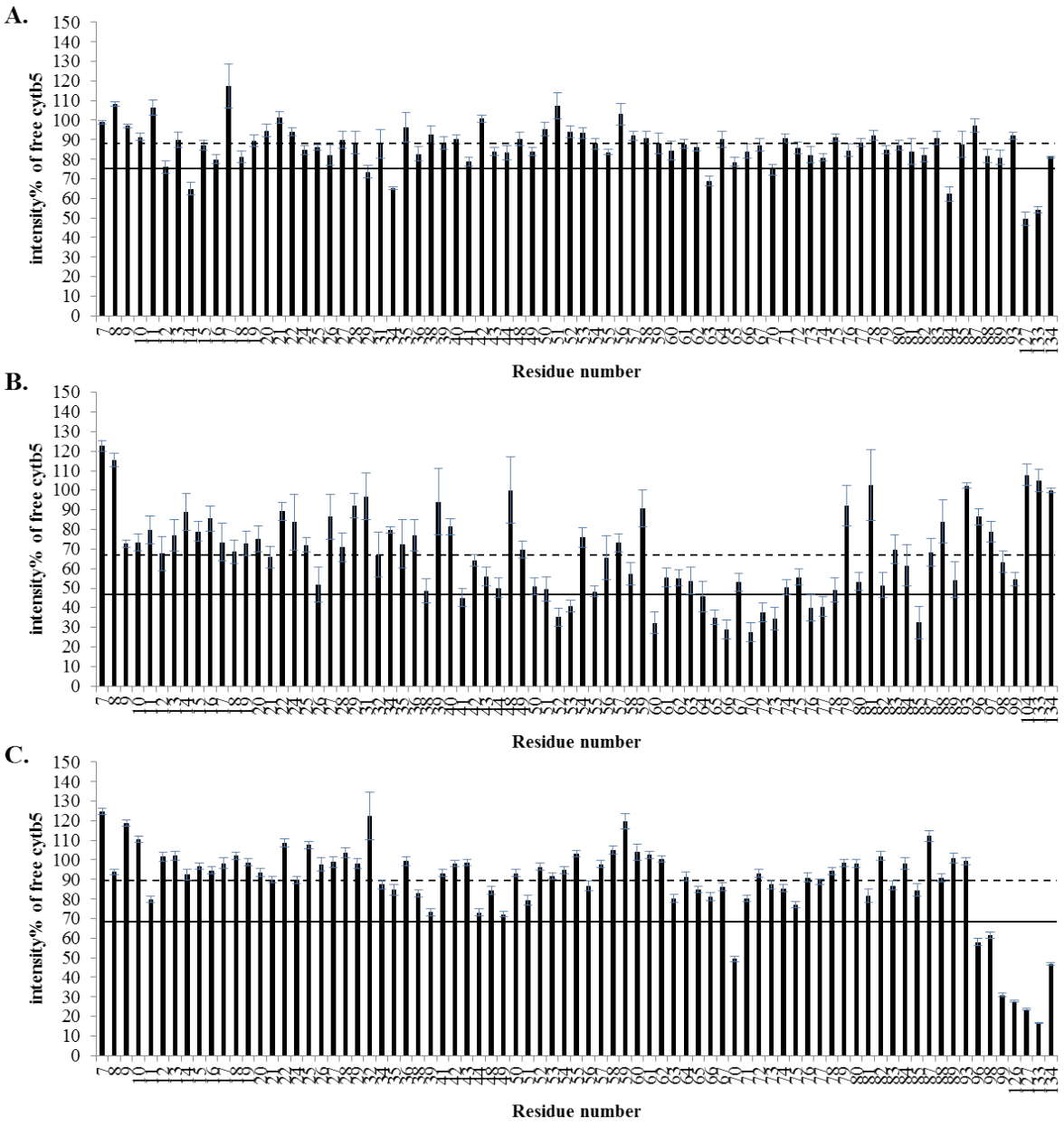

Figure 2.4 Differential line-broadening of cytb_5 resonances upon complex formation with wt-CYP2B4. Relative intensities for backbone amides of cytb_5 at 1:1 molar ratio with *wt*-CYP2B4 shown as a percentage of free cytb_5 resonance intensities, demonstrate differential line-broadening for cytb_5 upon interaction with *wt*-CYP2B4 in (A) a lipid-free solution, (B) a solution containing DLPC/DHPC isotropic bicelles and (C) a solution containing DPC micelles. The dashed line represents the average relative intensity, and the solid line represents the mean value minus one standard deviation. Error bars are calculated based on signal-to-noise ratio extracted from Sparky [48]. Residues of which the relative intensities are below the solid line are mapped onto the three-dimensional structure of cytb_5 and colored blue in Figure 2.3. The structure of cytb_5 in solution has been previously determined by our group [11].

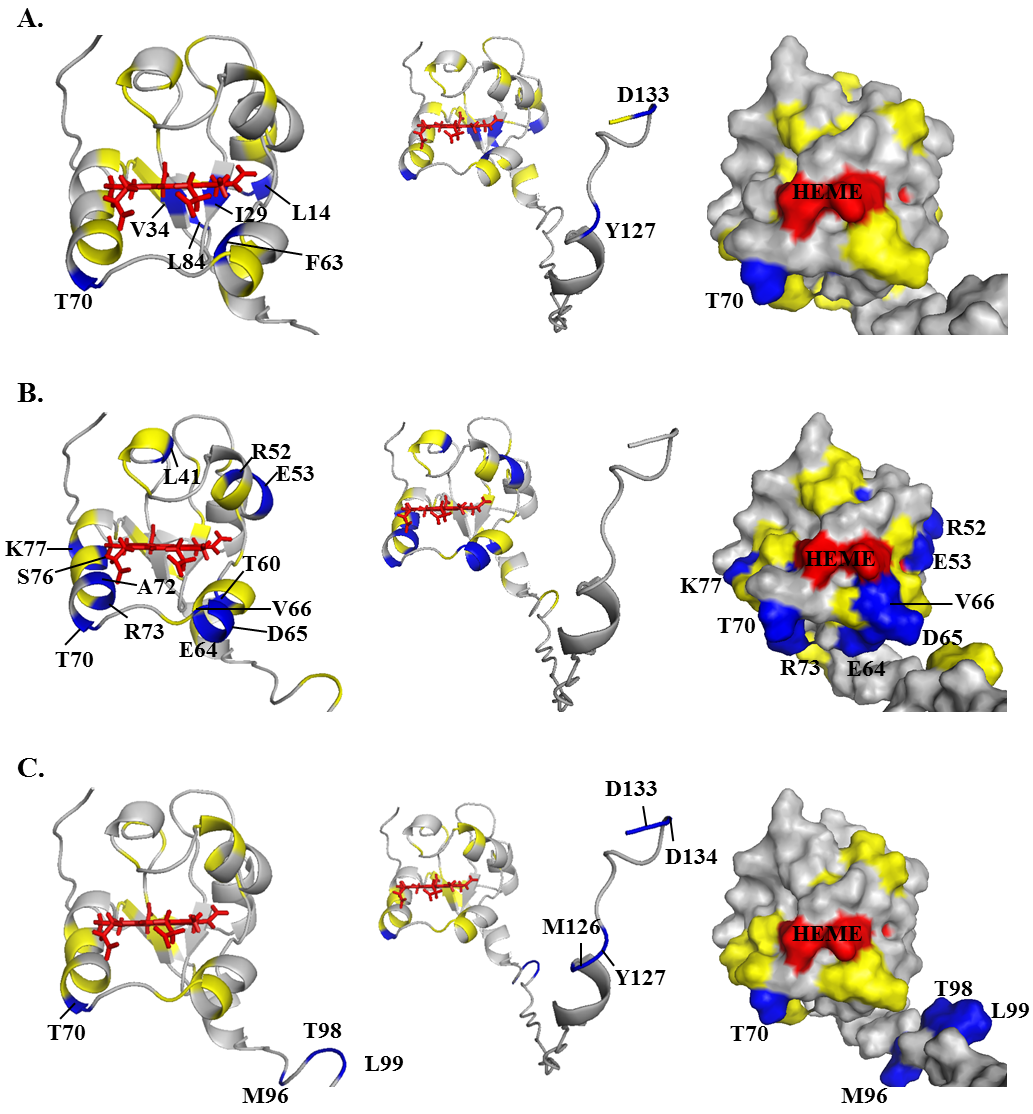

Figure 2.5 Mapping of differential line-broadening of cytb_5 residues upon interaction with wt-CYP2B4. Differential line-broadening of cytb_5 residues are mapped onto cytb_5 structure upon interaction with *wt*-CYP2B4 at the molar ratio of 1:1 in (A) a lipid-free solution, (B) a solution containing DLPC/DHPC isotropic bicelles and (C) a solution containing DPC micelles. Residues are categorized and color-coded according to their relative intensities: blue for significantly perturbed residues upon interaction with *wt*-CYP2B4 with the relative intensities more than one standard deviation below the average, yellow for moderately perturbed residues with the relative intensities in the range from average value to one standard deviation below the average, and grey for residues with negligible to no perturbation of which the relative intensities are above the average value. Heme is colored in red. Significantly perturbed residues are also labeled by amino acid name and the sequence number. Ribbon representations of the soluble domain of cytb_5 are presented in the *left panel*. The active site of cytb_5 (front face around the heme edge) is presented in surface representations in the *right panel.* The full-length structure of cytb_5 is shown by ribbon representations in the *middle panel* to demonstrate the perturbations in the TM domain if present.

Histograms showing the weighted chemical shift perturbations ($\Delta\delta_{avg}$) observed for the amide resonances of cytb_5 upon interaction with *wt*-CYP2B4 at 1:1 molar ratio in different membrane mimetic environments are presented in Figure 2.3. Residues of cytb_5 with $\Delta\delta_{avg}$ larger than the average value plus one standard deviation are considered to be most perturbed among all residues and are therefore most likely to be involved in the interaction with CYP2B4.

Spectra obtained in lipid-free solution reveal only six most perturbed residues, and they are spread over an extensive area of cytb_5 (Fig. 2.3A). Whereas the spectra acquired in bicelles indicate 10 most perturbed residues, which are mostly localized on the front face of cytb_5 around the heme edge and in the linker region (Fig. 2.3B). These areas largely overlap with our previously published CSP mapping [11]: around Y35 and region D88 – D104. The perturbations in the active site of cytb_5 (T60 – T70) are more pronounced in the current work than in our previous work. The discrepancies could be attributable to the fact that bicelles used in our previous work were DMPC/DHPC bicelles, while the bicelles used in the current work is DLPC/DHPC bicelles. The different membrane compositions (varying the hydrophobic thickness of the lipid bilayer) might induce different membrane topologies of CYP2B4 in terms of its depth of insertion into the lipid membrane and its soluble domain orientation on the membrane surface, which could lead to different binding epitopes on cytb_5 while the major areas still roughly overlap. Results obtained from DPC micelles also indicate 10 most perturbed residues located on the front face of cytb_5 around the heme edge, the flexible loop region on the back of cytb_5 and the linker region (Fig. 2.3C). Among all three different sample conditions, bicelles exhibited the largest average CSP value, implying the ability of bicelles in facilitating stronger interactions between *wt*-CYP2B4 and cytb_5.

In addition to the modest chemical shift perturbations, interaction between cytb_5 and *wt*-CYP2B4 also causes a global decrease in signal intensities. In Figure 2.2, the relative resonance peak heights measured from the 1:1 cytb_5-*wt*-CYP2B4 complex, represented as a percentage of the corresponding resonance peak heights in free cytb_5 are plotted as a function of cytb_5 residue number for lipid-free solution (Fig. 2.4A), bicelles (Fig. 2.4B) and micelles (Fig. 2.4C). A significant loss in signal intensity is defined as more than one standard deviation below the average relative peak height of cytb_5 upon complex formation with *wt*-CYP2B4 at 1:1 molar ratio. For spectra obtained from lipid-free solution, only a slight reduction in signal intensities is observed, with an average relative cytb_5 peak height of 87% at 1:1 molar ratio with *wt*-CYP2B4. Residues

considered significantly affected upon interaction with *wt*-CYP2B4 are spread over an extensive area on the soluble domain of cytb_5 (Fig. 2.5A *left* and *right panel*), therefore no specific region could be highlighted as the interaction interface between cytb_5 and *wt*-CYP2B4. Additionally, residues in the C-terminus of the TM domain of cytb_5 are also significantly affected upon the addition of *wt*-CYP2B4 (Fig. 2.5A, *middle panel*), which is probably due to non-native interactions between cytb_5 TM domain and the hydrophobic patches on *wt*-CYP2B4 due to the absence of a membrane environment. On the other hand, in bicelles, the average relative cytb_5 peak height drops to as low as 67%, and a closer inspection of Figure 2.4B reveals differential line broadening of cytb_5 resonances upon interaction with *wt*-CYP2B4. The majority of the significantly affected residues lie on the front face of cytb_5 around the solvent-exposed edge of the heme: among which L41, R52, and E53 lying on the upper cleft and T60, E64, D65, V66, T70, A72, R73, S76 and K77 lying on the lower cleft of cytb_5 exhibit the most significant line broadening upon interaction with *wt*-CYP2B4 (Fig. 2.5B *left* and *right panels*). This is consistent with our previous study of cytb_5-*wt*-CYP2B4 complex formation in DMPC/DHPC isotropic bicelle solution [11]. However, the binding interface mapped out in the current study differs from a previous study [37] on the interaction between a truncated cytb_5 and truncated CYP17A1 in a lipid-free environment, in which residues E47-V50 were shown to form the major complex interface. This could be attributed to the following reasons: first, the membrane environment regulates the interactions between cytb_5 and P450, resulting in a different binding interface; second, rabbit full-length cytb_5-CYP2B4 complex could intrinsically possess a different binding interface than the human truncated cytb_5-CYP17A1 complex. As we have shown in this study, the presence of membrane enhances the binding affinity between the two proteins. In addition, the absence of membrane does not render a specific binding interface between the proteins. Therefore, it is more likely that the presence of membrane is the dominant factor contributing to the discrepancy between our results and the published study. Residue L99 in the linker domain is also observed to be affected, which can be attributed to the restriction of motions in the linker upon complex formation [56]. No significant perturbation is observed in the C-terminal TM domain (Fig. 2.5B, *middle panel*) in contrast to the observation in lipid-free solution. This could be attributable to the primary interaction between cytb_5 TM domain and the bicelles, which aids in proper anchoring of the protein and diminishes non-native interactions. In DPC micelles, the average relative cytb_5 peak height is 89%, similar to that observed in lipid-free solution and is significantly higher than that observed in bicelles.

Differential line broadening is also observed in micelles, where the subset of residues showing significant intensity loss are not localized around the functionally active heme edge but centered at the end of C-terminal TM domain and the flexible linker region (Fig. 2.5C, *left* and *right panels*). CO assay of CYP2B4 suggests marked inactivation of the protein upon addition of DPC. (Fig. 2.6) Moreover, CD titration experiments reveal partial unfolding of CYP2B4 helices induced by the presence of DPC. (Fig. 2.7) It is likely that the disruption in both the secondary structure and the conformation of the CYP2B4 active site accounts for why cytb_5 and *wt*-CYP2B4 cannot properly interact with each other in the presence of DPC micelles.

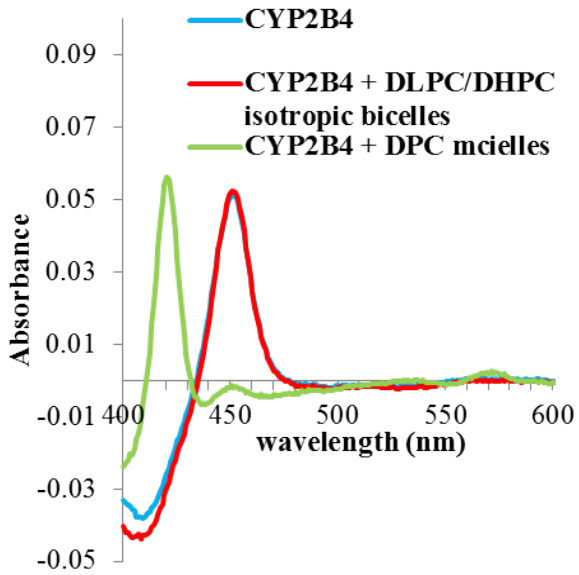

Figure 2.6 Carbon Monoxide assay of wt-CYP2B4 in different membrane environments. CO assays were performed on 1 µM CYP2B4 at 25 ℃ in 100 mM potassium phosphate buffer with 5 % (w/v) glycerol, pH 7.4, containing no lipid (blue curve) as control, 10 % (w/v) DLPC/DHPC isotropic bicelles (red curve) and 2 mM DPC micelles (green curve). An absorption maximum at 450 nm is observed in DLPC/DHPC isotropic bicelle solution, indicative of CYP2B4 in a functionally active P450 form. In DPC micelle solution, CYP2B4 turns into an inactive cytochrome P420 form as shown by a peak at 420 nm in the green curve.

In order to investigate the role of membrane in the interaction between cytb_5 and the *tr-CYP2B4*, a series of $^{15}N/^{1}H$ TROSY HSQC NMR spectra were recorded to monitor ^{15}N-labeled-cytb_5-unlabeled-*tr*-CYP2B4 interaction in lipid-free solution and DLPC/DHPC isotropic bicelles. The addition of *tr*-CYP2B4 to a solution of cytb_5 leads to a general increase in line-width and moderate chemical shift perturbation ($\Delta\delta_{avg} \leq 0.1$ ppm) for amide resonances of cytb_5 in aqueous

solution and bicelles. For bicelles, the average chemical shift change is 0.019 ppm, and in lipid-free solution the value is even smaller (0.012 ppm).

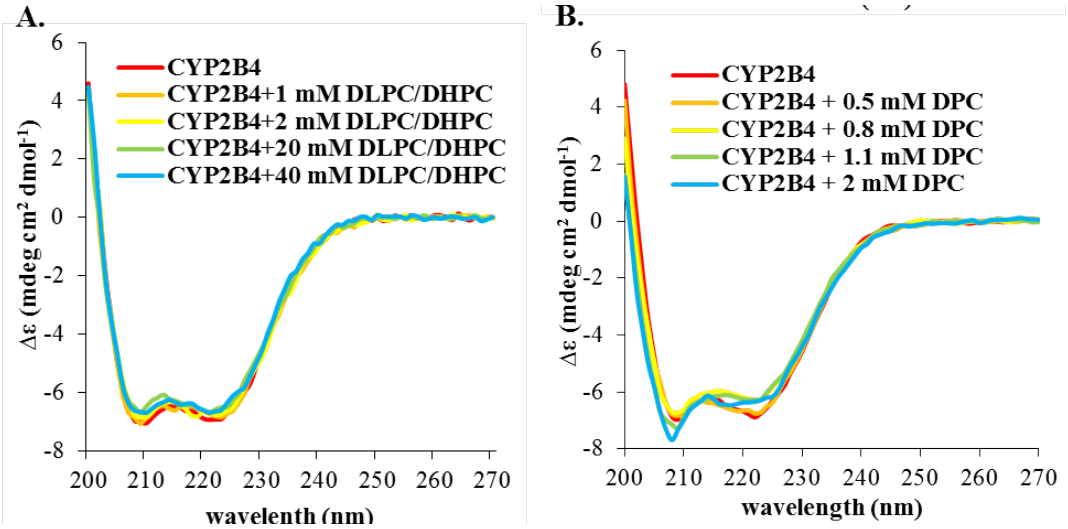

Figure 2.7 Circular Dichroism titration experiments of wt-CYP2B4. CD titrations of (A) DLPC/DHPC isotropic bicelles and (B) DPC micelles into 1 μM CYP2B4 were performed at 25 ℃ in 100 mM potassium phosphate buffer with 5 % (w/v) glycerol, pH 7.4. Loss in α-helix content is observed in DPC titration (from 49.1 ± 2.1% at the beginning of the titration to 40.1 ± 2.2% at the end of the titration). While in DLPC/DHPC titration, CYP2B4 secondary structure stays roughly unperturbed throughout the experiment (with α-helix content changing from 48.5 ± 2.0% to 46.5 ± 2.2%).

2.4.3 Interaction between cytb_5 and tr-CYP2B4

Perturbations of chemical shifts at a 1:1 molar ratio of the two proteins are depicted in the histograms presented in Figure 2.8. Residues of cytb_5 most affected upon interaction with *tr*-CYP2B4 are observed across all regions of cytb_5 under both sample conditions. However, among the most affected residues, three residues are found to be located on the front face of cytb_5 surrounding the heme edge in bicelles (Fig. 2.8B), while only one is found in this area in lipid free solution (Fig. 2.8A), though the affected areas observed in bicelles are not as specific as those observed for the cytb_5 –*wt*-CYP2B4 complex under the same condition.

Line-broadening of cytb_5 resonances caused by interaction with *tr*-CYP2B4 is presented in Figure 2.9, in which the relative cytb_5 resonance peak heights are plotted against cytb_5 residue number at 1:1 molar ratio with *tr*-CYP2B4. Residues with relative peak heights of more than one standard deviation below the average value are considered to be significantly affected upon interaction with *tr*-CYP2B4. Similar to cytb_5-*wt*-CYP2B4 interaction in lipid-free solution, no

significant line broadening is observed for cytb_5 upon addition of *tr*-CYP2B4 under the same condition.

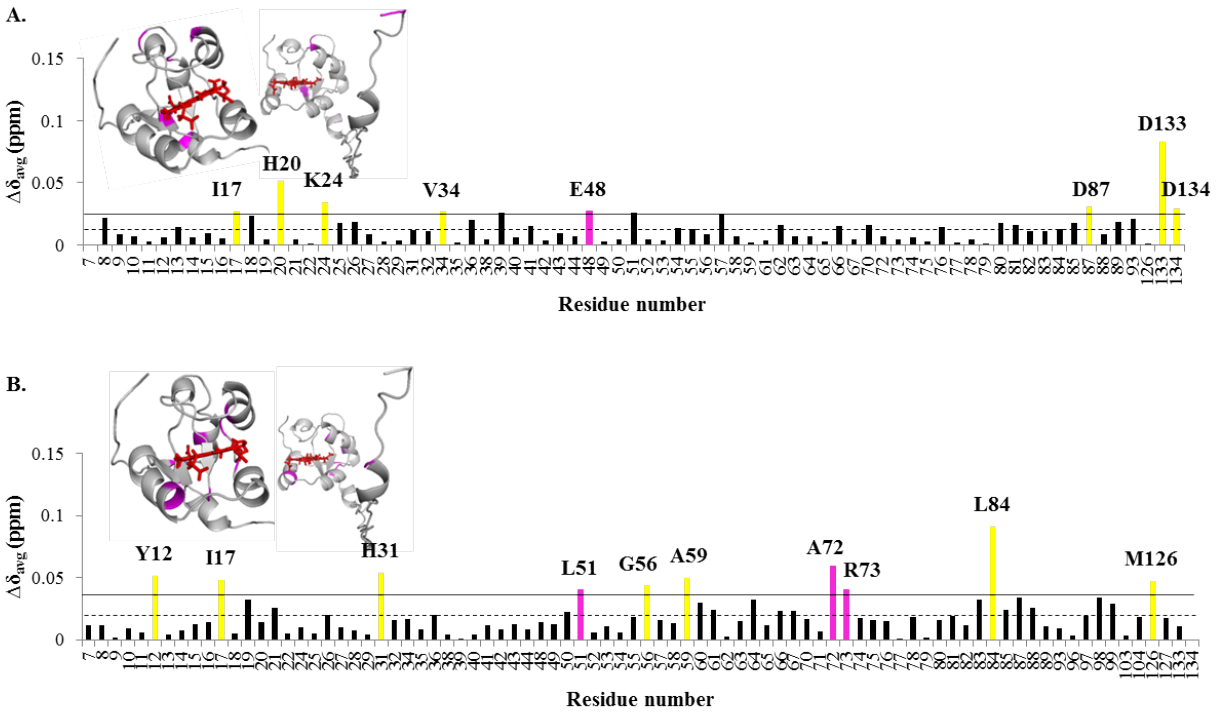

Figure 2.8 Chemical shift perturbation of cytb_5 resonances upon complex formation with tr-CYP2B4. As with *wt*-CYP2B4-cytb_5 interactions, CSPs from *tr*-CYP2B4-cytb_5 are also characterized by the small magnitude and wide dispersion, rendering it impossible for accurate binding interface mapping but provide rough estimations of epitopes involved in *tr*-CYP2B4-cytb_5 interactions. Weighted average of chemical shift differences ($\Delta\delta_{avg}$) for backbone amides of cytb_5 upon interaction with *tr*-CYP 2B4 at 1:1 molar ratio in a (A) lipid-free solution and (B) solution containing DLPC/DHPC isotropic bicelles are plotted against cytb_5 residue number. The dashed line represents the mean chemical shift change among all residues, and the solid line represents the mean chemical shift change plus one standard deviation. Residues with $\Delta\delta_{avg}$ above the solid line are considered to be the most affected among all the cytb_5 residues upon addition of *tr*-CYP2B4. Residues most affected are highlighted in magenta for those located on the front face of cytb_5 around the heme edge and yellow for those not in this area, both on the histogram and in the three dimensional structures of cytb_5 above each corresponding histogram. The structure of the soluble domain of cytb_5 is shown on the left and that of the full-length cytb_5 is shown on the right.

The average relative peak height of cytb_5 at 1:1 molar ratio of the two proteins is 86%. Small perturbations could be found around the heme edge of cytb_5, and the residues significantly affected are located on the back of cytb_5 and in the C-terminus of the TM domain (Fig. 2.10A). This is consistent with the case of cytb_5-*wt*-CYP2B4 complex in a lipid-free environment, which is likely due to non-native interactions between the cytb_5 TM domain and the hydrophobic patches

on *tr*-CYP2B4, likely the F-G loop region. In contrast to the results from lipid-free solution, cytb_5 resonances exhibit extensive reduction in signal intensity when interacting with *tr*-CYP2B4 in bicelles, with an average relative peak height of only 55%. This result reveals that even in the absence of the TM domain, CYP2B4 still interacts with cytb_5 in a membrane mimetic environment created by the bicelles, in a similar manner to cytb_5-*wt*-CYP2B4 interaction. The majority of the residues involved in the interaction between cytb_5 and *tr*-CYP2B4 are localized around the solvent exposed heme edge (Fig. 2.10B), overlapping with cytb_5-*wt*-CYP2B4 interface under the same condition. The area highlighted by the most significantly affected residues—including N62, F63, E64, D65, V66, G67, T70, A72 and S73—are located mostly on α4 helix, the loop between α4 and α5 helix, and the beginning of α5 helix (Fig. 2.10B, *left* and *right panels*), which is slightly different from what is observed for the cytb_5-*wt*-CYP2B4 complex (Fig. 2.5B).

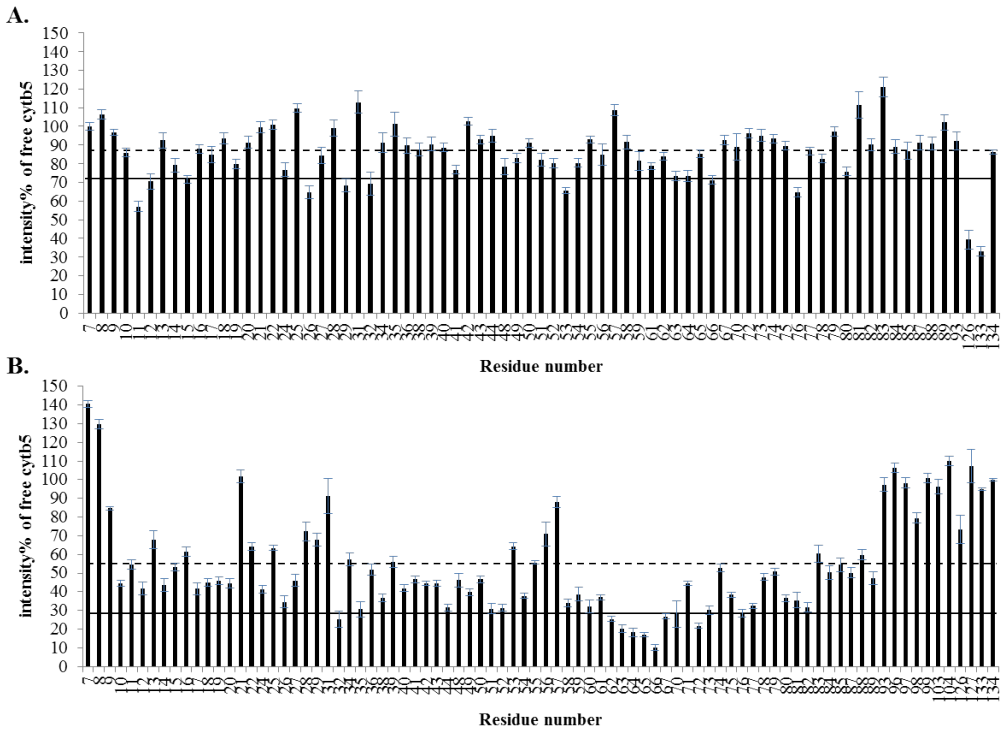

Figure 2.9 Differential line-broadening of cytb_5 resonances upon complex formation with wt-CYP2B4. Relative intensities of backbone amides of cytb_5 at 1:1 molar ratio with *tr*-CYP2B4 shown as a percentage of free cytb_5 resonance intensities, demonstrate differential line broadening for cytb_5 upon interaction with *tr*-CYP2B4 in (A) a lipid-free solution and (B) a solution containing DLPC/DHPC isotropic bicelles. The dashed line represents the average resonance intensity, and the solid line represents the mean value minus one standard deviation. Error bars are calculated based on signal-to-noise ratio extracted from Sparky [48]. Residues of which the relative intensities are below the solid line are mapped onto the three-dimensional structure of cytb_5 and colored blue in Figure 7.

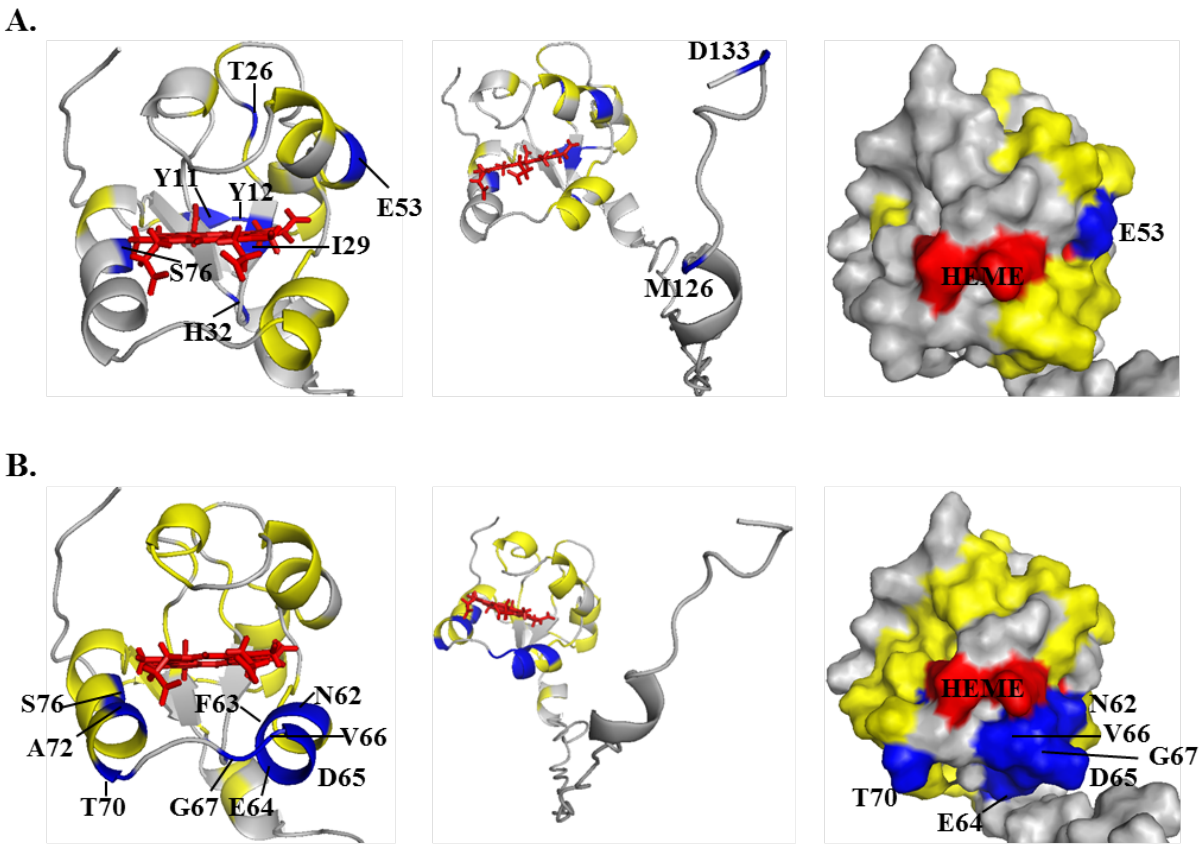

Figure 2.10 Mapping of differential line-broadening of cytb_5 residues upon interaction with tr-CYP2B4. Differential line-broadening of cytb_5 residues are mapped onto cytb_5 structure upon interaction with *tr*-CYP2B4 at the molar ratio of 1:1 in (A) a lipid-free solution and (B) a solution containing DLPC/DHPC isotropic bicelles. Residues are color-coded according to the same category in Figure 2. Heme is colored in red. Significantly perturbed residues are also labeled by amino acid name and the sequence number. Ribbon representations of the soluble domain of cytb_5 are presented in the *left panel*. The active site of cytb_5 (front face around the heme edge) is presented in surface representations in the *right panel.* The full-length structure of cytb_5 is shown by ribbon representations in the *middle panel* to demonstrate the perturbations in the TM domain if present.

2.5 Discussion

2.5.1 Effect of DLPC/DHPC isotropic bicelles on CYP2B4-cytb$_5$ interaction

The importance of phospholipids in cytochrome P450 reconstituted system has been known since the first successful reconstitution of cytochrome P450 dependent activities [13–16,57,58]. It has been reported that the addition of phospholipids into cytochrome P450 reconstituted system has a remarkable stimulating effect as shown by an increase in P450 catalytic activity [16,26,30,59,60].

Although evidence has shown that the interaction between cytochrome P450 and its reductase is affected by the presence of phospholipids [27–30,61], especially phosphatidylcholine-containing lipids, the mechanism of how membrane affects P450-cytb_5 interactions at the atomic level still remains unknown.

In order to provide insights into the role that membrane plays in the interaction between P450 and cytb_5, we have investigated the interaction between *wt*-CYP2B4 and full-length rabbit cytb_5 in the presence and absence of DLPC/DHPC isotropic bicelles by NMR. A titration of unlabeled *wt*-CYP2B4 into ^{15}N-labeled cytb_5 in DLPC/DHPC isotropic bicelles results in extensive line-broadening and modest chemical shift perturbation, which is characteristic of binding on an intermediate exchange time scale (ns - μs). A subset of residues exhibiting the most significant reductions in signal intensity is found to be localized around the catalytically active heme edge on the front face of cytb_5, suggesting a predominant site for interaction with *wt*-CYP2B4. Chemical shift perturbations, though small in magnitude, also show the largest changes at the same site, with an additional site in the flexible linker region probably due to conformational change upon interaction with *wt*-CYP2B4. In contrast, when *wt*-CYP2B4 is added to cytb_5 in a lipid-free solution, no significant line-broadening or CSPs are observed for cytb_5 resonances, suggesting very weak interactions between the two proteins in the absence of a membrane environment. The average CSP is only 0.009 ppm, much smaller than that observed in bicelles (0.023 ppm). The average relative cytb_5 resonance peak height, when mixed with a molar equivalent of *wt*-CYP2B4, is 87% of the corresponding free cytb_5 resonances, which is significantly higher than the 67% observed in DLPC/DHPC isotropic bicelles. Furthermore, in lipid-free solution, the potential residues involved in the interactions are quite dispersed with almost no area specified for a predominant binding site judged by differential line-broadening, while the interaction gives a specific binding interface in bicelles as mentioned above. The largest signal intensity reductions in lipid-free solution are found for residues at the C-terminus of the TM domain (Fig. 2.4A), which is most likely due to non-native interactions when the TM domain is not anchored in the membrane mimetic, implying inefficient interactions between the two proteins, while such interaction is not observed in bicelles. Our results indicate that in the presence of bicelles, the interaction between *wt*-CYP2B4 and cytb_5 is greatly enhanced and the binding site is much more specific, which would allow more efficient electron transfer between the two redox

partners, in comparison with that in lipid-free solution. This might be one of the reasons why P450 catalytic activities are promoted by the presence of phospholipids.

The possible reasons for the capability of isotropic bicelles to enhance cytb_5-CYP2B4 interactions could be: 1) both proteins are anchored into the membrane through their TM domains so that they are in close proximity to each other; 2) the membrane directly interacts with the non-TM part of CYP2B4 – the *tr*-CYP2B4, which assists in orienting the protein for optimal contact with cytb_5. Although a large body of evidence has been reported to support the hypothesis that interactions between the membrane surface and *tr*-P450s (lacking the TM domain) exist [17–22,62–66], it remains vague what role this potential interaction plays in the complex formation between cytb_5 and P450. Therefore, it is of great interest to explore the interactions between cytb_5 and the *tr*-P450 under the influence of a membrane environment.

In the present study, we have investigated the interaction between *tr*-CYP2B4 and cytb_5 in the presence and absence of DLPC/DHPC isotropic bicelle environment by NMR spectroscopy. Similar with *wt*-CYP2B4, titration of *tr*-CYP2B4 into cytb_5 in bicelles leads to extensive line-broadening and modest chemical shift perturbations. Again, this is characteristic of an intermediate exchange process on the NMR time scale. The predominant interaction interface on cytb_5 highlighted by differential line-broadening is on the front face of cytb_5 surrounding the heme edge. The significant decrease in the signal intensities and the specific interaction interface identified are indicative of strong interactions between cytb_5 and *tr*-CYP2B4. The *tr*-CYP2B4-cytb_5 interactions reveal overlapping but non-identical binding interface compared to *wt*-CYP2B4-cytb_5: in both cases the interfaces are located surrounding the heme edge; however, N62, F63 and G67 are only observed on the *tr*-CYP2B4-cytb_5 interface (Fig. 2.10B) while L41, R52, E53, T60, R73 and K77 can only be found on the *wt*-CYP2B4-cytb_5 interface (Fig. 2.5B). The difference between the interfaces most likely results from the presence/absence of the TM domain of CYP2B4. The TM domain of wt-CYP2B4 serves as an anchor of the protein to the membrane which leads to tighter binding between the wt-CYP2B4 and the membrane than the *tr*-CYP2B4 alone and/or aids in better orientation of CYP2B4 for interacting with cytb_5 and transferring electrons [66]. Solid-state NMR study on the TM domain of CYP2B4 revealed a 17^o tilting angle between the TM helix and the membrane normal, suggesting a characteristic orientation of the TM domain of CYP2B4 when anchored to the membrane, which likely restricts the soluble domain into certain orientations on the membrane [67,68]. The absence of the TM domain could therefore lead to different membrane

topologies of the *tr*-CYP2B4 in terms of its depth of insertion into the lipid bilayer and its orientation on the surface of the bicelle, which may result in different surface areas of CYP2B4 being exposed and available for interacting with cytb_5 and hence divergent binding epitopes on cytb_5. The dissimilar interaction interfaces between *wt*-CYP2B4-cytb_5 and *tr*-CYP2B4-cytb_5 are probably the dominating factors contributing to the distinct average relative intensities observed for the two cases (Fig. 2.4B & 9B). In lipid-free solution, only slight decrease in signal intensities could be observed, with widely dispersed perturbations found on cytb_5. This indicates weak interactions between cytb_5 and *tr*-CYP2B4 in lipid-free solution compared to what is observed in bicelles. Our results show that a bicelle environment could enhance not only cytb_5-*wt*-CYP2B4 but also cytb_5-*tr*-CYP2B4 interactions. The possible explanation for this observation could be that parts of the *tr*-CYP2B4, most likely the F-G and B-C loops [23,24], directly interacts with the lipid bilayer of bicelles. This hypothesis is well supported by studies reported in the literature: both *tr*-CYP2B4 and a number of other P450 isoforms lacking the NH_2-terminal membrane anchor region expressed in bacteria [17–20], yeast [21] and mammalian cells [22] have been shown to retain much of their membrane localizations, suggesting that the TM domain is not the sole determinant for membrane binding and that direct interaction exists between the *tr*-P450s and the membrane; both AFM study [64] and Langmuir-Blodgett Monolayer study [69] have suggested that a segment of the *tr*-P450 is buried into the membrane; the observed slow rotation rate for membrane-embedded cytochrome P450s could be well explained by a secondary binding interaction between the *tr*-P450 and the membrane [62,63]; a recent simulation study on CYP3A4 also supports partial insertion of the *tr*-P450 into a membrane mimetic [65]. We propose this potential interaction between *tr*-CYP2B4 and the membrane could lead to some specific orientations of the *tr*-CYP2B4 on the membrane, which facilitates a more efficient interaction with cytb_5 and probably further stimulates electron transfer between the two redox partners, as compared to what would be achieved if the *tr*-P450 simply tumbles isotropically in the solution flexibly coupled to the TM domain through a linker, like that in cytb_5. A model depicting P450-cytb_5 interaction facilitated by lipid bilayers is proposed in Figure 2.11.

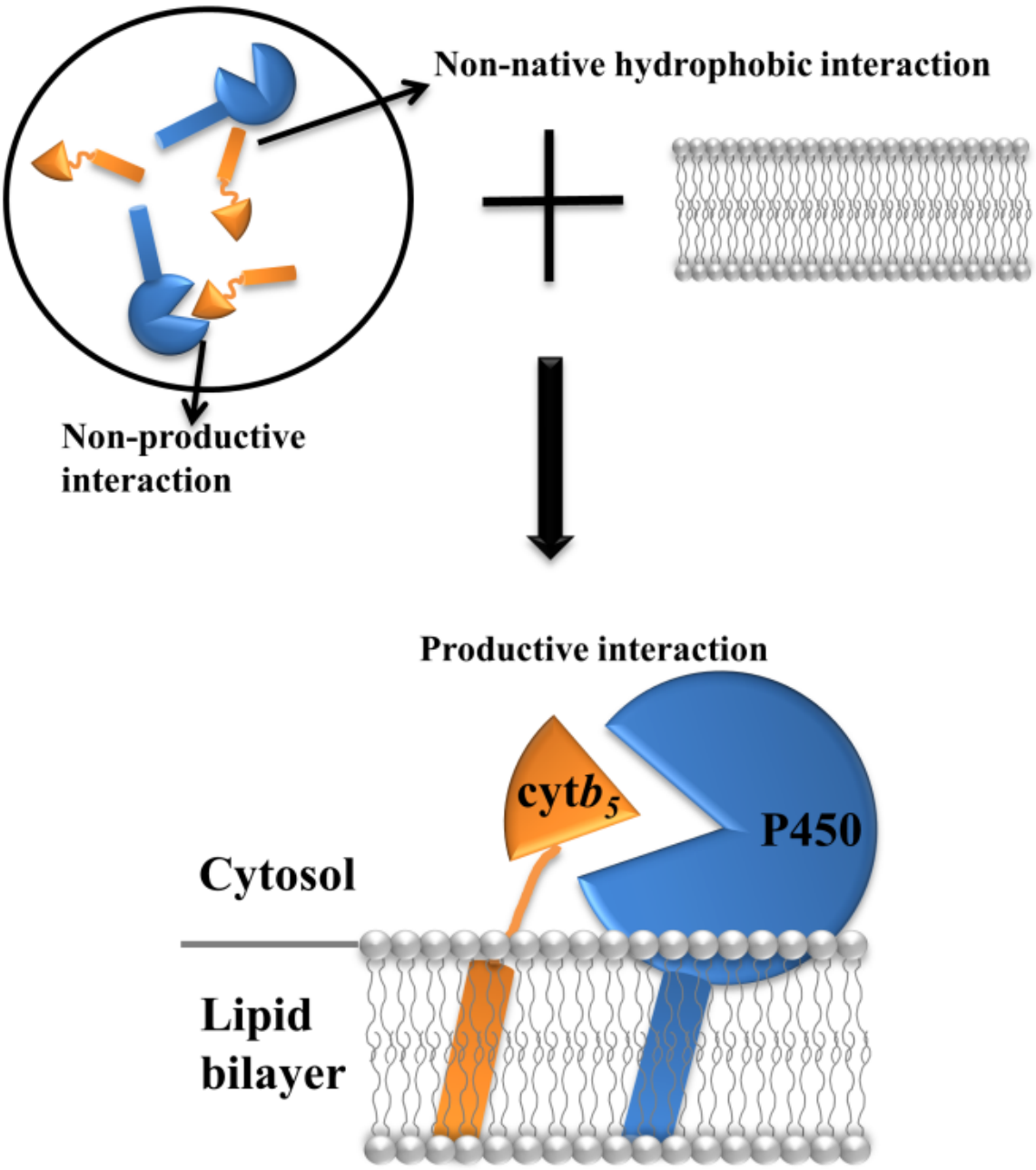

Figure 2.11 A model of the role of lipid bilayer in the interaction between P450 and cytb_5. P450 and cytb_5 are randomly oriented in membrane-free environment (top-left), giving rise to non-native hydrophobic interactions and non-productive interactions. With the assistance of lipid bilayers (top-right and bottom), both proteins are anchored to the membrane, rendering them in close proximity to each other. Additionally, the interaction between the soluble domain of P450 and the lipid bilayer poses the protein in certain orientations that favor the interaction with cytb_5, leading to more productive complex formation between the two redox partners.

2.5.2 Comparison between DLPC/DHPC isotropic bicelles and DPC micelles on their influence on wt-CYP2B4-cytb_5 interaction

Experiments carried out for studying *wt*-CYP2B4-cytb_5 interactions in DPC micelles generally revealed less significant line-broadening of cytb_5 resonances and smaller CSPs as compared to that observed in bicelles, implying much weaker interactions between the two proteins in DPC micelles as compared to bicelles. Interestingly, in DPC micelles, resonances in both the flexible linker region and the C-terminus of the TM domain demonstrate exceptionally large line-broadening effects (relative intensity around 20%) as compared to the rest of cytb_5 residues (average relative intensity 89%). The perturbation observed in the linker region could be due to restriction of motions upon interactions between the soluble domains of the two proteins [11,56]. On the other hand, this observation could also be due to direct interaction with CYP2B4. Judging from the fact that the residues perturbed in this region mostly contain hydrophobic side chains (M96, L99), it is likely that the perturbation in this region, together with the perturbations found at the C-terminus of the TM domain, mostly comes from direct non-native hydrophobic interactions with CYP2B4. An additional region exhibiting chemical shift perturbations is observed in the loop region on the back of cytb_5 soluble domain. Residues involved mostly contain positively charged side chains (K19, H20 and K24), which probably participate in the non-specific, long-range electrostatic interactions with the negatively charged area of the surface of CYP2B4. Overall, unlike the strong and specific *wt*-CYP2B4-cytb_5 interactions observed in bicelles, the interaction observed in DPC micelles is weak and involves more non-specific/artificial interactions, which could lead to the formation of nonproductive complexes. This observation could be attributed to the fact that both the catalytically active site and the secondary structure of CYP2B4 are disturbed upon interaction with DPC micelles (Fig. 2.6, Fig. 2.7), which probably further affects its interaction with cytb_5. Other membrane proteins have also been reported to suffer a loss in activity when embedded in micelles [70,71]. The monolayer lipid packing in micelles and the large curvature at the micelle surface render them unsuitable for mimicking the natural membrane environment, which might be the major reason leading to both structural and functional disruption of CYP2B4 [72,73].

2.6 Conclusion

In summary, a phospholipid bilayer containing membrane mimetic environment regulates strong and specific interactions between *wt-/tr*-CYP2B4 and cytb_5, as revealed by two-dimensional $^{15}N/^{1}H$ TROSY HSQC NMR titration experiments. Proper interactions between *tr*-CYP2B4 and the lipid bilayer likely pose the protein into optimal orientations that favor interactions with cytb_5, which could lead to more efficient productive complex formation between the two proteins. Unlike in bicelles, the interaction between CYP2B4 and cytb_5 is less evident both in complex affinity and interface specificity in DPC micelles. The loss of activity and partial structure unfolding of CYP2B4 upon interaction with DPC micelles might the cause of unfavorable complex formation between CYP2B4 and cytb_5 in this membrane condition.

2.7 References

1. Dürr, U. H. N., Waskell, L. & Ramamoorthy, A. The cytochromes P450 and b5 and their reductases--promising targets for structural studies by advanced solid-state NMR spectroscopy. *Biochim. Biophys. Acta* **1768,** 3235–59 (2007).
2. Danielson, P. B. The cytochrome P450 superfamily: biochemistry, evolution and drug metabolism in humans. *Curr. Drug Metab.* **3,** 561–597 (2002).
3. Guengerich, F. P., Wu, Z.-L. & Bartleson, C. J. Function of human cytochrome P450s: characterization of the orphans. *Biochem. Biophys. Res. Commun.* **338,** 465–9 (2005).
4. Nelson, D. R. Comparison of P450s from human and fugu: 420 million years of vertebrate P450 evolution. *Arch. Biochem. Biophys.* **409,** 18–24 (2003).
5. Nebert, D. W. & Russell, D. W. Clinical importance of the cytochromes P450. *Lancet* **360,** 1155–62 (2002).
6. Ortiz de Montellano, P. R. Hydrocarbon hydroxylation by cytochrome P450 enzymes. *Chem. Rev.* **110,** 932–48 (2010).
7. Zhang, H., Hamdane, D., Im, S.-C. & Waskell, L. Cytochrome b5 inhibits electron transfer from NADPH-cytochrome P450 reductase to ferric cytochrome P450 2B4. *J. Biol. Chem.* **283,** 5217–25 (2008).
8. Guengerich, F. P. Cytochrome P450s and other enzymes in drug metabolism and toxicity. *AAPS J.* **8,** E101–11 (2006).
9. Konopka, K. The Stoichiometry of the Cytochrome P-450-catalyzed Metabolism of

Methoxyflurane and Benzphetamine in the Presence and Absence of Cytochrome b(5). *J. Biol. Chem.* **270,** 24707–24718 (1995).

10. Guengerich, F. P. Cytochromes P450, drugs, and diseases. *Mol. Interv.* **3,** 194–204 (2003).
11. Ahuja, S. *et al.* A model of the membrane-bound cytochrome b5-cytochrome P450 complex from NMR and mutagenesis data. *J. Biol. Chem.* **288,** 22080–95 (2013).
12. Coleman, R. Membrane-bound enzymes and membrane ultrastructure. *Biochim. Biophys. Acta - Rev. Biomembr.* **300,** 1–30 (1973).
13. Lu, A. Y. H., Strobel, H. W. & Coon, M. J. Hydroxylation of benzphetamine and other drugs by a solubilized form of cytochrome P-450 from liver microsomes: Lipid requirement for drug demethylation. *Biochem. Biophys. Res. Commun.* **36,** 545–551 (1969).
14. Lu, A. Y. H., Junk, K. W. & Coon, M. J. Resolution of the Cytochrome P-450-containing ohgr-Hydroxylation System of Liver Microsomes into Three Components. *J. Biol. Chem.* **244,** 3714–3721 (1969).
15. Lu, A. Y. H., Strobel, H. W. & Coon, M. J. Properties of a Solubilized Form of the Cytochrome P-450-Containing Mixed-Function Oxidase of Liver Microsomes. *Mol. Pharmacol.* **6,** 213–220 (1970).
16. Strobel, H. W., Lu, A. Y. H., Heidema, J. & Coon, M. J. Phosphatidylcholine Requirement in the Enzymatic Reduction of Hemoprotein P-450 and in Fatty Acid, Hydrocarbon, and Drug Hydroxylation. *J. Biol. Chem.* **245,** 4851–4854 (1970).
17. Pernecky, S. J., Larson, J. R., Philpot, R. M. & Coon, M. J. Expression of truncated forms of liver microsomal P450 cytochromes 2B4 and 2E1 in Escherichia coli: influence of NH2-terminal region on localization in cytosol and membranes. *Proc. Natl. Acad. Sci. U. S. A.* **90,** 2651–5 (1993).
18. Gillam, E. M., Baba, T., Kim, B. R., Ohmori, S. & Guengerich, F. P. Expression of modified human cytochrome P450 3A4 in Escherichia coli and purification and reconstitution of the enzyme. *Arch. Biochem. Biophys.* **305,** 123–31 (1993).
19. Sagara, Y., Barnes, H. J. & Waterman, M. R. Expression in Escherichia coli of functional cytochrome P450c17 lacking its hydrophobic amino-terminal signal anchor. *Arch. Biochem. Biophys.* **304,** 272–8 (1993).
20. Larson, J., Coon, M. & Porter, T. Alcohol-inducible cytochrome P-450IIE1 lacking the hydrophobic NH2- terminal segment retains catalytic activity and is membrane-bound when

expressed in Escherichia coli. *J. Biol. Chem.* **266,** 7321–7324 (1991).

21. Cullin, C. Two distinct sequences control the targeting and anchoring of the mouse P450 1A1 into the yeast endoplasmic reticulum membrane. *Biochem. Biophys. Res. Commun.* **184,** 1490–1495 (1992).
22. Clark, B. & Waterman, M. The hydrophobic amino-terminal sequence of bovine 17 alpha-hydroxylase is required for the expression of a functional hemoprotein in COS 1 cells. *J. Biol. Chem.* **266,** 5898–5904 (1991).
23. Williams, P. A., Cosme, J., Sridhar, V., Johnson, E. F. & McRee, D. E. Mammalian Microsomal Cytochrome P450 Monooxygenase. *Mol. Cell* **5,** 121–131 (2000).
24. Zhao, Y. *et al.* Structure of microsomal cytochrome P450 2B4 complexed with the antifungal drug bifonazole: insight into P450 conformational plasticity and membrane interaction. *J. Biol. Chem.* **281,** 5973–81 (2006).
25. Baylon, J. L., Lenov, I. L., Sligar, S. G. & Tajkhorshid, E. Characterizing the membrane-bound state of cytochrome P450 3A4: structure, depth of insertion, and orientation. *J. Am. Chem. Soc.* **135,** 8542–51 (2013).
26. van der Hoeven, T. A. & Coon, M. J. Preparation and Properties of Partially Purified Cytochrome P-450 and Reduced Nicotinamide Adenine Dinucleotide Phosphate-Cytochrome P-450 Reductase from Rabbit Liver Microsomes. *J. Biol. Chem.* **249,** 6302–6310 (1974).
27. Muller-Enoch, D., Churchill, P., Fleischer, S. & Guengerich, F. Interaction of liver microsomal cytochrome P-450 and NADPH-cytochrome P- 450 reductase in the presence and absence of lipid. *J. Biol. Chem.* **259,** 8174–8182 (1984).
28. Miwa, G. T. & Lu, A. Y. H. Studies on the stimulation of cytochrome P-450-dependent monooxygenase activity by dilauroylphosphatidylcholine. *Arch. Biochem. Biophys.* **211,** 454–458 (1981).
29. Coon, M. J., Haugen, D. A., Guengerich, F. P., Vermilion, J. L. & Dean, W. L. in *The Structural Basis of Membrane Function* 409–427 (1976). doi:10.1016/B978-0-12-332450-4.50035-4
30. Imaoka, S., Imai, Y., Shimada, T. & Funae, Y. Role of phospholipids in reconstituted cytochrome P450 3A form and mechanism of their activation of catalytic activity. *Biochemistry* **31,** 6063–6069 (1992).

31. Kominami, S., Noriyuki, O., Reiko, M., Huang, D.-Y. & Shigeki, T. The role of cytochrome b5 in adrenal microsomal steroidogenesis. *J. Steroid Biochem. Mol. Biol.* **42,** 57–64 (1992).
32. Finn, R. D. *et al.* Defining the in Vivo Role for cytochrome b5 in cytochrome P450 function through the conditional hepatic deletion of microsomal cytochrome b5. *J. Biol. Chem.* **283,** 31385–93 (2008).
33. Morgan, E. & Coon, M. Effects of cytochrome b5 on cytochrome P-450-catalyzed reactions. Studies with manganese-substituted cytochrome b5. *Drug Metab. Dispos.* **12,** 358–364 (1984).
34. Canova-Davis, E., Chiang, J. Y. L. & Waskell, L. Obligatory role of cytochrome b5 in the microsomal metabolism of methoxyflurane. *Biochem. Pharmacol.* **34,** 1907–1912 (1985).
35. Shimada, T., Mernaugh, R. L. & Guengerich, F. P. Interactions of mammalian cytochrome P450, NADPH-cytochrome P450 reductase, and cytochrome b(5) enzymes. *Arch. Biochem. Biophys.* **435,** 207–16 (2005).
36. Im, S.-C. & Waskell, L. The interaction of microsomal cytochrome P450 2B4 with its redox partners, cytochrome P450 reductase and cytochrome b(5). *Arch. Biochem. Biophys.* **507,** 144–53 (2011).
37. Estrada, D. F., Laurence, J. S. & Scott, E. E. Substrate-modulated cytochrome P450 17A1 and cytochrome b5 interactions revealed by NMR. *J. Biol. Chem.* **288,** 17008–18 (2013).
38. Bridges, A. *et al.* Identification of the binding site on cytochrome P450 2B4 for cytochrome b5 and cytochrome P450 reductase. *J Biol Chem* **273,** 17036–17049 (1998).
39. DePierre, J. W. & Ernster, L. Enzyme topology of intracellular membranes. *Annu. Rev. Biochem.* **46,** 201–62 (1977).
40. Depierre, J. W. & Dallner, G. Structural aspects of the membrane of the endoplasmic reticulum. *Biochim. Biophys. Acta - Rev. Biomembr.* **415,** 411–472 (1975).
41. Dürr, U. H. N., Gildenberg, M. & Ramamoorthy, A. The magic of bicelles lights up membrane protein structure. *Chem. Rev.* **112,** 6054–74 (2012).
42. Arora, A. & Tamm, L. K. Biophysical approaches to membrane protein structure determination. *Curr. Opin. Struct. Biol.* **11,** 540–7 (2001).
43. Dürr, U. H. N., Yamamoto, K., Im, S.-C., Waskell, L. & Ramamoorthy, A. Solid-state NMR reveals structural and dynamical properties of a membrane-anchored electron-carrier protein, cytochrome b5. *J. Am. Chem. Soc.* **129,** 6670–1 (2007).

44. Saribas, A. S., Gruenke, L. & Waskell, L. Overexpression and purification of the membrane-bound cytochrome P450 2B4. *Protein Expr Purif* **21,** 303–309 (2001).
45. Scott, E. E., Spatzenegger, M. & Halpert, J. R. A truncation of 2B subfamily cytochromes P450 yields increased expression levels, increased solubility, and decreased aggregation while retaining function. *Arch. Biochem. Biophys.* **395,** 57–68 (2001).
46. van Stokkum, I. H. M., Spoelder, H. J. W., Bloemendal, M., van Grondelle, R. & Groen, F. C. A. Estimation of protein secondary structure and error analysis from circular dichroism spectra. *Anal. Biochem.* **191,** 110–118 (1990).
47. Provencher, S. W. & Gloeckner, J. Estimation of globular protein secondary structure from circular dichroism. *Biochemistry* **20,** 33–37 (1981).
48. Kneller, D. G. & Kuntz, I. D. UCSF Sparky-an NMR display, annotation, and assignment tool. *J. Cell. Biochem.* **53,** 254–254 (1993).
49. Williamson, R. A., Carr, M. D., Frenkiel, T. A., Feeney, J. & Freedman, R. B. Mapping the binding site for matrix metalloproteinase on the N-terminal domain of the tissue inhibitor of metalloproteinases-2 by NMR chemical shift perturbation. *Biochemistry* **36,** 13882–9 (1997).
50. Williamson, M. P. Using chemical shift perturbation to characterise ligand binding. *Prog. Nucl. Magn. Reson. Spectrosc.* **73,** 1–16 (2013).
51. Prudêncio, M. & Ubbink, M. Transient complexes of redox proteins: structural and dynamic details from NMR studies. *J. Mol. Recognit.* **17,** 524–39 (2004).
52. Volkov, A. N., Ferrari, D., Worrall, J. A. R., Bonvin, A. M. J. J. & Ubbink, M. The orientations of cytochrome c in the highly dynamic complex with cytochrome b5 visualized by NMR and docking using HADDOCK. *Protein Sci.* **14,** 799–811 (2005).
53. Tang, C., Iwahara, J. & Clore, G. M. Visualization of transient encounter complexes in protein-protein association. *Nature* **444,** 383–6 (2006).
54. Volkov, A. N., Ubbink, M. & van Nuland, N. A. J. Mapping the encounter state of a transient protein complex by PRE NMR spectroscopy. *J. Biomol. NMR* **48,** 225–36 (2010).
55. Suh, J.-Y., Tang, C. & Clore, G. M. Role of electrostatic interactions in transient encounter complexes in protein-protein association investigated by paramagnetic relaxation enhancement. *J. Am. Chem. Soc.* **129,** 12954–5 (2007).
56. Koberova, M. *et al.* Photo-cytochrome b5 -- A New Tool to Study the Cytochrome P450

Electron-transport Chain. *Int. J. Electrochem. Sci.* **8,** 125–134 (2013).

57. Lu, A. Y. H. & Coon, M. J. Role of Hemoprotein P-450 in Fatty Acid ohgr-Hydroxylation in a Soluble Enzyme System from Liver Microsomes. *J. Biol. Chem.* **243,** 1331–1332 (1968).
58. French, J. S., Guengerich, F. P., Coon, M. J. & Pcm-, G. Interactions of Cytochrome P-450, NADPH-Cytochrome P450 Reductase, Phospholipid, and Substrate in the Reconstituted Liver Microsomal Enzyme System. *J Biochem* **255,** 4112–4119 (1980).
59. Yang, C. S. Interactions between solubilized cytochrome P-450 and hepatic microsomes. *J. Biol. Chem.* **252,** 293–298 (1977).
60. Ingelman-Sundberg, M. & Glaumann, H. Reconstitution of the liver microsomal hydroxylase system into liposomes. *FEBS Lett.* **78,** 72–6 (1977).
61. Blanck, J., Smettan, G., Ristau, O., Ingelman-Sundberg, M. & Ruckpaul, K. Mechanism of rate control of the NADPH-dependent reduction of cytochrome P-450 by lipids in reconstituted phospholipid vesicles. *Eur. J. Biochem.* **144,** 509–513 (1984).
62. Kawato, S., Gut, J., Cherry, R. J., Winterhalter, K. H. & Richter, C. Rotation of cytochrome P-450. I. Investigations of protein-protein interactions of cytochrome P-450 in phospholipid vesicles and liver microsomes. *J. Biol. Chem.* **257,** 7023–7029 (1982).
63. Ohta, Y., Sakaki, T., Yabusaki, Y., Ohkawa, H. & Kawato, S. Rotation and membrane topology of genetically expressed methylcholanthrene-inducible cytochrome P-450IA1 lacking the N-terminal hydrophobic segment in yeast microsomes. *J. Biol. Chem.* **269,** 15597–15600 (1994).
64. Bayburt, T. H. & Sligar, S. G. Single-molecule height measurements on microsomal cytochrome P450 in nanometer-scale phospholipid bilayer disks. *Proc. Natl. Acad. Sci. U. S. A.* **99,** 6725–30 (2002).
65. Baylon, J. L., Lenov, I. L., Sligar, S. G. & Tajkhorshid, E. Characterizing the membrane-bound state of cytochrome P450 3A4: structure, depth of insertion, and orientation. *J. Am. Chem. Soc.* **135,** 8542–51 (2013).
66. Pernecky, S. J., Olken, N. M., Bestervelt, L. L. & Coon, M. J. Subcellular localization, aggregation state, and catalytic activity of microsomal P450 cytochromes modified in the NH2-terminal region and expressed in Escherichia coli. *Arch. Biochem. Biophys.* **318,** 446–56 (1995).

67. Yamamoto, K. *et al.* Dynamic interaction between membrane-bound full-length cytochrome P450 and cytochrome b5 observed by solid-state NMR spectroscopy. *Sci. Rep.* **3,** 2538 (2013).
68. Yamamoto, K. *et al.* Probing the transmembrane structure and topology of microsomal cytochrome-p450 by solid-state NMR on temperature-resistant bicelles. *Sci. Rep.* **3,** 2556 (2013).
69. Shank-Retzlaff, M. L., Raner, G. M., Coon, M. J. & Sligar, S. G. Membrane topology of cytochrome P450 2B4 in Langmuir-Blodgett monolayers. *Arch. Biochem. Biophys.* **359,** 82–8 (1998).
70. Sanders, C. R. & Landis, G. C. Reconstitution of Membrane Proteins into Lipid-Rich Bilayered Mixed Micelles for NMR Studies. *Biochemistry* **34,** 4030–4040 (1995).
71. Garavito, R. M. & Ferguson-Miller, S. Detergents as tools in membrane biochemistry. *J. Biol. Chem.* **276,** 32403–6 (2001).
72. Lee, D. *et al.* Bilayer in small bicelles revealed by lipid-protein interactions using NMR spectroscopy. *J. Am. Chem. Soc.* **130,** 13822–3 (2008).
73. Matthews, E. E., Zoonens, M. & Engelman, D. M. Dynamic helix interactions in transmembrane signaling. *Cell* **127,** 447–50 (2006).

CHAPTER 3

Reconstitution of Cytb_5–CytP450 Complex in Nanodiscs for Structural Studies by NMR[*†]

3.1 Summary

Cytochrome P450s (P450) are a superfamily of enzymes responsible for the catalysis of a wide range of substrates. Dynamic interactions between full-length membrane-bound P450 and its redox partner cytochrome b_5 (cytb_5) have been found to be highly important for the enzymatic activity of P450. However, the stability of the ~70-kDa membrane-bound complex in model membranes poses tremendous challenges for high-resolution structural studies by NMR. To overcome these challenges, we demonstrate the successful reconstitution of P450-cytb_5 complex in peptide-based nanodiscs devoid of detergents, which are characterized by a combination of size exclusion chromatography and NMR. In addition, NMR experiments are used to identify the binding interface of the P450-cytb_5 complex in the nanodisc. This first successful demonstration of protein-protein complex in nanodisc for NMR structural studies paves the way to obtaining valuable structural information on membrane bound protein complexes.

3.2 Introduction

Cytochrome P450s (P450s) are a ubiquitous superfamily of monooxygenases found in all living kingdoms, including plants, animals, bacteria and fungi.[1] They are responsible for the metabolism of a wide variety of endogenous and exogenous substrates, including over 70% of the pharmaceuticals in the current market.[1] In order for P450s to carry out their function, two electrons

[*] This chapter is based on the published paper: Zhang, M., Huang, R., Ackermann, R., Im, S., Waskell, L., Schwendeman, A., and Ramamoorthy, A. (2016) Membrane Proteins Reconstitution of the Cyt b_5 – CytP450 Complex in Nanodiscs for Structural Studies using NMR Spectroscopy. *Angew. Chemie Int. Ed.* **55**, 4497–4499

[†] This thesis research was supported by funds from the National Institutes of Health (NIH to A.R.).

are required to be sequentially delivered to the heme of P450s from their redox partners – cytochrome b_5 (cytb_5) and cytochrome P450 reductase (CPR).[2] Mammalian P450s and redox partners (CPR and cytb_5), consisting of a soluble heme-containing domain and a single α-helical transmembrane (TM) domain, are primarily found on the cytoplasmic side of the endoplasmic reticulum (ER) membrane of hepatic cells.[1] Cytb_5 has been reported to stimulate, inhibit or have no effect on the activities of P450s depending on various factors, including the relative amount of cytb_5 versus CPR, the particular substrate under investigation and other experimental conditions.[3] Even though it is known that only the full-length membrane-bound P450 and cytb_5 form a productive complex, the vast majority of crystallographic studies have focused only on the structures of the soluble domains of P450s. While it is necessary to characterize the dynamic interactions between cytb_5 and P450 at high-resolution in a membrane environment, its size and stability pose tremendous challenges.

Our previous study suggested that bicelles composed of lipids and detergents better facilitate the interactions between P450 and cytb_5, as compared to detergent micelles or a non-membrane environment.[4] Additionally, detergents were found to partially unfold the α-helices of P450 2B4 (CYP2B4), as well as convert P450 into an inactive form (P420).[4] Therefore, the elimination of detergents from the membrane mimetic used for structural and functional studies of P450, and its interactions with cytb_5, becomes necessary in order to provide a more physiological environment for P450.

Nanodiscs, comprised of a planar lipid bilayer and membrane scaffold proteins (MSPs) forming the rim, have been widely recognized as a promising membrane mimetic for studying membrane proteins, including P450s.[56] This discoidal nano-scale membrane model is well-defined in size and demonstrates a high stability for reconstituted membrane proteins whose activities are deteriorated by the detergents present in other membrane mimetics such as micelles.[7] However, the use of nanodiscs to investigate protein-protein interactions is limited by the sample preparation process and difficulties in the reconstitution of protein-protein complexes with both proteins properly oriented with respect to each other. Only several examples of study on membrane protein complexes in nanodiscs have been reported to date.[8–15]

In this study, we demonstrate the first successful incorporation of the CYP2B4-cytb_5 complex into a peptide-based nanodisc comprised of DMPC lipids; a 22 residue peptide is used in place of the large MSPs to form the rim of the nanodiscs. The protocol to prepare peptide-based

nanodiscs is simple and it's easy to control the size of resultant nanodiscs.[16,17] With the use of size exclusion chromatography (SEC) and NMR experiments, we have characterized the effect of lipid bilayer on the aggregation of full-length cytb_5 and the reconstitution of productive CYP2B4-cytb_5 complexes into nanodiscs. We believe that this study paves ways to better understand the structure and function of membrane protein complexes in a more physiologically-relevant lipid membrane environment.

3.3 Materials and Methods

3.3.1 Materials

Phosphate buffer components (potassium phosphate monobasic and dibasic), glycerol and 3,5-di-*tert*-butyl-4-hydroxytoluene (BHT) were purchased from Sigma-Aldrich (St. Louis, MO). 1,2-dihexanoyl-*sn*-glycero-3-phosphocholine (DHPC) and 1,2-dimyristoyl-*sn*-glycero-3-phosphocholine (DMPC) were purchased from Avanti Polar Lipids, Inc. (Alabaster, AL). The 22 residue peptide (PVLDLFRELLNELLEALKQKLK) was purchased from Genescript and American Peptide. Full-length ^{15}N labeled and unlabeled cytb_5, and full-length CYP2B4 were expressed and purified as reported in the literature[3,18–20].

3.3.2 Preparation of empty nanodiscs

DMPC powder was suspended into buffer A (10 mM potassium phosphate, pH 7.4) to make a stock solution at 20 mg/mL. The 22A peptide was dissolved in buffer B (40 mM potassium phosphate, pH 7.4) to make a stock solution at 10 mg/mL. The DMPC stock solution was vortexed thoroughly immediately before use. 50 μL of each stock solution was mixed together and incubated at 50 ºC for 10 min. Then the mixture was allowed to cool down at room temperature for 10 min. This cycle was repeated 3 to 5 times until the mixture became clear, followed by several cycles of freeze and thaw between -80 ºC and room temperature to make the nanodsics more homogeneous. The resulting solution containing nanodiscs were characterized by size exclusion chromatography (SEC). A Superdex 200 Increase 300/10 GL column was operated on an ÄKTA purifier (GE Healthcare, Freiburg, Germany). The flow rate of the SEC buffer (buffer A) was 0.75 mL/min.

3.3.3 Preparation of nanodiscs containing cytb_5 or CYP2B4-cytb_5 complex

To incorporate cytb_5 into nanodiscs, stock solutions of DMPC vesicle suspension at 121.7 mg/mL in buffer A, 22A peptide in buffer B at 60.8 mg/mL and uniformly ^{15}N labeled cytb_5 in buffer A were mixed together at the following volumes respectively: 65.74, 65.74 and 68.52 µL. The resulting mixture was incubated at 37 ºC, 200 rpm overnight until the solution became optically clear. SEC was subsequently operated on a Superdex 200 Increase 300/10 GL column at the flow rate of 0.75 mL/min of buffer A for purification of nanodiscs containing cytb_5 from unincorporated cytb_5 and empty nanodiscs. Fractions at the center of the peak on the elution profile were collected and concentrated to around 0.1 mM using Amicon. 10% D_2O was added to the sample prior to use for NMR experiments.

Method 1 for reconstitution of the CYP2B4-cytb_5 complex into nanodiscs: nanodiscs containing cytb_5 were reconstituted and purified. Unlabeled full-length CYP2B4 in buffer A was subsequently added at a molar ratio of 1:1.2 (cytb_5:CYP2B4). The resulting mixture was incubated at 37 ºC, 200 rpm overnight. Nanodiscs containing CYP2B4-cytb_5 were purified and prepared for NMR experiments the same way as explained above.

Method 2 for reconstitution of the CYP2B4-cytb_5 complex into nanodiscs: in close analogy to the assembling of cytb_5 containing nanodiscs, the aforementioned stock solutions of DMPC vesicles in buffer A, the 22A peptide in buffer B, uniformly ^{15}N labeled cytb_5 and unlabeled full-length CYP2B4 in buffer A were mixed and incubated at 37 ºC, 200 rpm overnight until the solution became optically clear. The molar ratio between CYP2B4 and cytb_5 was 1:1. The sample was purified and prepared for NMR experiments the same way as demonstrated above.

3.3.4 NMR experiments

NMR experiments were performed at 298 K on a Bruker Avance II 600 MHz spectrometer equipped with a cryoprobe. 2D ^{15}N/^{1}H TROSY HSQC spectra were recorded with 0.1 mM ^{15}N-cytb_5 in buffer A, nanodiscs containing ^{15}N-cytb_5, and nanodiscs containing both ^{15}N-cytb_5 and unlabeled CYP2B4 prepared from Method 1 or Method 2. All nanodisc samples were in buffer A and contained ^{15}N-cytb_5 at a concentration around 0.1 mM. BHT was subsequently added to nanodiscs containing both ^{15}N-cytb_5 and unlabeled CYP2B4 at a BHT:CYP2B4 molar ratio of 4:1, and 2D ^{15}N/^{1}H TROSY HSQC spectra were collected

All NMR spectra were recorded with 64 scans and 256 t1 increments. Data was processed using TopSpin 2.0 (Bruker) and analyzed with Sparky [21]. The cytb_5 backbone chemical shift assignments have been previously reported [3]. The weighted amide chemical shift perturbation ($\Delta\delta_{avg}$) was calculated using the equation below:

$$\Delta\delta_{avg} = \sqrt{(\Delta\delta N \times \frac{F_2\ SW}{F_1\ SW})^2 + \Delta\delta H^2}$$

where $\Delta\delta N$ and $\Delta\delta H$ are the changes in the chemical shifts of amide nitrogen and hydrogen respectively, while $F_1\ SW$ and $F_2\ SW$ represent the spectral width in the first and second dimensions respectively; chemical shift values are given in ppm [22,23].

3.4 Results and Discussion

Lipid bilayer containing nanodiscs were prepared using an amphipathic 22 residue peptide (PVLDLFRELLNELLEALKQKLK).[16,17,24] This peptide was designed based on the helical structure and the consensus amino acid sequence of the amphipathic α-helical segments in the apolipoprotein A-I (Apo A-I);[17] previous studies have used Apo A-I mutants as membrane scaffold proteins for nanodisc reconstitution.[5] Application of this 22-residue peptide (referred to as **22A** hereafter) renders a greatly simplified preparation protocol for nanodiscs and an easy control of the size of the nanodiscs simply through the variation of 22A:lipid molar ratio.[16,25,26] Incorporation of a lipid bilayer in 22A-nanodisc resulted in a single peak on the SEC elution profile (Figure 3.1 dotted line), suggesting high homogeneity in the size distribution of nanodiscs.

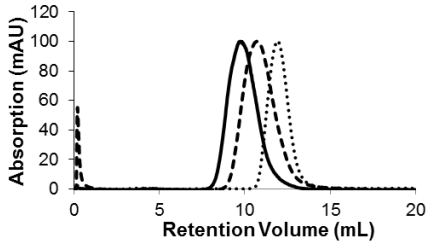

Figure 3.1 Size Exclusion Chromatography. Elution profiles of 22A-nanodiscs containing CYP2B4-cytb_5 after purification (solid line), 22A-nanodiscs containing cytb_5 after purification (dashed line) and empty 22A-nanodiscs (dotted line).

In order to examine the influence of nanodiscs on the overall folding of cytb_5, 2D $^{15}N/^{1}H$ TROSY HSQC NMR spectrum was recorded for cytb_5 alone in buffer (Fig. 3.2A cyan) and cytb_5 incorporated into nanodiscs (Fig. 3.2A magenta). Chemical shift perturbation (CSP) and changes in peak heights were observed for cytb_5 resonances upon incorporation in nanodsics (Fig. 3.2B&C). Largest CSPs are found for residues I17, H20, H31, H32 and H68, which are primarily located on the lower cleft of cytb_5; and residues L92, T101, Y127 and D134, which are located on the linker and the transmembrane domain of cytb_5 (Fig. 3.2B, right panel). Perturbations observed in these areas are likely due to the dissociation of cytb_5 aggregates and direct interaction between cytb_5 and the nanodisc. Mapping of these residues, therefore, provides information on the cytb_5-cytb_5 aggregate interface and/or membrane binding interface. In addition to CSPs, a significant increase in peak height was observed in the linker region for residues including E97, T98, L99, T101, V103 and D104 (Fig. 3.2C right panel). Changes in the line-width of resonances in this region imply a change in the dynamics of the linker likely due to the liberation of cytb_5 from its aggregates upon incorporation in the lipid bilayer of a nanodisc. Significant line-broadening in the linker region of cytb_5 has been reported upon complex formation between cytb_5 and P450 as a result of motional restriction of the linker.[3]

Dissociation of cytb_5 aggregates, as revealed by SEC (Figure. 3.2) and NMR (Figure. 3.3), was achieved through successful reconstitution of cytb_5 into 22A-nanodiscs (Figure. 1 dashed line).

In an effort to incorporate the CYP2B4-cytb_5 complex into the 22A-nanodisc, a variety of sample preparation methods were screened, among which the two procedures (Method 1 and Method 2) reported in **Materials and Methods** generated successful incorporation of both proteins into nanodiscs as suggested by their SEC elution profiles (Figures 3.1 (solid line) & 3.4). The nanodiscs containing both proteins were stable for more than a week at room temperature, as revealed by no precipitation and a reproducible SEC profile after 10 days (Figure 3.4B). In contrast, CYP2B4-cytb_5 complexes incorporated in isotropic bicelles, which consist lipids and detergents at 1:4 molar ratio, are only stable for around 3 days (Figure 3.4C), after which the sample start to precipitate. Higher stability of the protein complex achieved by nanodiscs compared to isotropic bicelles is likely the result of the complete elimination of detergents throughout the sample preparation process. Existence of detergents not only disturbs the overall folding of CYP2B4 but also hampers the activity of the protein.[4] Although both sample preparation methods resulted in

identical SEC elution profiles suggesting successful reconstitution of both proteins to the nanodiscs, distinction needs to be made between the following two situations: 1) both CYP2B4 and cytb_5 are anchored to the same side of the nanodisc, and a productive complex is formed between the two proteins; 2) CYP2B4 and cytb_5 are reconstituted to opposite sides of the nanodiscs, which hampers the formation of the CYP2B4-cytb_5 complex.

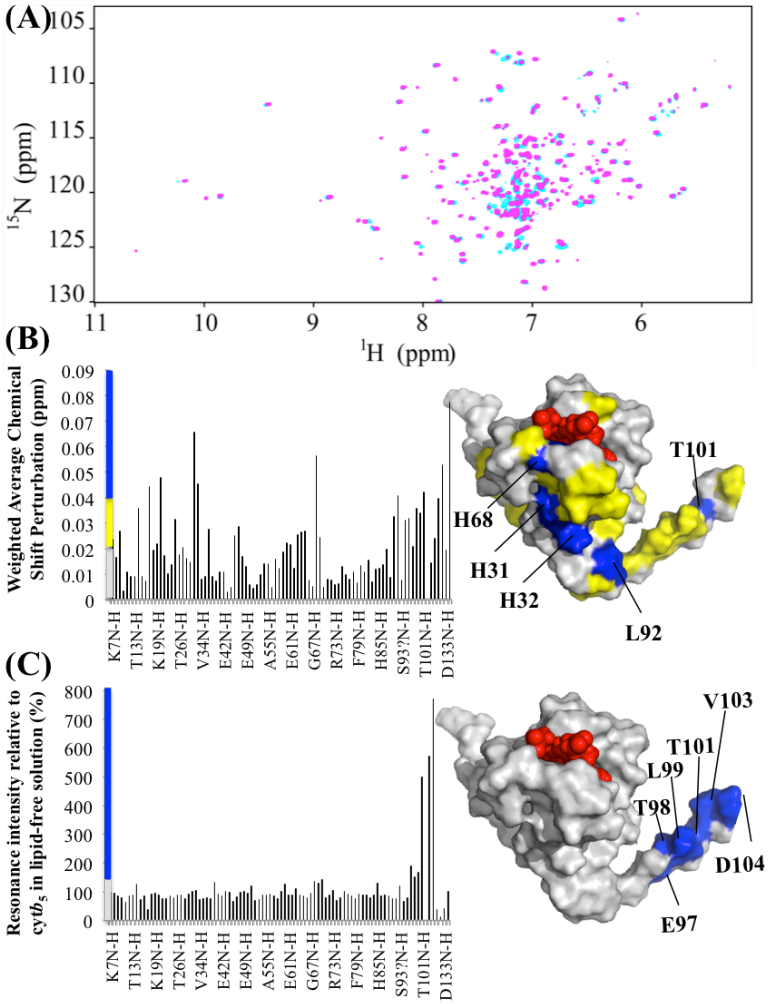

Figure 3.2 2D ^{15}N/^{1}H TROSY HSQC spectrum of cytb_5. (A) Overlay of the 2D ^{15}N/^{1}H TROSY HSQC spectra of cytb_5 in buffer (cyan) and cytb_5 reconstituted in the 22A-nanodiscs (magenta). (B) *Left panel:* A histogram presenting the changes in the weighted average amide chemical shifts of cytb_5 resonances upon incorporation into 22A-nanodiscs. The chemical shift perturbations are categorized into significant (blue), medium (yellow) and not significant (grey), presented by the vertical color strip, and is also mapped onto the structure of cytb_5 (in the *right panel)*. (C) *Left panel:* A histogram presenting the resonance intensities of cytb_5 incorporated in 22A-nanodiscs normalized to free cytb_5 in buffer. The relative resonance intensities are categorized into significant (blue) and not significant (grey), presented by the vertical color strip, and is also mapped onto the structure of cytb_5 in the *right panel.*

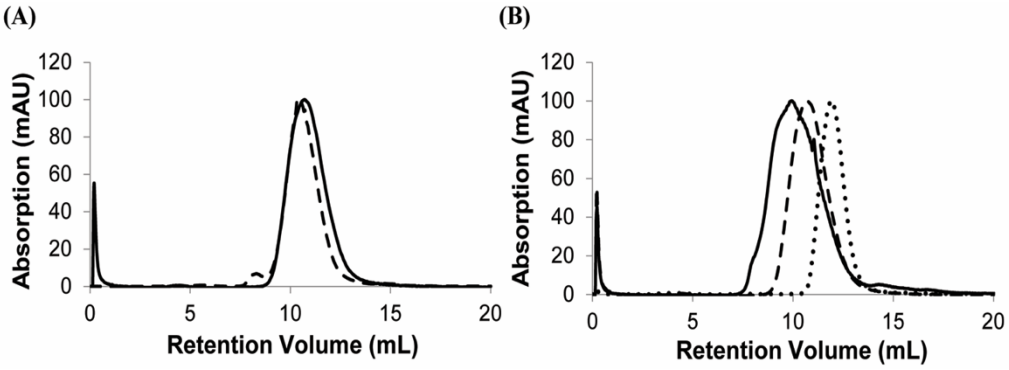

Figure 3.3 Size Exclusion Chromatography of cytb_5. (A) Elution profile of 22A-nanodiscs containing cytb_5 before (dashed line) and after (solid line) purification through SEC. (B) Comparison of the SEC elution profiles between cytb_5 alone in buffer (solid line), 22A-nanodiscs containing cytb_5 after purification (dashed line), and empty 22A-nanodiscs (dotted line). Reconstitution of cytb_5 into 22A-nanodiscs resulted in a single major peak, representing the nanodiscs containing cytb_5, and a minor peak on the SEC elution profile (Fig. S1A, dashed line). This minor peak coincides with the peak observed for cytb_5 alone in buffer. A comparison of the elution profiles between cytb_5 in nanodiscs (Fig. S1B, dashed line) and cytb_5 alone (Fig. S1B, solid line) reveals a large particle size for cytb_5 in a membrane free environment, which implies the aggregation of cytb_5 in the absence of nanodiscs and the ability of nanodiscs to dissociate cytb_5 aggregates. Aggregation of cytb_5 has also been observed by other research groups,[27] and is most likely attributed to the amphipathic nature of this protein, which consists of a globular soluble domain and an α-helical transmembrane domain.[3]

In order to verify the nature of the CYP2B4-cytb_5 complex formed in a nanodisc, 2D $^{15}N/^{1}H$ TROSY HSQC spectra were recorded for the samples prepared by both methods with ^{15}N-cytb_5. Significant differential line-broadening and modest chemical shift perturbation (< 0.01 ppm) were observed only for the sample prepared via Method 1, implying productive CYP2B4-cytb_5 complex formation in the nanodiscs.(Figure 3.5A&B) This observation agrees with our previous studies on the interaction between CYP2B4 and cytb_5 in bicelles.[4] In contrast, in detergent micelles, the interaction between the two proteins is very weak and negligible as compared to that in nanodiscs (Figure 3.6A).[4]

The small magnitude of the CSP could be attributable to the formation of an ensemble of encounter complexes and/or protein-protein interactions on a fast-to-intermediate time scale.[3] Mapping of differential line-broadening on the cytb_5 (Figure 3.5C) reveals potential binding interface for the CYP2B4-cytb_5 complex in nanodiscs, including residues H68, S69, T70, R73 and L75, which are located on the lower cleft of the front face of cytb_5 around the heme edge. These

residues, with the exception of L75, have been found on the binding interface of the CYP2B4-cytb_5 complex structure in bicelles.[3] In addition, previous studies have shown that T70 is involved in stereospecific complex formation between CYP2B4 and cytb_5.[28]

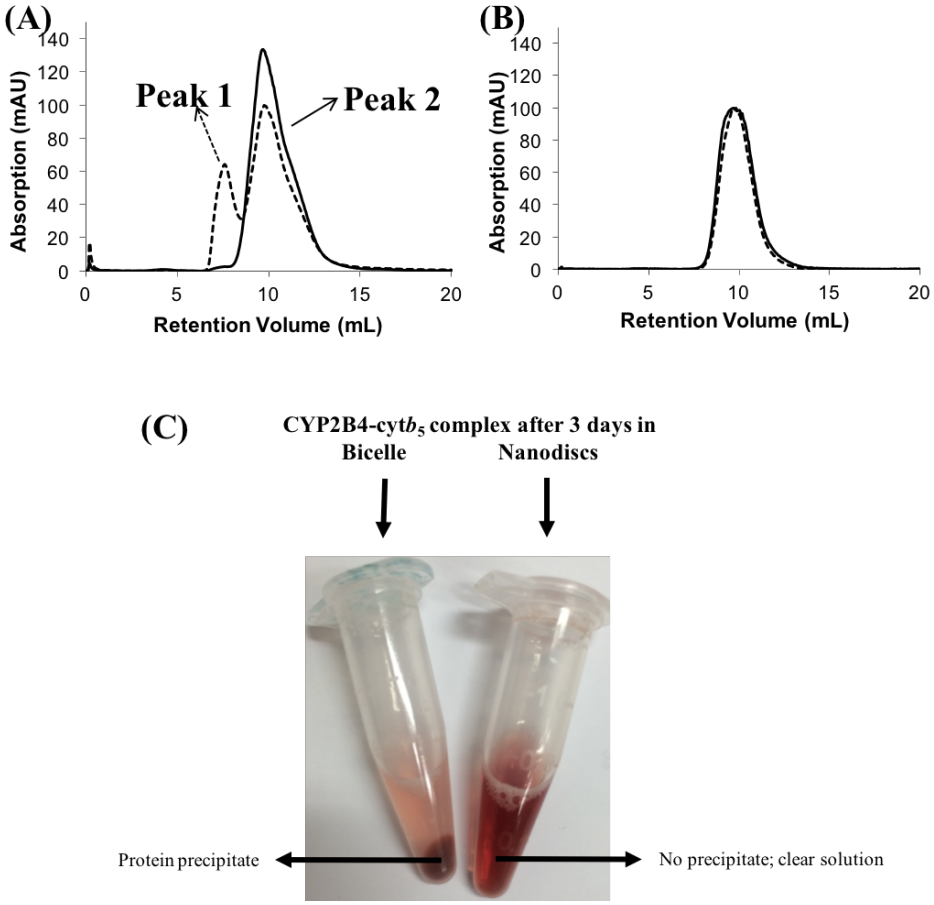

Figure 3.4 Characterization of the size and stability of CYP2B4-cytb_5 in nanodiscs. (A) Elution profile of 22A-nanodiscs containing CYP2B4-cytb_5 after incubation for 2 hours (dashed line) and 10 hours (solid line) before purification. The elution profile contains a slightly distorted major peak (peak 2) corresponding to 22A-nanodisc containing CYP2B4 and cytb_5, and a minor peak preceding the major one (peak 1) revealing existence of the protein aggregates in solution. The minor peak (peak 1) becomes smaller and the major peak becomes bigger as the incubation time gets longer (solid line), implying a time-dependent reconstitution of both proteins into nanodiscs. After 10-hour incubation, more than 90% protein incorporation could be achieved. (B) Purification through SEC leads to a single peak (peak 2 in A) on the elution profile, indicating nanodiscs homogeneously incorporated with both the proteins. The dashed line represents elution profile immediately after purification; the solid line represents the elution profile of the same sample after 10 days at room temperature. The reproducible elution profile after 10 days at room temperature implies stability of the nanodiscs containing CYP2B4-cytb_5 complexes for more than a week. (C) A photo showing that the CYP2B4-cytb_5 complexes form precipitate in bicelle after 3 days, which leads to loss of protein in solution. In contrast, the complexes in nanodiscs remain a clear solution and no sign of precipitate is found.

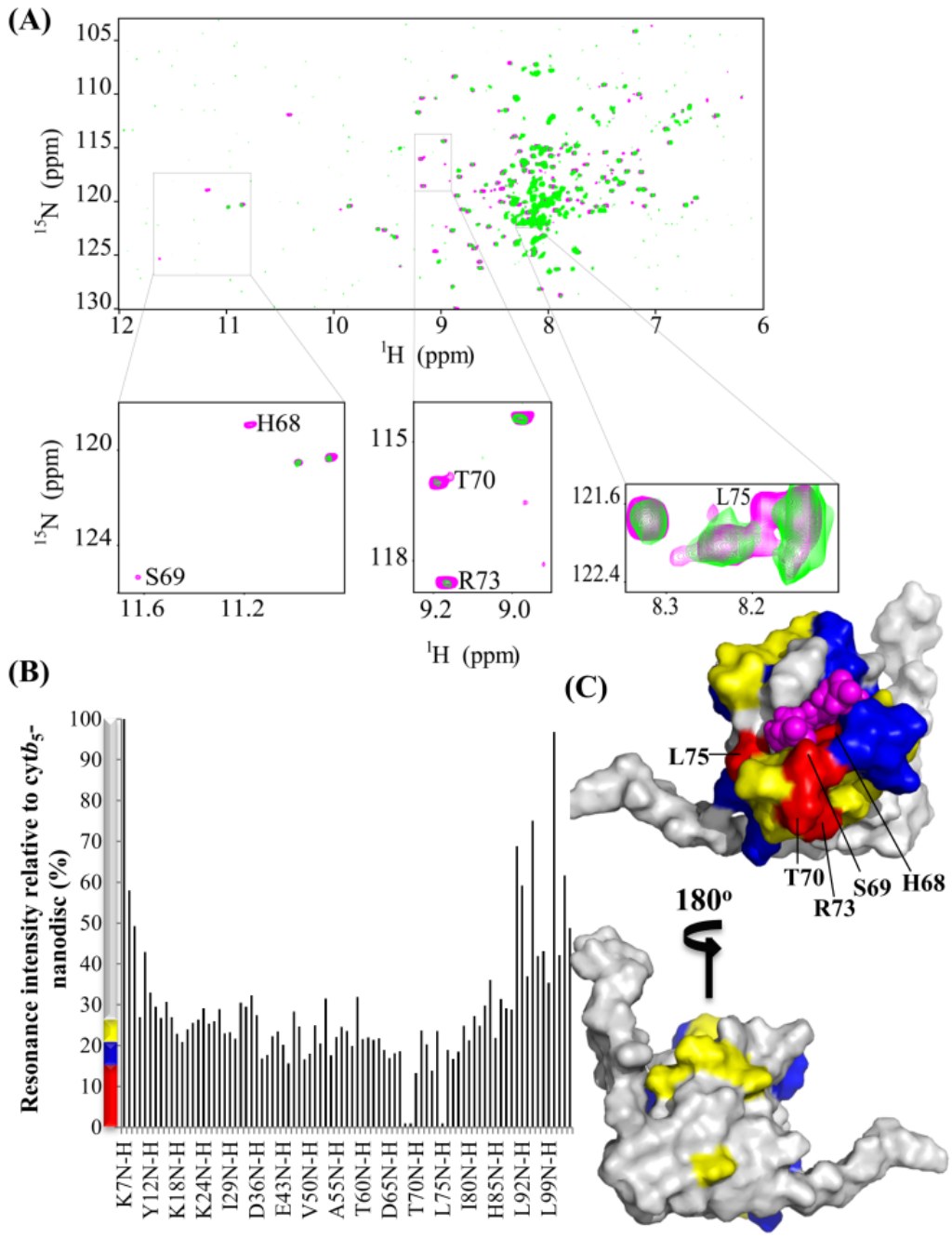

Figure 3.5 2D ^{15}N/^{1}H TROSY HSQC spectrum of cytb_5. (A) Overlay of the 2D ^{15}N/^{1}H TROSY HSQC spectra of cytb_5 alone in 22A-nanodiscs (magenta) and cytb_5 in complex with CYP2B4 reconstituted in 22A-nanodiscs (green). (B) A histogram of the resonance intensities of cytb_5 in complex with CYP2B4 incorporated in 22A-nanodiscs normalized to free cytb_5 in 22A-nanodiscs, which exhibits a differential line-broadening pattern. The line-broadening is categorized into significant (red), medium (blue), not significant (yellow) and negligible (grey), presented by the vertical color strip, and is also mapped onto the structure of cytb_5 in (C).

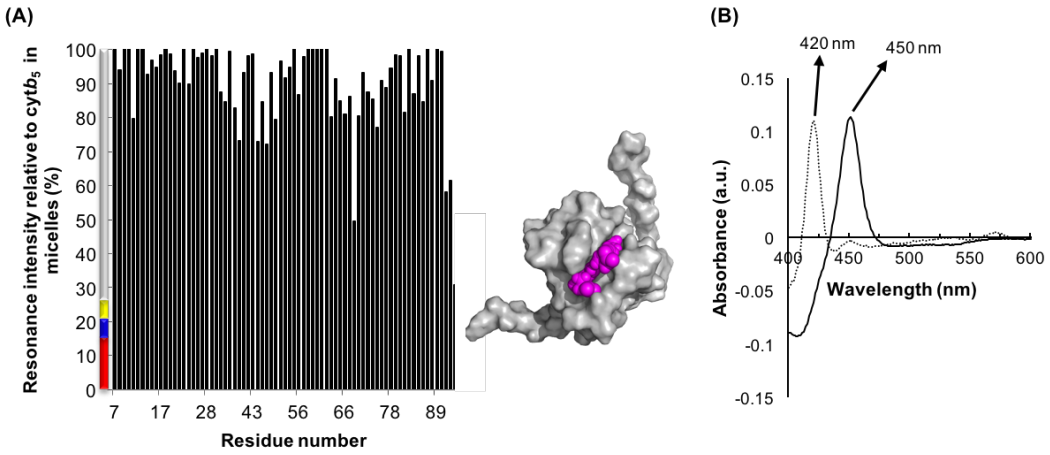

Figure 3.6 Effect of nanodiscs and detergent micelles on CYP2B4-cytb_5 complex formation (A) and CYP2B4 catalytic activity (B). (A) NMR resonance intensity for backbone amides of cytb_5 at a 1:1 molar ratio with CYP2B4 in DPC micelles, shown as a percentage of free cytb_5 resonance intensities. The line-broadening is categorized the same as Figure 3.2 into significant (red), medium (blue), not significant (yellow) and negligible (grey), presented by the vertical color strip, and is also mapped onto the structure of cytb_5 on the Right. Heme is colored in magenta. Mapping of the binding interface shows that no residue is significantly perturbed during titration of CYP2B4, implying negligible interaction between cytb_5 and CYP2B4 in the micelles. [4] (B) Carbon monoxide (CO) activity assay of CYP2B4 in DPC micelles (dotted line) and 22A-nanodiscs (solid line). An absorption maximum at 450 nm is observed in nanodiscs, indicative of CYP2B4 in a functionally active P450 form. In contrast, CYP2B4 completely turns into an inactive cytochrome P420 form in DPC micelles, as shown by a peak at 420 nm.

For the first time, L75 is reported to be likely involved in CYP2B4-cytb_5 interactions. This could be attributed to potential changes in membrane topology of the two proteins in terms of their orientations in lipid bilayers as well as the depth of insertion into the membrane; as nanodiscs, unlike bicelles, completely devoid of detergents, membrane interaction of CYP2B4 could be enhanced and its folding may be slightly different.[29,30] Above all, identification of this binding interface that matches previous findings implies successful formation of productive complexes between CYP2B4 and cytb_5. On the other hand, the sample prepared through Method 2, although resulted in identical SEC profiles with that from Method 1, failed to produce a differential broadening pattern of cytb_5 resonances. Instead, uniform broadening was observed as expected for the overall increase in the total correlation time of the entire particle when CYP2B4 was anchored to the opposite side of the disc (data not shown). Addition of substrates resulted in enhanced protein-protein interactions for samples prepared via Method 1 (Figure 3.7) but not Method 2, which further supports productive complex formation in the former.

It is worth pointing out that, our results cannot fully rule out the possible existence of a fraction of nanodiscs with CYP2B4 and cytb_5 located on opposite sides in Method 1. Yet given the fact that Method 1 sample predominantly displays the character of CYP2B4-cytb_5 productive complexes as revealed by the NMR experiments, it is highly likely that the situation where both proteins are on the same side of the nanodiscs dominates in Method 1.

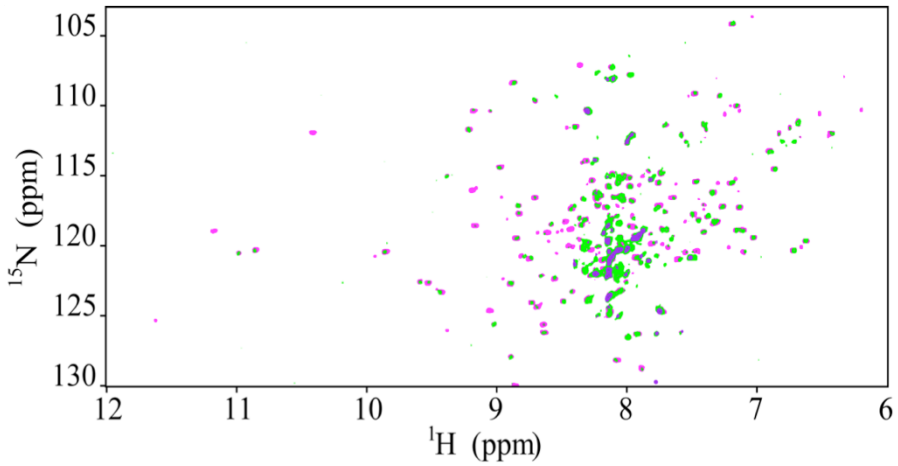

Figure 3.7 Effect of BHT on CYP2B4-cytb_5 binding. An overlay of 2D ^{15}N/^{1}H TROSY HSQC spectra of cytb_5 alone (magenta), cytb_5 in complex with CYP2B4 (green), and cytb_5 in complex with BHT-bound CYP2B4 (purple) reconstituted in the 22A-nanodisc. Butylated hydroxytoluene (BHT), a substrate of CYP2B4, was added to nanodiscs containing CYP2B4 and cytb_5 for samples prepared via Method 1 (sample 1) and Method 2 (sample 2), and 2D ^{15}N/^{1}H TROSY HSQC spectra were obtained to further confirm complex formation in nanodiscs. The addition of BHT to Sample 1 exhibited extensive line-broadening resulting in the disappearance of a majority of resonances in the spectrum (purple). This observation is consistent with our previous finding in DMPC/DHPC isotropic bicelles as BHT enhances CYP2B4-cytb_5 binding by promoting short-range stereospecific interactions between the two proteins.[3,28] This observation suggests that the two proteins are in close proximity to each other, implying reconstitution of both proteins to the same side of the nanodisc. In contrast, no change was observed on the cytb_5 spectrum when BHT was added to Sample 2, which implies the absence of complex formation between CYP2B4 and cytb_5 in the reconstituted nanodiscs via Method 2.

3.5 Conclusion

In summary, we demonstrate successful reconstitution of CYP2B4-cytb_5 complexes into peptide-based nanodiscs. NMR experiments have provided the evidence for productive complex formation in nanodiscs, implying that both proteins are reconstituted to the same side of the nanodsics. The use of the 22A peptide as the belt protein enables simplified preparation protocol for nanodiscs. Additionally, the complete elimination of detergents from samples renders a high

stability of membrane proteins such as CYP2B4 whose structure and function are sensitive to the presence of detergents. In addition, the high spectral resolution and sample stability demonstrated by this approach would enable high-resolution structure and dynamics studies using NMR techniques.

3.6 Reference

1. Dürr, U. H. N., Waskell, L. & Ramamoorthy, A. The cytochromes P450 and b5 and their reductases--promising targets for structural studies by advanced solid-state NMR spectroscopy. *Biochim. Biophys. Acta* **1768,** 3235–59 (2007).
2. Zhang, H., Hamdane, D., Im, S.-C. & Waskell, L. Cytochrome b5 inhibits electron transfer from NADPH-cytochrome P450 reductase to ferric cytochrome P450 2B4. *J. Biol. Chem.* **283,** 5217–25 (2008).
3. Ahuja, S. *et al.* A model of the membrane-bound cytochrome b5-cytochrome P450 complex from NMR and mutagenesis data. *J. Biol. Chem.* **288,** 22080–95 (2013).
4. Zhang, M., Huang, R., Im, S.-C., Waskell, L. & Ramamoorthy, A. Effects of Membrane Mimetics on Cytochrome P450-Cytochrome b5 Interactions Characterized by NMR Spectroscopy. *J. Biol. Chem.* (2015). doi:10.1074/jbc.M114.597096
5. Denisov, I. G. & Sligar, S. G. Cytochromes P450 in nanodiscs. *Biochim. Biophys. Acta* **1814,** 223–9 (2011).
6. Raschle, T. *et al.* Structural and functional characterization of the integral membrane protein VDAC-1 in lipid bilayer nanodiscs. *J Am Chem Soc* **131,** 17777–17779 (2009).
7. Hagn, F., Etzkorn, M., Raschle, T. & Wagner, G. Optimized phospholipid bilayer nanodiscs facilitate high-resolution structure determination of membrane proteins. *J. Am. Chem. Soc.* **135,** 1919–1925 (2013).
8. Alami, M., Dalal, K., Lelj-Garolla, B., Sligar, S. G. & Duong, F. Nanodiscs unravel the interaction between the SecYEG channel and its cytosolic partner SecA. *EMBO J.* **26,** 1995–2004 (2007).
9. Katayama, H. *et al.* Three-dimensional structure of the anthrax toxin pore inserted into lipid nanodiscs and lipid vesicles. *Proc. Natl. Acad. Sci. U. S. A.* **107,** 3453–3457 (2010).
10. Frauenfeld, J. *et al.* Cryo-EM structure of the ribosome-SecYE complex in the membrane environment. *Nat. Struct. Mol. Biol.* **18,** 614–621 (2011).

11. Hernández-Rocamora, V. M., García-Montañés, C., Rivas, G. & Llorca, O. Reconstitution of the Escherichia coli cell division ZipA-FtsZ complexes in nanodiscs as revealed by electron microscopy. *J. Struct. Biol.* **180,** 531–538 (2012).
12. D'Antona, A. M., Xie, G., Sligar, S. G. & Oprian, D. D. Assembly of an activated rhodopsin-transducin complex in nanoscale lipid bilayers. *Biochemistry* **53,** 127–134 (2014).
13. Kedrov, A. *et al.* Elucidating the native architecture of the YidC: Ribosome complex. *J. Mol. Biol.* **425,** 4112–4124 (2013).
14. Denisov, I. G., Baas, B. J., Grinkova, Y. V. & Sligar, S. G. Cooperativity in cytochrome P450 3A4: Linkages in substrate binding, spin state, uncoupling, and product formation. *J. Biol. Chem.* **282,** 7066–7076 (2007).
15. Denisov, I. G., Frank, D. J. & Sligar, S. G. Cooperative properties of cytochromes P450. *Pharmacol. Ther.* **124,** 151–167 (2009).
16. Dasseux, J.-L. Peptide/lipid complex formation by co-lyophilization. (2007). at <https://www.google.com/patents/US7189411>
17. Louis, D. J., Sekul, R., Buttner, K., Cornut, I. & Metz, G. Apolipoprotein a-i agonists and their use to treat dyslipidemic disorders. (1999). at <http://www.google.com/patents/WO1999016408A2?cl=en>
18. Dürr, U. H. N., Yamamoto, K., Im, S.-C., Waskell, L. & Ramamoorthy, A. Solid-state NMR reveals structural and dynamical properties of a membrane-anchored electron-carrier protein, cytochrome b5. *J. Am. Chem. Soc.* **129,** 6670–1 (2007).
19. Saribas, A. S., Gruenke, L. & Waskell, L. Overexpression and purification of the membrane-bound cytochrome P450 2B4. *Protein Expr Purif* **21,** 303–309 (2001).
20. Bridges, A. *et al.* Identification of the binding site on cytochrome P450 2B4 for cytochrome b5 and cytochrome P450 reductase. *J Biol Chem* **273,** 17036–17049 (1998).
21. Kneller, D. G. & Kuntz, I. D. UCSF Sparky-an NMR display, annotation, and assignment tool. *J. Cell. Biochem.* **53,** 254–254 (1993).
22. Williamson, R. A., Carr, M. D., Frenkiel, T. A., Feeney, J. & Freedman, R. B. Mapping the binding site for matrix metalloproteinase on the N-terminal domain of the tissue inhibitor of metalloproteinases-2 by NMR chemical shift perturbation. *Biochemistry* **36,** 13882–9 (1997).
23. Williamson, M. P. Using chemical shift perturbation to characterise ligand binding. *Prog.*

Nucl. Magn. Reson. Spectrosc. **73,** 1–16 (2013).

24. Li, D., Gordon, S., Schwendeman, A. & Remaley, A. T. *Apolipoprotein Mimetics in the Management of Human Disease*. (Springer International Publishing, 2015). doi:10.1007/978-3-319-17350-4
25. Homan, R., Esmaeil, N., Mendelsohn, L. & Kato, G. J. A fluorescence method to detect and quantitate sterol esterification by lecithin:cholesterol acyltransferase. *Anal. Biochem.* **441,** 80–6 (2013).
26. Vaisman, B. L. & Remaley, A. T. Measurement of lecithin-cholesterol acyltransferase activity with the use of a Peptide-proteoliposome substrate. *Methods Mol. Biol.* **1027,** 343–52 (2013).
27. Calabro, M. A., Katz, J. T. & Holloway, P. W. Self-association of cytochrome b5 in aqueous solution. Gel filtration and ultracentirfugational studies. *J. Biol. Chem.* **251,** 2113–2118 (1976).
28. Zhang, M. *et al.* Insights into the Role of Substrates on the Interaction between Cytochrome b5 and Cytochrome P450 2B4 by NMR. *Sci. Rep.* **5,** 8392 (2015).
29. Kawato, S., Gut, J., Cherry, R. J., Winterhalter, K. H. & Richter, C. Rotation of cytochrome P-450. I. Investigations of protein-protein interactions of cytochrome P-450 in phospholipid vesicles and liver microsomes. *J. Biol. Chem.* **257,** 7023–7029 (1982).
30. Bayburt, T. H. & Sligar, S. G. Single-molecule height measurements on microsomal cytochrome P450 in nanometer-scale phospholipid bilayer disks. *Proc. Natl. Acad. Sci. U. S. A.* **99,** 6725–30 (2002).

CHAPTER 4

Insights into the Role of Substrates on the Interaction between Cytochrome b_5 and Cytochrome P450 2B4 by NMR[*†]

4.1 Summery

Mammalian cytochrome b_5 (cyt b_5) is a membrane-bound protein capable of donating the second electron to cytochrome P450 (P450) in the P450 catalytic cycle. The interaction between cyt b_5 and P450 has been reported to be affected by the substrates of P450; however, the mechanism of substrate modulation on the cyt b_5-P450 complex formation is still unknown. In this study, the complexes between full-length rabbit cyt b_5 and full-length substrate-free/substrate-bound cytochrome P450 2B4 (CYP2B4) are investigated using NMR techniques. Our findings reveal that the population of complexes is ionic strength dependent, implying the importance of electrostatic interactions in the complex formation process. The observation that the cyt b_5-substrate-bound CYP2B4 complex shows a weaker dependence on ionic strength than the cyt b_5-substrate-free CYP2B4 complex suggests the presence of a larger fraction of specific complexes when CYP2B4 is substrate-bound. These results suggest that a CYP2B4 substrate likely promotes specific interactions between cyt b_5 and CYP2B4. Residues D65, V66, T70, D71 and A72 are found to be most likely involved in specific interactions between the two proteins due to their weak response to ionic strength change. These findings provide insights into the mechanism underlying substrate modulation on the cyt b_5-P450 complexation process.

[*] This chapter is based on the published paper: Zhang, M., Le Clair, S. V, Huang, R., Ahuja, S., Im, S.-C., Waskell, L., and Ramamoorthy, A. (2015) Insights into the Role of Substrates on the Interaction between Cytochrome b5 and Cytochrome P450 2B4 by NMR. *Sci. Rep.* **5**, 8392

[†]This thesis research was supported by funds from the National Institutes of Health (NIH to A.R.).

4.2 Introduction

Cytochrome P450s (P450s) are a ubiquitous superfamily of monooxygenases responsible for the metabolism of numerous endogenous and exogenous compounds, including over 50% of marketed pharmaceuticals.[1–3] Mammalian P450 and its redox partners, cytochrome P450 reductase (CPR) and cytochrome b_5 (cyt b_5), are membrane-bound proteins, each comprised of a large soluble domain and a single α-helical transmembrane domain.[4] To carry out the well-known oxidation of non-activated hydrocarbon molecules, P450 requires two electrons to be sequentially delivered from its redox partners.[5] CPR is capable of donating both electrons, while cyt b_5 is only able to provide the second electron to oxyferrous P450 but not the first electron to ferric P450 due to its high redox potential.[6–9] It has been proposed that electron transfer proteins follow a two-step model for complex formation: first, the formation of an ensemble of encounter complexes in which the two partners adopt different orientations relative to one another; second, the formation of well-defined complex(es), referred to as the stereospecific complex(es), in which electron transfer can occur.[10,11] Long-range, non-specific electrostatic interactions have been found to be the main driving forces behind encounter complex formation, while it is the specific, short-range interactions (*e.g.* hydrogen bonds, salt bridges and hydrophobic interactions) that hold the stereospecific complex(es) together.[11–15] It has been reported that encounter complexes exhibit stronger dependence on ionic strength than the stereospecific complex.[16]

Cyt b_5 has been shown to stimulate, inhibit, or have no effect on the activity of P450s, both *in vitro* and *in vivo* in humans and genetically engineered mice.[9,17–19] Although our understanding of the novel effects of cyt b_5 on P450 catalysis is incomplete, significant progress has been made towards understanding its mechanism of action. Its stimulatory effects are due to its ability to generate the active oxidizing species of P450 more quickly than CPR.[20] The more rapid rate of catalysis in the presence of cyt b_5 also allows less time for side product formation, thereby increasing the utilization of NADPH for product formation. Cyt b_5 inhibits P450 activity by competing with CPR for a binding site on the basic proximal surface of P450.[8,9] No effect of cyt b_5 is observed when these two opposite effects cancel one another. It has also been reported that cyt b_5 exhibits different stimulatory effects on substrate turn-over depending on the substrate under investigation.[17,21] It has also been found that a higher affinity between cyt b_5 and P450 could be achieved in the presence of substrates.[22] A solution NMR study on truncated P450 also revealed substrate modulation of the interactions between cyt b_5 and P450.[23] Our previous work on the full-

length cytochrome P450 2B4 (CYP2B4) showed that the substrate 3,5-di-*tert*-butyl-4-hydroxytoluene (BHT) enhances complex formation between full-length CYP2B4 and full-length cyt b_5 in a membrane mimetic environment.[24] Crystal structures of P450s have demonstrated that substrate binding causes conformational changes on the proximal surface of P450 where the redox partners bind.[25–35] A more detailed look into cyt b_5-P450 complex formation process under the influence of substrates, in a native-like environment, will lead to a better understanding of the role that substrates play in modulating the interactions between these two redox partners.

In this study, NMR techniques are used to investigate the interactions, at the atomic level, between full-length substrate-free/BHT-bound CYP2B4 and full-length rabbit cyt b_5 in a membrane mimetic environment under different ionic strength conditions. By titrating NaCl into the complexes, we explored the important role of electrostatic interactions in the cyt b_5-CYP2B4 complex formation. We found that varying the ionic strength affected complex formation between cyt b_5 - substrate-free CYP2B4 and cyt b_5 - BHT-bound CYP2B4 in different ways, revealing different encounter/stereospecific complex population ratios in the two cases. The findings unveil the role that the substrate BHT plays in the complexation process. Furthermore, a detailed analysis of the differential ionic strength dependence of resonance intensities of cyt b_5 residues allowed for identification of residues most likely involved in specific interactions with CYP2B4, leading to a better understanding of the complex interface.

4.3 Materials and Methods

4.3.1 Materials

Phosphate buffer components (potassium phosphate monobasic and dibasic), glycerol and 3,5-di-*tert*-butyl-4-hydroxytoluene (BHT) were purchased from Sigma-Aldrich (St. Louis, MO). Sodium chloride was purchased from Fisher Scientific. 1,2-dihexanoyl-*sn*-glycero-3-phosphocholine (DHPC) and 1,2-dimyristoyl-*sn*-glycero-3-phosphocholine (DMPC) were purchased from Avanti Polar Lipids, Inc. (Alabaster, AL).

4.3.2 NMR experiments

Full-length ^{15}N-labeled cyt b_5 and unlabeled full-length CYP2B4 were expressed and purified as reported previously.[36,37] NMR experiments were performed at 298 K on a Bruker 900

MHz spectrometer equipped with a 5 mm triple-resonance TXI cryo-probe. All NMR samples were prepared in 100 mM potassium phosphate buffer, pH 7.4, with 5% (w/v) of glycerol. DMPC/DHPC isotropic bicelles (q = [DMPC]/[DHPC] = 0.25) were prepared by co-solubilizing DMPC and DHPC in chloroform. The solvent was then evaporated with N_2 gas to form a thin film at the bottom of a test tube; any residual chloroform was completely removed by lyophilizing in a vacuum oven overnight. The lipid film was rehydrated prior to preparing the NMR sample.[38] The final concentration of bicelles in all NMR samples was 10% (w/v).

The NaCl titration experiments on cyt b_5 alone were done on 0.2 mM ^{15}N-cyt b_5 incorporated in DMPC/DHPC isotropic bicelles (q = 0.25). A series of ^{1}H/^{15}N-SOFAST-HMQC spectra of ^{15}N-cyt b_5 were collected under the following four conditions: 0, 100, 250 and 400 mM NaCl.

For studies of the cyt b_5-CYP2B4 complex, complexes of cyt b_5 and CYP2B4 were prepared with 0.2 mM concentration of each protein and incorporated in 10% (w/v) DMPC/DHPC isotropic bicelles (q = 0.25). The complex samples were titrated with NaCl and monitored by recording ^{1}H/^{15}N-TROSY-HSQC spectra. The complex samples containing BHT had a molar ratio of 2:1 of BHT to CYP2B4. NaCl titrations were performed on both the protein complex samples with and without BHT. The titrations were carried out with 0, 100, 250 and 400 mM NaCl.

A ^{1}H/^{15}N-TROSY-HSQC reference spectrum of 0.1 mM ^{15}N-labeled cyt b_5 incorporated in 10% (w/v) DMPC/DHPC isotropic bicelles (q = 0.25) was also recorded (referred to as "free cyt b_5" in the text). The free cyt b_5 backbone amide resonance peak heights from this spectrum were used to calculate the relative intensities of each cyt b_5 residue when in complex with CYP2B4, under the various conditions tested. For this calculation, the free cyt b_5 resonance peak heights were taken as 100% and the peak heights in complex with CYP2B4 were taken as a percentage of the free cyt b_5 peak heights, referred to as relative intensities, in all analyses. For the spectra in which certain cyt b_5 resonances were not visible in the spectrum (where the resonances broadened beyond detection), a relative intensity of 0% was assigned to these residues.

All spectra were processed in TopSpin 2.0. Peak assignments were accomplished using Sparky, and chemical shifts as well as peak heights were also obtained from Sparky.[39] Assignment of resonances from the soluble domain of ferric cyt b_5 in the ^{1}H/^{15}N-TROSY-HSQC spectra was previously reported.[24]

To calculate ΔI, the difference between the relative intensity of cyt b_5 at a given ionic strength and 0 mM NaCl was taken (*e.g.* ΔI for 100 mM NaCl = $I_{100mM\ NaCl} - I_{0mM\ NaCl}$). The value ΔI_{avg} is the average of ΔI values over all cyt b_5 residues at that ionic strength.

4.3.3 Circular dichroism (CD) experiments of CYP2B4

CD experiments were performed on a Jasco J-715 spectropolarimeter fitted with a 150-W xenon lamp at 25°C using a 1 mm cuvette. Bandwidth was set at 1.0 nm and the time constant was 1.0 s. Spectra were recorded in the far UV region from 190 to 270 nm, with 8 scans accumulated and averaged for each spectrum. Background (with everything present except CYP2B4) was subtracted for all experiments. NaCl was titrated into a solution containing 1 μM CYP2B4 and 2% (w/v) DMPC/DHPC bicelle (q = 0.25) in 100 mM potassium phosphate buffer, pH 7.4, containing 5% (w/v) glycerol. The following concentrations of NaCl were tested: 1 μM, 250 μM, 500 μM, 675 μM, 1 mM, 1.25 mM and 2 mM. These concentrations cover the molar ratios of CYP2B4 to NaCl that are equivalent to those in the NMR samples.

4.4 Results

4.4.1 NaCl does not affect the structures of cyt b_5 and CYP2B4

Through the use of CD experiments, in which NaCl was titrated into CYP2B4 incorporated in isotropic bicelles composed of DMPC (1,2-dimyristoyl-*sn*-glycero-3-phosphocholine) and DHPC (1,2-dihexanoyl-*sn*-glycero-3-phosphocholine) (q = 0.25), we confirm that the overall secondary structure of CYP2B4 does not change with the addition of NaCl (Fig. 4.1). This is in agreement with a previous study which showed no secondary structure changes in CYP2B4 at different sodium phosphate and NaCl concentrations.[40]

To assess whether the structure of cyt b_5, incorporated in DMPC/DHPC isotropic bicelles (q = 0.25), is affected upon the addition of NaCl, a series of 2D $^{1}H/^{15}N$-SOFAST-HMQC (band-Selective Optimized-Flip-Angle Short-Transient Heteronuclear Multiple Quantum Correlation) spectra of cyt b_5 were recorded during NaCl titration. The spectra reveal no significant structural changes of cyt b_5 since only slight to negligible chemical shift perturbations are observed (average perturbation < 0.009 ppm) (Fig. 4.2). In addition, no significant perturbations in signal intensities are observed (average intensity change of 2.3% relative to free cyt b_5 intensities) except for the N-

terminal loop region (K7 and D8), residues S93 to D104 in the linker region and the residue E48. All of these residues show intensity changes of more than one standard deviation away from the average change and are therefore not included in the data analysis of the salt titration on the cyt b_5-CYP2B4 complexes. These residues are highly solvent-exposed and the perturbations they experience are likely due to changes in buffer conditions. Addition of BHT to cyt b_5 also causes no spectral changes, neither in intensities nor chemical shifts (Fig. 4.3).

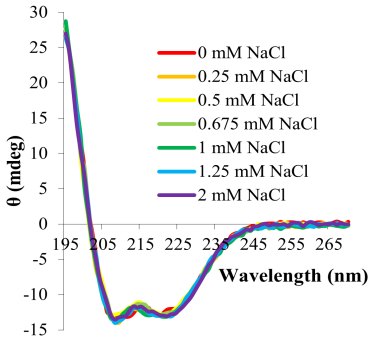

Figure 4.1 The secondary structure of CYP2B4 is not affected upon the addition of NaCl. Circular Dichroism spectra of CYP2B4, incorporated in 2% (w/v) DMPC/DHPC isotropic bicelles (q = 0.25), collected before and during titration of NaCl.

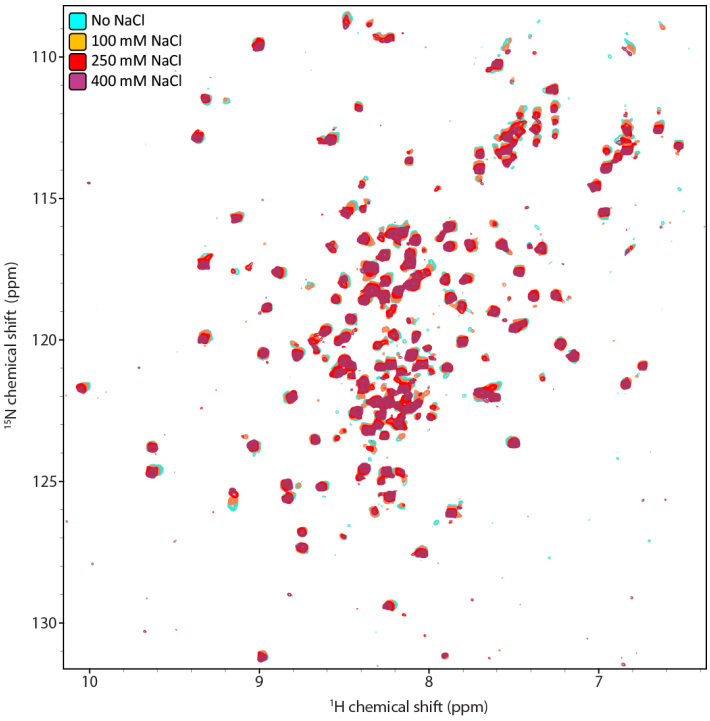

Figure 4.2 The overall structure of cyt b_5 is not affected by the addition of NaCl. $^{1}H/^{15}N$-SOFAST-HMQC spectra of ^{15}N-cyt b_5, incorporated in DMPC/DHPC isotropic bicelles (q = 0.25), collected at the indicated salt conditions.

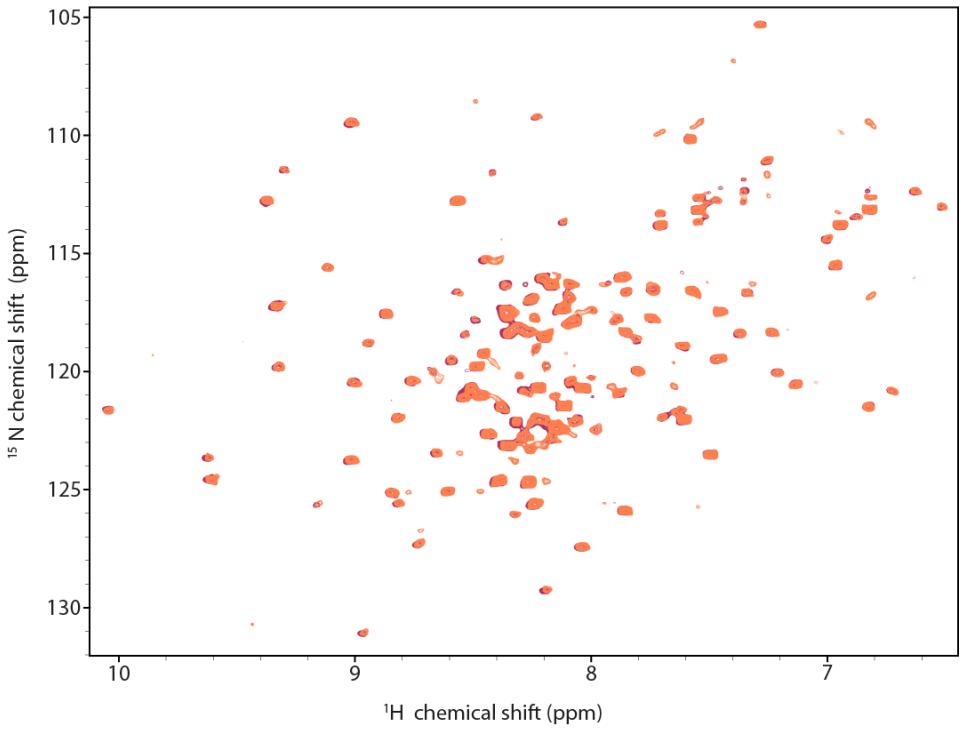

Figure 4.3 Addition of BHT affects neither intensities nor chemical shifts of cyt b_5 backbone NH resonances. The $^{1}H/^{15}N$-SOFAST-HMQC spectrum of ^{15}N-cyt b_5 in isotropic bicelles (maroon) and the spectrum obtained after addition of BHT in a 2:1 molar ratio of BHT to cyt b_5 (coral) superimposed above it.

4.4.2 Interaction between cyt b_5 and substrate-free CYP2B4 during NaCl titration

In order to study the influence of ionic strength on the interaction between cyt b_5 and substrate-free CYP2B4, cyt b_5-CYP2B4 complexes were first formed and incorporated in DMPC/DHPC bicelles (q = 0.25), and then titrated with NaCl. A series of 2D $^{1}H/^{15}N$-TROSY-HSQC (Transverse Relaxation Optimized SpectroscopY Heteronuclear Single Quantum Correlation) spectra were recorded at the following NaCl concentrations: 0, 100, 250 and 400 mM.

When CYP2B4 and ^{15}N-cyt b_5 form a 1:1 complex, general broadening of resonances (Fig. 4.4A, blue) and modest chemical shift perturbation (CSP) (average < 0.01 ppm) are observed for cyt b_5 backbone amides. These two findings suggest the interaction takes place on a fast-to-intermediate time scale (ns - µs).[23,24] The relative intensities of each cyt b_5 backbone amide resonance, represented as a percentage of the corresponding resonance intensities in the $^{1}H/^{15}N$-TROSY-HSQC spectrum of free cyt b_5 (see Materials and Methods), are plotted against cyt b_5 residue number for each NaCl titration point in Figure 4.4A. When cyt b_5 interacts with one molar equivalent of substrate-free CYP2B4 at 0 mM NaCl, the average relative intensity of cyt b_5

resonances drops down to 34.1% of that observed in the free cyt b_5 spectrum. Residues significantly affected (with a relative intensity more than one standard deviation below the average) upon complex formation with CYP2B4 include E43, F63, E64, D65, V66, D71 and S76. These residues are located on the proximal side of cyt b_5 where the heme is solvent-exposed (Fig. 4.4B), and are consistent with our previous findings.[24]

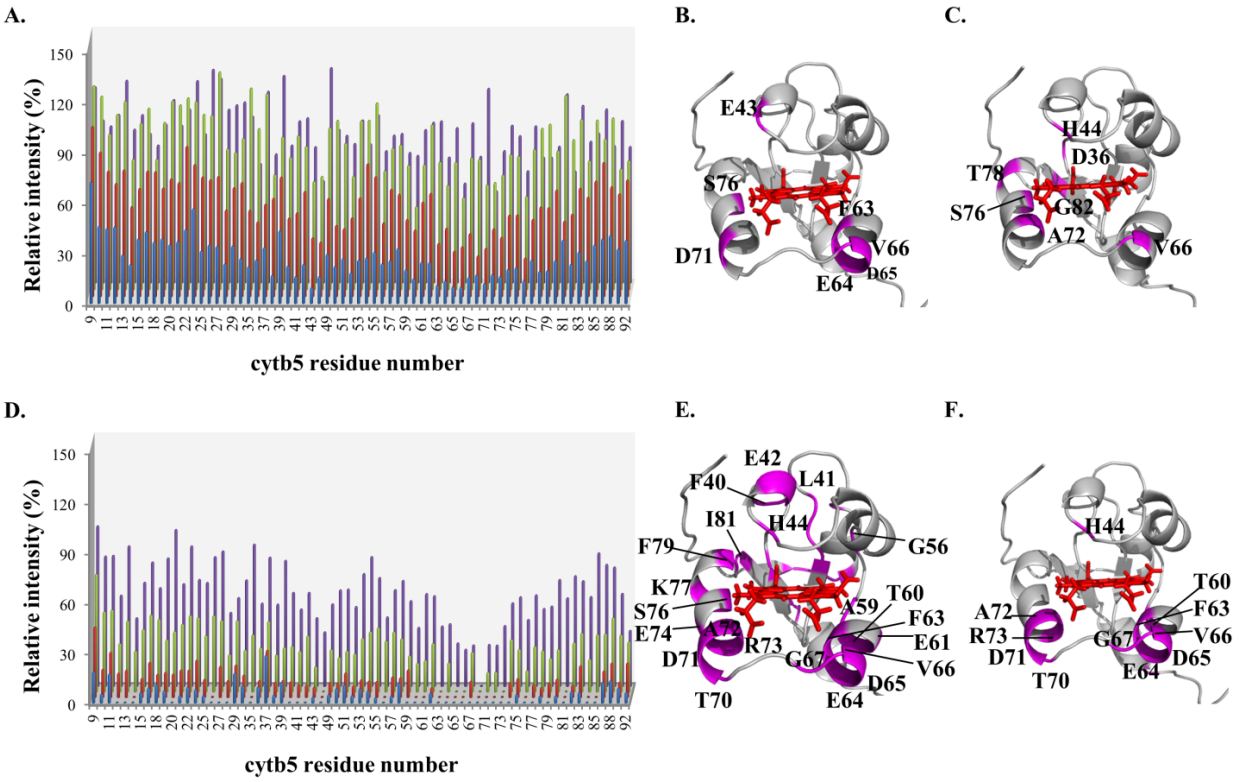

Figure 4.4 Relative intensity recovery of cyt b_5 resonances in complex with substrate-free (A-C)/BHT-bound (D-F) CYP2B4 during NaCl titration. Relative intensities of backbone amides of cyt b_5 in a 1:1 molar ratio with CYP2B4, represented as a percentage of the corresponding resonance intensity in free cyt b_5, are plotted for each cyt b_5 residue for (A) the complex between cyt b_5 and substrate-free CYP2B4 and (D) the complex between cyt b_5 and BHT-bound CYP2B4 at the following NaCl concentrations: 0 mM (blue), 100 mM (red), 250 mM (green) and 400 mM (purple). Residues with relative intensities of more than one standard deviation below the average are mapped onto the cyt b_5 structure (magenta) before and after NaCl titration: cyt b_5-substrate-free CYP2B4 at 0 mM (B) and 400 mM (C) NaCl; and cyt b_5-BHT-bound CYP2B4 at 400 mM NaCl (F). All the residues that broadened beyond detection for the cyt b_5-BHT-bound CYP2B4 complex at 0 mM NaCl are shown in (E), but mapping of these residues does not provide information on the specific binding interface of cyt b_5-BHT-bound CYP2B4 (see Results). However, it demonstrates the remarkable line-broadening of cyt b_5 upon complexation with BHT-bound CYP2B4. The cyt b_5 structure in these figures is the NMR-derived structure previously reported (PDB code: 2M33).[24]

NaCl was subsequently titrated into the cyt b_5-CYP2B4 complex and a general increase in relative resonance intensities was observed with increasing NaCl concentration (Fig. 4.4A). The average relative intensities of cyt b_5 resonances at 0, 100, 250 and 400 mM NaCl are 31.4, 59.1, 89.2 and 92.2% respectively and start to reach a plateau at 250 mM NaCl (Fig. 4.5, black). The first three titration points (before reaching the plateau) could be fit using a linear trend line with a slope of 0.23 ($R^2 = 0.99$), which approximately represents the rate of intensity increase with respect to NaCl concentration. To assess how individual residues are influenced by ionic strength, the relative intensities of the cyt b_5 resonances at each NaCl titration step are also compared to those at 0 mM NaCl to determine the change in intensity, ΔI (see Materials and Methods), and plotted for each cyt b_5 residue (Fig. 4.6A). The average intensity difference values (ΔI_{avg}) for each NaCl concentration are listed in Table I. By identifying residues with a ΔI more than one standard deviation below ΔI_{avg}, certain cyt b_5 residues can be identified as being insignificantly affected upon salt addition. These residues include H44, L51, T70, S76 and I81 at 100 mM NaCl (Fig. 4.6B); T60, R89 and L92 at 250 mM NaCl (Fig. 4.6C); and A72 at 400 mM NaCl (Fig. 4.6D). It can be seen that no residue is found to maintain weak salt dependence throughout the entire NaCl titration. At 400 mM NaCl, however, certain cyt b_5 residues still remain relatively low in intensity (with a relative intensity more than one standard deviation below the average relative intensity) and include D36 and G82 on the back of cyt b_5, as well as H44, V66, A72, S76 and T78 on the upper and lower cleft of cyt b_5, around the heme edge (Fig. 4.4C).

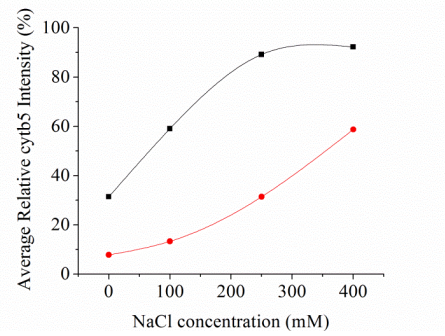

Figure 4.5 Ionic strength dependence of the average relative intensity of cyt b_5 resonances in the cyt b_5-substrate-free CYP2B4 complex (black) and cyt b_5-BHT-bound CYP2B4 complex (red). The black curve reaches a plateau at 250 mM NaCl (the third data point) while the red curve still increases even at 400 mM NaCl (the last data point). The first three data points (before reaching the plateau) of the cyt b_5-substrate-free CYP2B4 complex (black) increase linearly with a slope of 0.23 and R^2 value of 0.99. The cyt b_5-BHT-bound CYP2B4 complex data points (red) increase linearly with a slope of 0.12 and R^2 value of 0.96. Excel was used to fit the linear trend lines.

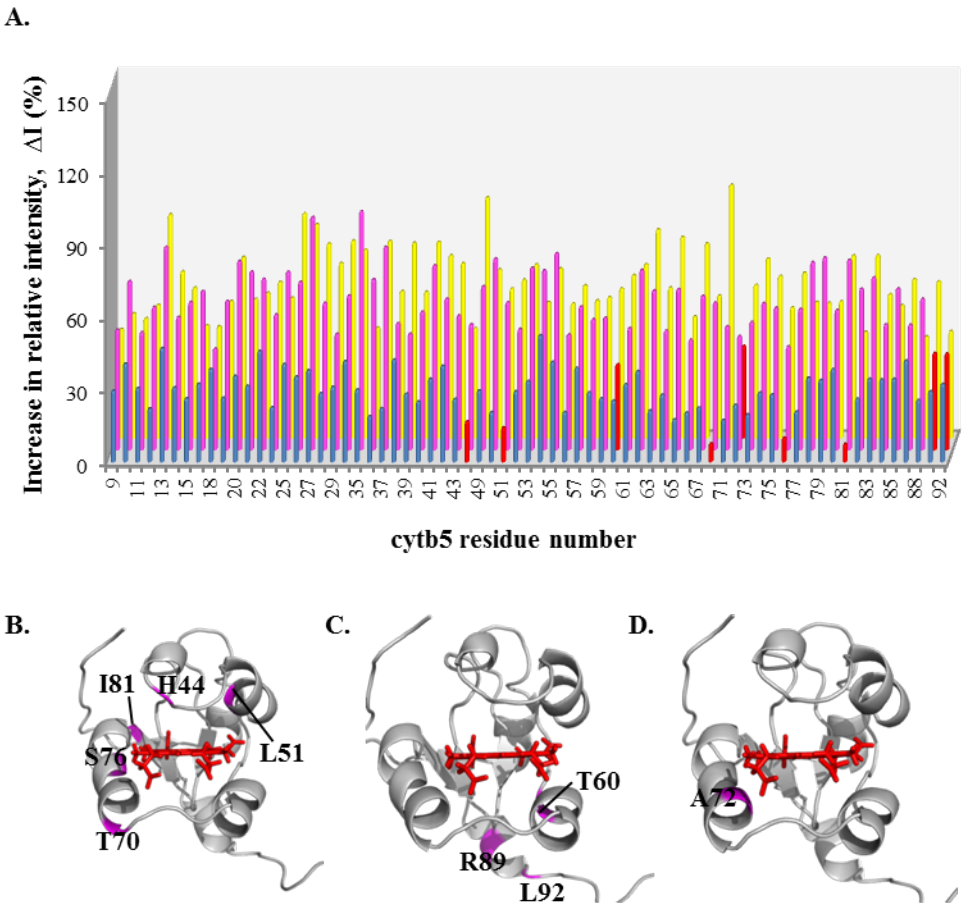

Figure 4.6 Mapping of cyt b_5 residues minimally affected by the increasing ionic strength when in complex with substrate-free CYP2B4. (A) Relative intensity increase (ΔI) of cyt b_5 resonances at 100 mM (blue), 250 mM (magenta) and 400 mM (yellow) NaCl, each calculated relative to 0 mM NaCl (*e.g.* ΔI for 250 mM NaCl = $I_{250mM\ NaCl} - I_{0mM\ NaCl}$). Residues with ΔI more than one standard deviation below the average are considered insignificantly affected by the ionic strength increment and highlighted in red in the histogram in (A), and are mapped in magenta onto the cyt b_5 structure for 100 mM NaCl (B), 250 mM NaCl (C) and 400 mM NaCl (D). No common residue is found in B, C and D

4.4.3 Interaction between cyt b_5 and substrate-bound CYP2B4 during NaCl titration

We previously showed that the interaction between cyt b_5 and CYP2B4 is altered by the presence of a CYP2B4 substrate.[24] To understand the changes in the protein-protein interaction caused by a substrate, the effect of ionic strength on the 1:1 full-length complex between cyt b_5 and CYP2B4, incorporated in DMPC/DHPC isotropic bicelles (q = 0.25), was studied in the presence of the CYP2B4 type I substrate 3,5-di-*tert*-butyl-4-hydroxytoluene (BHT). The complex

between cyt b_5 and BHT-bound CYP2B4 was monitored during the titration of 0, 100, 250 and 400 mM NaCl with a series of two-dimensional $^{1}H/^{15}N$-TROSY-HSQC spectra.

As shown in Figure 4.4D (blue), formation of the complex between cyt b_5 and BHT-bound CYP2B4 leads to extensive line-broadening of ^{15}N-labeled cyt b_5 amide resonances, among which ~50% of the residues disappear from the spectrum (Fig. 4.4D, blue), which suggests intermediate-to-slow chemical exchange between free- and bound-cyt b_5.[24] All cyt b_5 residues that disappear from the spectrum are mapped onto the cyt b_5 structure in Figure 4.4E. However, due to the disappearance of the majority of cyt b_5 resonances from the spectrum, the interaction interface on cyt b_5 cannot be accurately defined. The majority of the residues that broaden beyond detection upon the addition of BHT-bound CYP2B4 are located on the proximal side of cyt b_5, surrounding the solvent-exposed heme edge. The more significant line-broadening of cyt b_5 resonances observed when cyt b_5 interacts with BHT-bound CYP2B4, as compared to its interaction with substrate-free CYP2B4, suggests tighter binding between the two proteins as a result of the presence of the substrate BHT.[24]

Subsequent titration of NaCl causes an increase in relative intensities of cyt b_5 resonances (Fig. 4.4D). The average relative intensities at 0, 100, 250 and 400 mM NaCl are 7.78, 13.3, 31.3 and 58.7% respectively. Unlike in the substrate-free complex, the average relative intensities of cyt b_5 resonances in the CYP2B4 BHT-bound complex show no sign of reaching a plateau at the highest ionic strength of 400 mM NaCl (Fig. 4.5, red). The four data points fit a linear trend line with a slope of 0.12 (R^2 = 0.96), which approximately represents the rate of relative intensity increase as a function of NaCl concentration. Residue-wise relative intensity increase (ΔI) and the average intensity increase (ΔI_{avg}) observed at each titration step, relative to 0 mM NaCl, are plotted in Figure 4.7A and listed in Table I respectively. At 100 mM NaCl, twenty-two cyt b_5 residues can be identified as having insignificant relative intensity increase (ΔI more than one standard deviation below ΔI_{avg}), the majority of which are located on the proximal side of cyt b_5 around the heme edge (Fig. 4.7B). At 250 mM NaCl, residues exhibiting insignificant ΔI include E43, H44, F63, D65, V66, T70, D71, A72, R73 and I81 (Fig. 4.7C). At 400 mM NaCl, residues D65, V66, G67, T70, D71, A72 and L92 are observed to show insignificant ΔI (Fig. 4.7D). The following residues therefore demonstrate weak dependence on NaCl concentration throughout the entire titration: D65, V66, T70, D71 and A72. These five residues are located on the proximal side of cyt b_5, surrounding the heme edge, and were previously hypothesized to be at the binding interface

with CYP2B4.[24] At 400 mM NaCl, certain cyt b_5 residues remain significantly line-broadened (relative intensity more than one standard deviation below the average relative intensity): H44 on the upper cleft of cyt b_5, as well as T60, F63, E64, D65, V66, G67, T70, D71, A72 and R73 on the lower cleft of cyt b_5, around the heme edge (Fig. 4.4F).

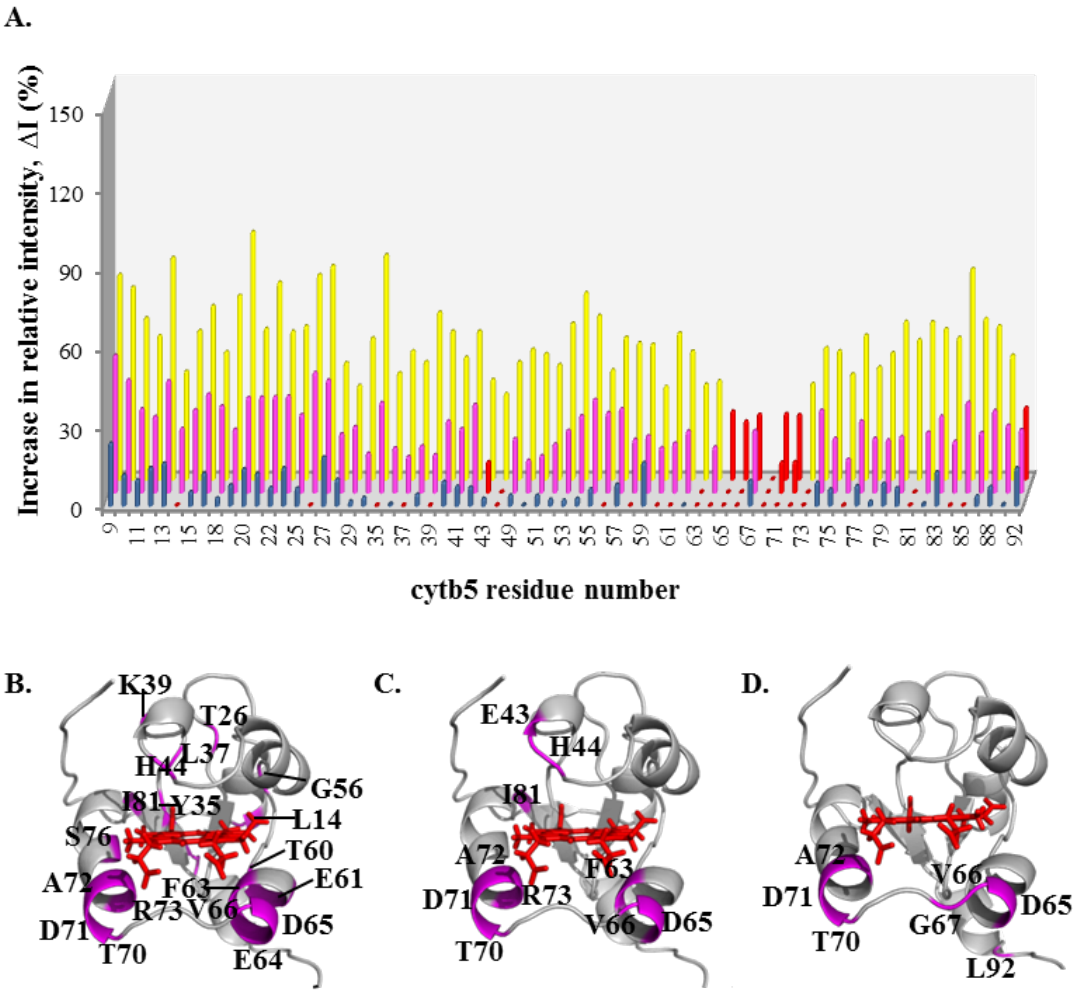

Figure 4.7 Mapping of cyt b_5 residues minimally affected by the increasing ionic strength when in complex with BHT-bound CYP2B4. (A) Increase in relative intensities (ΔI) of cyt b_5 resonances at 100 mM (blue), 250 mM (magenta) and 400 mM (yellow) NaCl, each calculated relative to 0 mM NaCl. Residues with ΔI more than one standard deviation below the average are highlighted in red in the histogram in (A), and are mapped in magenta onto the cyt b_5 structure for 100 mM NaCl (B), 250 mM NaCl (C) and 400 mM NaCl (D). The following residues are found to be highlighted in all the three figures (B, C and D): D65, V66, T70, D71 and A72. These residues are most likely involved in specific interactions during complex formation.

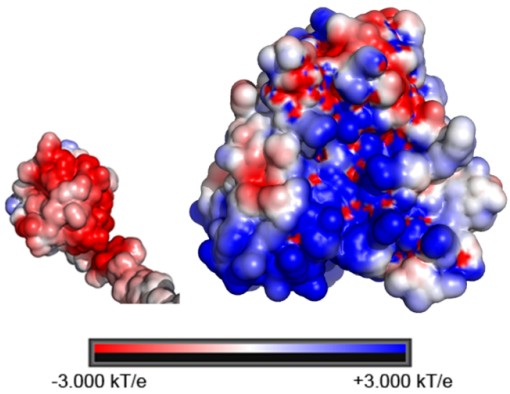

Figure 4.8 Electrostatic potential surfaces of the proximal sides of cyt b_5 (left) and CYP2B4 (right), showing the negatively charged convex surface of cyt b_5 (PDB code: 2M33)[24] and the positively charged concave surface of CYP2B4 (PDB code: 1SUO[34]). The electrostatic potential surfaces were calculated using the PDB2PQR[50,51] server and PyMOL[52] with the APBS plugin 2.1[53].

4.5 Discussion

4.5.1 Cyt b_5-CYP2B4 complex population decreases with increasing ionic strength

Our results reveal that complex formation between cyt b_5 and CYP2B4, both substrate-free and BHT-bound, is ionic strength dependent. The broadening of ^{15}N-labeled cyt b_5 amide resonances observed in the ^{1}H/^{15}N-TROSY-HSQC spectrum upon complexation with CYP2B4 can be reversed by the introduction of NaCl into the system (Fig. 4.4A, Fig. 4.4D and Fig. 4.5), implying liberation of free cyt b_5 and dissociation of the complex. These observations are indicative of the importance of the attractive electrostatic interactions in complex formation. This is not surprising given the net charges of the two proteins at pH 7.4: +6.9 for CYP2B4 and -8.4 for cyt b_5. The opposite electrostatic surface potentials of the two proteins (Fig. 4.8) could promote favorable electrostatic docking between the two proteins. Long-range electrostatic interactions are known to facilitate protein-protein complexation in two ways:[14,15,41] first, Coulombic attraction between oppositely charged surfaces, like the acidic convex surface of cyt b_5 and the concave basic proximal side of CYP2B4 (Fig. 4.8), keeps the two proteins in close proximity and lengthens the lifetime of the macro-collision, enabling more extensive surface sampling through translational and rotational movements; second, pre-orientation of the two proteins is steered by the interactions between complimentary charged patches of residues on each protein, which results in a significant reduction of the searching area and increases the probability of reaching a productive orientation in which electron transfer can occur. Therefore, the salt screening effect caused by high ionic

strength should, to some extent, hinder the part of complex formation in which electrostatic interactions play an important role. Similar results have been observed for a number of other protein complexes, where the complex association constant decreases with increasing ionic strength, especially for complexes between redox partners, *e.g.* cytochrome f and cytochrome c_6,[42] Ana-PSI and Ana-Pc,[43] and barnase and barstar,[13,44].

4.5.2 Substrates promote specific interactions between CYP2B4 and cyt b_5

As mentioned, it has been proposed that macromolecular association can be divided into two steps [11,13,15,16,45]: first, the formation of an ensemble of encounter complexes through three dimensional random collisions of the two molecules, in which long-range non-specific electrostatic interactions have been suggested to play an important role by increasing the collision rate constants and reducing the searching dimensionality on the surfaces of the binding partners; second, subsequent rotations and translations along each other's surfaces rearrange the two molecules to satisfy the stringent orientational requirements for specific interactions, which leads to the formation of the final well-defined stereospecific complex(es). Because the interfaces of encounter complexes are much less compact than that of stereospecific complex(es), ions have easier access to the encounter complexes' interfaces and the salt screening effect of interfacial charges for encounter complexes is more significant than for the stereospecific complex(es), upon an increase in ionic strength.[16] For these reasons, encounter complexes have been found to be more sensitive to ionic strength than the stereospecific complex(es).[16]

In the present study, the dependence of complex formation on ionic strength is investigated for both cyt b_5-substrate-free CYP2B4 and cyt b_5-BHT-bound CYP2B4 complexes. The average relative cyt b_5 resonance intensity increase (ΔI_{avg}) at each NaCl titration step are listed in Table I for both cases. It is apparent that the average relative intensity increase is greater for the cyt b_5-substrate-free CYP2B4 complex than for the cyt b_5-BHT-bound CYP2B4 complex when adding 100 mM (> 5x greater) and 250 mM (> 2x greater) NaCl. At 400 mM NaCl, however, the intensity increase is similar in the two cases, with cyt b_5-substrate-free CYP2B4 being slightly bigger (ΔI_{avg} of 60% versus 50%), which is a result of the fact that saturation in intensity is reached at 250 mM NaCl in the case of cyt b_5-substrate-free CYP2B4 (average relative intensity of 92.2%) while the relative intensity is still increasing for cyt b_5-BHT-bound CYP2B4 (average relative intensity of 58.7%) (Fig. 4.5). By looking at Figure 4.5 and comparing the slopes of the linear portions for

each complex type, a higher dependence on salt concentration is observed when CYP2B4 is substrate-free (slope of 0.23 for cyt b_5-substrate-free CYP2B4 and 0.12 for cyt b_5-BHT-bound CYP2B4). These observations indicate that the complex between cyt b_5 and CYP2B4 is more sensitive to ionic strength in the absence of a substrate than when CYP2B4 is bound to the substrate BHT. Considering that stereospecific complexes have been shown to be affected by ionic strength to a smaller degree than encounter complexes,[16] our results thereby suggest that there is a larger fraction of stereospecific complexes for cyt b_5-BHT-bound CYP2B4 than when CYP2B4 is substrate-free. In other words, the substrate BHT likely promotes specific interactions between cyt b_5 and CYP2B4, causing a higher population ratio of stereospecific complex(es) to encounter complexes. This might be due to a conformational change of CYP2B4 in order to accommodate BHT. Crystal structures of CYP2B4 have demonstrated ligand-induced structural rearrangements of the protein when bound to diverse substrates,[25–35] and have highlighted five plastic regions (PR1-5) subject to conformational variability; PR2 includes the C helix and the C-D loop region on the proximal side of CYP2B4.[46] Interestingly, mutagenesis studies have shown that six out of seven interface residues on CYP2B4, when complexed with cyt b_5, are on the C helix and the C-D loop.[37] Our previously reported complex structure of cyt b_5-CYP2B4 also showed that the binding interface on CYP2B4 was predominantly located on the C helix and the C-D loop.[24] Therefore, a possible explanation for the capability of BHT to promote specific interactions during cyt b_5-CYP2B4 complex formation could be that a conformational rearrangement of the CYP2B4 C helix and C-D loop region is induced upon accommodation of BHT; this might place the key binding sites on CYP2B4 into specific orientations such that favorable contacts with the binding interface on cyt b_5 can occur, thus leading to a shift in equilibrium from the encounter complexes to the stereospecific complex(es).

Since short-range specific interactions are much stronger than long-range non-specific electrostatic interactions, this shift towards the stereospecific complexes also explains our observation that interactions between cyt b_5 and BHT-bound CYP2B4 lead to more extensive line-broadening in the NMR spectrum, implying higher affinity between the two proteins, than that observed for cyt b_5-substrate-free CYP2B4 (Figs. 1A and 1D, blue).[24] Additionally, at 400 mM NaCl (the highest ionic strength tested in our experiments), the average relative intensity for cyt b_5 in complex with substrate-free CYP2B4 returns to almost 100% (Fig. 4.5, black), and the residues that remain relatively low in intensity compared to other residues are spread over an

extensive area on cyt b_5 (Fig. 4.4C), suggesting very weak (nearly negligible) and non-specific interactions between the two proteins at this ionic strength. These two observations also suggest that cyt b_5-substrate-free CYP2B4 predominantly comprises encounter complexes. The salt screening effect caused by high ionic strength should thus lead to a markedly reduced lifetime of these encounter complexes,[47,48] thereby leaving insufficient time for the necessary re-orientation of the two partners that would allow for the formation the well-defined stereospecific complex(es)[15]. For cyt b_5-substrate-free CYP2B4, the probability of reaching the stereospecific complex(es) is therefore greatly reduced with increasing ionic strength, and this explains the observation that the cyt b_5-substrate-free CYP2B4 complexes are nearly all dissociated at 400 mM NaCl. In contrast, at the same ionic strength (400 mM NaCl), cyt b_5-BHT-bound CYP2B4 still exhibits ~50% reduction in intensity (on average) relative to free cyt b_5 intensities (Fig. 4.5, red) and a very localized binding interface on cyt b_5 (Fig. 4.4F), indicating high affinity and specificity even at 400 mM NaCl. Since the stereospecific complexes are affected by ionic strength to a lesser extent than encounter complexes, this observation could be attributed to a higher population ratio of stereospecific/encounter complexes due to the equilibrium shift induced by BHT, as mentioned above. By looking at the binding interface observed at the titration point of 400 mM NaCl (Fig. 4.4F), we should therefore be able to better define the stereospecific interaction interface of cyt b_5.

4.5.3 Identification of cyt b_5 residues involved in specific interactions with CYP2B4

Cyt b_5 residues hardly perturbed by ionic strength changes are likely to be involved in short-range specific interactions with CYP2B4 due to the relatively more closely packed binding interface of the stereospecific complexes.[16] Following the relative intensity increase, ΔI, for each cyt b_5 residue, at each step of NaCl titration into cyt b_5-BHT-bound CYP2B4, we are able to narrow down the number of residues that are most likely involved in specific interactions with CYP2B4 to D65, V66, T70, D71 and A72. These residues experience small changes in intensity (ΔI more than one standard deviation below ΔI_{avg}) with increasing ionic strength throughout the entire titration (Fig. 4.7). These five residues were previously found at the interface of the cyt b_5-CYP2B4 complex generated by docking studies, with D65 and D71 forming hydrogen bonds and salt bridges with K433/R122 and D134/R133 on CYP2B4 respectively, and V66, T70 and A72 forming van der Waals interactions with K433/R125, A130/D134/G136 and R126 on CYP2B4 respectively.[24] D65 and V66 have also been shown by a mutagenesis study to be essential for the

formation of productive complexes between cyt b_5 and CYP2B4.[24] Although our identification of D71 as a likely interfacial residue is discrepant with published mutagenesis results demonstrating D71 to be unimportant for cyt b_5 binding to CYP2B4,[24] it is not uncommon for interfacial residues to contribute insignificant free energy of binding.[49] In contrast to cyt b_5-BHT-bound CYP2B4, no residue maintained weak salt dependence throughout the NaCl titration of cyt b_5-substrate-free CYP2B4 (Fig. 4.6), which could be attributable to the more pronounced encounter complex character of this complex, due to the larger encounter complex population.

4.6 Conclusion

In conclusion, our study demonstrates the importance of electrostatic interactions in complex formation between cyt b_5 and CYP2B4, both substrate-free and BHT-bound, as indicated by the ionic strength dependence of cyt b_5 resonance intensities. A comparison of the ionic strength dependence between cyt b_5-substrate-free CYP2B4 and cyt b_5-BHT-bound CYP2B4 reveals a higher ratio of stereospecific to encounter complex populations when CYP2B4 is BHT-bound. This finding suggests the ability of BHT to promote specific interactions between the two proteins, likely through conformational modulation of CYP2B4, which might lead to more efficient electron transfer and substrate turn-over. Additionally, five cyt b_5 residues, namely D65, V66, T70, D71 and A72 are identified to be most likely involved in specific interactions with CYP2B4, providing structural insights into the interactions between cyt b_5 and BHT-bound CYP2B4.

4.7 Reference

1. Dürr, U. H. N., Waskell, L. & Ramamoorthy, A. The cytochromes P450 and b5 and their reductases--promising targets for structural studies by advanced solid-state NMR spectroscopy. *Biochim. Biophys. Acta* **1768,** 3235–59 (2007).
2. Guengerich, F. P., Wu, Z.-L. & Bartleson, C. J. Function of human cytochrome P450s: characterization of the orphans. *Biochem. Biophys. Res. Commun.* **338,** 465–9 (2005).
3. Nebert, D. W. & Russell, D. W. Clinical importance of the cytochromes P450. *Lancet* **360,** 1155–62 (2002).
4. Danielson, P. B. The cytochrome P450 superfamily: biochemistry, evolution and drug metabolism in humans. *Curr. Drug Metab.* **3,** 561–597 (2002).

5. Ortiz de Montellano, P. R. Hydrocarbon hydroxylation by cytochrome P450 enzymes. *Chem. Rev.* **110,** 932–48 (2010).
6. Guengerich, F. P. Cytochrome P450s and other enzymes in drug metabolism and toxicity. *AAPS J.* **8,** E101–11 (2006).
7. Konopka, K. The Stoichiometry of the Cytochrome P-450-catalyzed Metabolism of Methoxyflurane and Benzphetamine in the Presence and Absence of Cytochrome b(5). *J. Biol. Chem.* **270,** 24707–24718 (1995).
8. Zhang, H., Hamdane, D., Im, S.-C. & Waskell, L. Cytochrome b5 inhibits electron transfer from NADPH-cytochrome P450 reductase to ferric cytochrome P450 2B4. *J. Biol. Chem.* **283,** 5217–25 (2008).
9. Im, S.-C. & Waskell, L. The interaction of microsomal cytochrome P450 2B4 with its redox partners, cytochrome P450 reductase and cytochrome b(5). *Arch. Biochem. Biophys.* **507,** 144–53 (2011).
10. Hulsker, R., Baranova, M. V, Bullerjahn, G. S. & Ubbink, M. Dynamics in the transient complex of plastocyanin-cytochrome f from Prochlorothrix hollandica. *J. Am. Chem. Soc.* **130,** 1985–91 (2008).
11. Bashir, Q., Scanu, S. & Ubbink, M. Dynamics in electron transfer protein complexes. *FEBS J.* **278,** 1391–400 (2011).
12. Worrall, J. A. R. *et al.* Myoglobin and cytochrome b5: a nuclear magnetic resonance study of a highly dynamic protein complex. *Biochemistry* **41,** 11721–30 (2002).
13. Schreiber, G. & Fersht, A. R. Rapid, electrostatically assisted association of proteins. *Nat. Struct. Biol.* **3,** 427–431 (1996).
14. Crowley, P. B. & Ubbink, M. Close encounters of the transient kind: protein interactions in the photosynthetic redox chain investigated by NMR spectroscopy. *Acc. Chem. Res.* **36,** 723–30 (2003).
15. Ubbink, M. The courtship of proteins: understanding the encounter complex. *FEBS Lett.* **583,** 1060–6 (2009).
16. Suh, J.-Y., Tang, C. & Clore, G. M. Role of electrostatic interactions in transient encounter complexes in protein-protein association investigated by paramagnetic relaxation enhancement. *J. Am. Chem. Soc.* **129,** 12954–5 (2007).
17. Zhang, H., Myshkin, E. & Waskell, L. Role of cytochrome b5 in catalysis by cytochrome

P450 2B4. *Biochem. Biophys. Res. Commun.* **338,** 499–506 (2005).

18. Finn, R. D. *et al.* Defining the in Vivo Role for cytochrome b5 in cytochrome P450 function through the conditional hepatic deletion of microsomal cytochrome b5. *J. Biol. Chem.* **283,** 31385–93 (2008).
19. McLaughlin, L. A., Ronseaux, S., Finn, R. D., Henderson, C. J. & Roland Wolf, C. Deletion of microsomal cytochrome b5 profoundly affects hepatic and extrahepatic drug metabolism. *Mol. Pharmacol.* **78,** 269–78 (2010).
20. Zhang, H., Im, S.-C. & Waskell, L. Cytochrome b5 increases the rate of product formation by cytochrome P450 2B4 and competes with cytochrome P450 reductase for a binding site on cytochrome P450 2B4. *J. Biol. Chem.* **282,** 29766–76 (2007).
21. Gruenke, L. D., Konopka, K., Cadieu, M. & Waskell, L. The stoichiometry of the cytochrome P-450-catalyzed metabolism of methoxyflurane and benzphetamine in the presence and absence of cytochrome b5. *J. Biol. Chem.* **270,** 24707–18 (1995).
22. Tamburini, P., White, R. & Schenkman, J. Chemical characterization of protein-protein interactions between cytochrome P-450 and cytochrome b5. *J. Biol. Chem.* **260,** 4007–4015 (1985).
23. Estrada, D. F., Laurence, J. S. & Scott, E. E. Substrate-modulated cytochrome P450 17A1 and cytochrome b5 interactions revealed by NMR. *J. Biol. Chem.* **288,** 17008–18 (2013).
24. Ahuja, S. *et al.* A model of the membrane-bound cytochrome b5-cytochrome P450 complex from NMR and mutagenesis data. *J. Biol. Chem.* **288,** 22080–95 (2013).
25. Shah, M. B. *et al.* A structural snapshot of CYP2B4 in complex with paroxetine provides insights into ligand binding and clusters of conformational states. *J. Pharmacol. Exp. Ther.* **346,** 113–20 (2013).
26. Zhang, H. *et al.* Potent mechanism-based inactivation of cytochrome P450 2B4 by 9-ethynylphenanthrene: implications for allosteric modulation of cytochrome P450 catalysis. *Biochemistry* **52,** 355–64 (2013).
27. Shah, M. B. *et al.* Conformational adaptation of human cytochrome P450 2B6 and rabbit cytochrome P450 2B4 revealed upon binding multiple amlodipine molecules. *Biochemistry* **51,** 7225–7238 (2012).
28. Gay, S. C. *et al.* Structural Analysis of Mammalian Cytochrome P450 2B4 Covalently Bound to the Mechanism-Based Inactivator tert-Butylphenylacetylene: Insight into Partial

Enzymatic Activity. *Biochemistry* **50,** 4903–4911 (2011).

29. Wilderman, P. R. *et al.* Plasticity of cytochrome P450 2B4 as investigated by hydrogen-deuterium exchange mass spectrometry and X-ray crystallography. *J. Biol. Chem.* **285,** 38602–11 (2010).
30. Gay, S. C. *et al.* Structures of cytochrome P450 2B4 complexed with the antiplatelet drugs ticlopidine and clopidogrel . *Biochemistry* **49,** 8709–20 (2010).
31. Gay, S. C., Sun, L., Maekawa, K., Halpert, J. R. & Stout, C. D. Crystal structures of cytochrome P450 2B4 in complex with the inhibitor 1-biphenyl-4-methyl-1H-imidazole: ligand-induced structural response through alpha-helical repositioning. *Biochemistry* **48,** 4762–71 (2009).
32. Zhao, Y. *et al.* Structural and thermodynamic consequences of 1-(4-chlorophenyl)imidazole binding to cytochrome P450 2B4. *Biochemistry* **46,** 11559–11567 (2007).
33. Zhao, Y. *et al.* Structure of microsomal cytochrome P450 2B4 complexed with the antifungal drug bifonazole: insight into P450 conformational plasticity and membrane interaction. *J. Biol. Chem.* **281,** 5973–81 (2006).
34. Scott, E. E. *et al.* Structure of mammalian cytochrome P450 2B4 complexed with 4-(4-chlorophenyl)imidazole at 1.9-A resolution: insight into the range of P450 conformations and the coordination of redox partner binding. *J. Biol. Chem.* **279,** 27294–301 (2004).
35. Scott, E. E. *et al.* An open conformation of mammalian cytochrome P450 2B4 at 1.6-A resolution. *Proc. Natl. Acad. Sci. U. S. A.* **100,** 13196–201 (2003).
36. Mulrooney, S. B. & Waskell, L. High-level expression in Escherichia coli and purification of the membrane-bound form of cytochrome b5. *Protein Expr. Purif.* **19,** 173–178 (2000).
37. Bridges, A. *et al.* Identification of the binding site on cytochrome P450 2B4 for cytochrome b5 and cytochrome P450 reductase. *J Biol Chem* **273,** 17036–17049 (1998).
38. Dürr, U. H. N., Yamamoto, K., Im, S.-C., Waskell, L. & Ramamoorthy, A. Solid-state NMR reveals structural and dynamical properties of a membrane-anchored electron-carrier protein, cytochrome b5. *J. Am. Chem. Soc.* **129,** 6670–1 (2007).
39. T. D. Goddard and D. G. Kneller, SPARKY 3, University of California, San Francisco.
40. Voznesensky, a I. & Schenkman, J. B. The cytochrome P450 2B4-NADPH cytochrome P450 reductase electron transfer complex is not formed by charge-pairing. *J. Biol. Chem.* **267,** 14669–14676 (1992).

41. Adam, G. & Delbruck, M. Reduction of dimensionality in biological diffusion processes in: Structural Chemistry and Molecular Biology (Rich, A. and Davidson, N., Ed.). 198 – 215 (1968).
42. Crowley, P. B. *et al.* The interactions of cyanobacterial cytochrome c6 and cytochrome f, characterized by NMR. *J. Biol. Chem.* **277,** 48685–9 (2002).
43. Hervás, M., Navarro, J. A., Díaz, A. & De la Rosa, M. A. A comparative thermodynamic analysis by laser-flash absorption spectroscopy of photosystem I reduction by plastocyanin and cytochrome c6 in Anabaena PCC 7119, Synechocystis PCC 6803 and Spinach. *Biochemistry* **35,** 2693–8 (1996).
44. Schreiber, G. & Fersht, A. R. Interaction of barnase with its polypeptide inhibitor barstar studied by protein engineering. *Biochemistry* **32,** 5145–50 (1993).
45. Garrett, D. S., Seok, Y. J., Peterkofsky, A., Gronenborn, A. M. & Clore, G. M. Solution structure of the 40,000 Mr phosphoryl transfer complex between the N-terminal domain of enzyme I and HPr. *Nat. Struct. Biol.* **6,** 166–73 (1999).
46. Halpert, J. R. Structure and function of cytochromes P450 2B: from mechanism-based inactivators to X-ray crystal structures and back. *Drug Metab. Dispos.* **39,** 1113–21 (2011).
47. Sheinerman, F. B., Norel, R. & Honig, B. Electrostatic aspects of protein-protein interactions. *Curr. Opin. Struct. Biol.* **10,** 153–159 (2000).
48. Janin, J. The kinetics of protein-protein recognition. *Proteins* **28,** 153–61 (1997).
49. Clackson, T. & Wells, J. A. A hot spot of binding energy in a hormone-receptor interface. *Science* **267,** 383–6 (1995).
50. Dolinsky, T. J. *et al.* PDB2PQR: expanding and upgrading automated preparation of biomolecular structures for molecular simulations. *Nucleic Acids Res.* **35,** W522–5 (2007).
51. Dolinsky, T. J., Nielsen, J. E., McCammon, J. A. & Baker, N. A. PDB2PQR: an automated pipeline for the setup of Poisson-Boltzmann electrostatics calculations. *Nucleic Acids Res.* **32,** W665–7 (2004).
52. DeLano, W. L. The PyMOL Molecular Graphics System, Version 1.5.0.4 Schrödinger, LLC. (2010). at <http://www.pymol.org/citing>
53. Baker, N. A., Sept, D., Joseph, S., Holst, M. J. & McCammon, J. A. Electrostatics of nanosystems: application to microtubules and the ribosome. *Proc. Natl. Acad. Sci. U. S. A.* **98,** 10037–41 (2001).

CHAPTER 5

Investigation on complex formation between the FMN binding domain of cytochrome P450 reductase and cytochrome P450, as well as the competitive binding mechanism in an trFBD-cyt P450-cyt b_5 tertiary protein system*

5.1 Summery

Electron transfer from cytochrome P450 reductase (CPR) and cytochrome b_5 (cyt b_5) to cytochromevP450s (cyt P450s) are essential steps in the catalytic cycle of the cyt P450 enzymes. A complete understanding of the electron transfer processes require detailed structural and dynamic information of the protein complexes. In this study, the structure and dynamics of (1) the FMN binding domain of CPR (trFBD) expressed and purified from E. coli; (2) the interaction between trFBD and cyt P450 2B4; (3) the interaction between cyt b_5 and cyt P450 2B4; and (4) the interplay among all three proteins in a tertiary trFBD-cyt P450-cyt b_5 system were investigated by solution NMR approaches. Analysis on differential line-broadening and solvent PRE results reveals residues of trFBD located surrounding the solvent exposed edge of the FMN cofactor to be potentially on the binding interface with cyt P450. Using HADDOCK and HARLEM programs, a trFBD-cyt P450 2B4 complex model was generated based on NMR restraints as well as previous mutagenesis studies, and an electron transfer pathway was predicted based on the complex structure. The proposed model allows identification of potential interactions including salt bridges, hydrogen bonds and van der Waals contacts on the binding interface and residues that are important for complex formation. Effect of substrates on complex formation was investigated for both cyt P450-trFBD and cyt P450-cyt b_5, which reveals distinct substrate modulation patterns between the two complexes. While most substrates enhance cyt P450-cyt b_5 interactions, complex

* This thesis research was supported by funds from the National Institutes of Health (NIH to A.R.).

formation between cyt P450 and trFBD is minimally affected by the substrates involved in the current study. Investigation on the tertiary trFBD-cyt P450-cyt b_5 system implies competitive binding between cyt b_5 and trFBD for P450, which is also regulated by different substrates. Enhancement of P450-cyt b_5 interaction by the substrate benzphetamine results in almost 100% dissociation of cyt P450-trFBD complexes in the tertiary system. Inhibition of cyt P450-trFBD interaction could result in inhibition of the first electron transfer step in the catalytic cycle of cyt P450, thereby contributes to a decrease in cyt P450 activity. In contrast, cyt P450-trFBD complexes remain partially bound in the presence of the substrate methoxyflurane in the tertiary system. These results explain why cyt b_5 stimulation effect on cyt P450 activity is different for different substrates. Our study unravels the mechanism of substrate regulation on the tertiary trFBD-cyt P450-cyt b_5 system, providing insights into the structural basis of the interplay of the three redox partners.

5.2 Introduction

Cytochrome P450s (cyt P450s) are a ubiquitous superfamily of enzymes found in all eukaryotes and most prokaryotes. They are responsible for metabolizing a dazzling array of exogenous and endogenous compounds, including carcinogens, steroids, hormones, and over 75% of the pharmaceuticals on the current market.[1–5] To complete the catalytic cycle of cyt P450s, two electrons are required to be delivered to cyt P450 from its redox partners.[6] For mammalian cyt P450s, there are two redox partners: cytochrome P450 reductase (CPR) and cytochrome b_5 (cyt b_5). While cyt b_5 is only capable of transferring the second electron to the oxyferrous cyt P450 due to its high redox potential (~ 25 mV) compared to the ferric cyt P450 (~ -330 mV), CPR is able to donate both the first and the second electron to cyt P450, which renders CPR essential to cyt P450 activities. [7,8]

CPR is a ~ 78 kDa multi-domain protein comprise of four major domains: an FAD/NADPH binding domain, an FMN binding domain, a connecting domain that links the aforementioned two domains together, and an N-terminus hydrophobic transmembrane domain. CPR shuttles electrons from the electron donor NADPH to the electron acceptor cyt P450 via the following pathway: NADPH → FAD → FMN → the heme iron of cyt P450, which involves both inter-domain and inter-protein electron transfers. The FMN binding domain thereby serves as the effective inter-protein electron transfer domain for cyt P450. In the crystal structure of CPR, the FMN binding

domain is buried deeply inside in close proximity to the FAD cofactor with an inter-flavin distance of 4 Å, which allows fast inter-domain electron transfers.[9–13] However, the deeply buried non-solvent-exposed FMN cofactor is not in an optimal orientation for donating electrons to cyt P450. It has been hypothesized that CPR goes through domain movement to coordinate both inter-domain and inter-protein electron transfer processes.[14–19] Numerous studies have been carried out in order to understand the interaction between cyt P450 and CPR, including site-directed mutagenesis studies,[20–25] cross-linking in combination with mass spectroscopy studies,[26] chemical modifications,[27,28] kinetic studies,[29–32] *etc*. These studies imply the critical role of electrostatic interactions between the positively charged concave proximal surface of cyt P450 and the negatively charged surface of the FMN binding domain of CPR. In addition, hydrophobic residues on cyt P450 have also been found to be involved in complex formation with CPR. Better understanding of cyt P450 – CPR complex formation and the electron transfer pathway from the FMN cofactor to the heme necessitates a high resolution complex structure. In the current study, NMR experiments have been performed to map out residue specific binding interface on the FMN binding domain of CPR, which, together with previously reported mutagenesis data on the binding interface on cyt P450 2B4, were used as experimental restraints for generating the complex structure of trFBD – cyt P450 2B4 using HADDOCK. This structure provides detailed information on the binding interface of both proteins and interactions involved in complex formation. An electron transfer pathway was subsequently predicted based on the complex structure indicating Met122 and Arg123 of cyt P450 2B4 are involved in shuttling the electron from FMN to the heme iron.

Cyt b_5 is a 134 amino acid amphipathic protein with a molecular weight of ~ 17 kDa. It is composed of a heme-containing soluble domain, a hydrophobic transmembrane domain and a 15 amino acid flexible linker connecting the aforementioned two domains together. As mentioned above, cyt b_5 is only able to donate the second electron to cyt P450 due to its high redox potential. The role of cyt b_5 in cyt P450 activities is very perplexing, since it has been reported to stimulate, inhibit or not affect cyt P450 activities depending on the substrates involved, the particular isoform of cyt P450, the experimental conditions, *etc.* [6,33–35] It has been found that rabbit cyt b_5 stimulates cyt P450 2B4 activities to different extents with different substrates: 8.5 fold increase in activity for the substrate methoxyflurane and 1.3 fold for the substrate benzphetamine.[6] To understand the mechanism of how substrates affect the role of cyt b_5 in the activities of cyt P450, it is necessary

carry out thorough investigations into the effect of substrates on complex formation between cyt b_5 and cyt P450, complex formation between trFBD and cyt P450, and eventually the interplay of the three proteins in a trFBD – cyt P450 – cyt b_5 tertiary protein system. In the current study, we have utilized solution NMR technologies to look into substrate regulation on both the binary and the tertiary protein systems at the atomic level resolution, based on which we were able to unravel of mechanism behind the perplexing behavior of cyt b_5 during cyt P450 catalysis process.

5.3 Materials and Methods

5.3.1 Materials

E. coli C41 cells for protein overexpression were purchased from Lucigen (Middleton, MI). Yeast extract, tryptone for unlabeled growth media were purchased from Sigma-Aldrich. [^{15}N] ammonium chloride, [^{13}C] glucose, [^{13}C, ^{15}N] CELTONE rich medium powder and D_2O were purchased from Cambridge Isotope Laboratories (Andover, MA). Resins, buffer components, and all the other chemicals were purchased from Sigma-Aldrich. Glycerol used in NMR experiments was purchased from Roche Applied Science. Gd-DTPA-BMA was a kind gift from Dr. Tobias Madl (Technische Universität München).

5.3.2 Expression and purification of the soluble FMN binding domain of rat CPR

The U-^{13}C, ^{15}N-labeled soluble FMN binding domain (residue 57-239) (trFBD) was expressed and purified from *E. coli* C41 cells, which were transformed with a pSC-rat CPR plasmid containing the FBD gene.[20] The transformed cells were first adapted in 100mL Luria Bertani (LB) medium for 4 – 5 hours before inoculation into 1 L M9 minimal medium (40 mM Na_2HPO_4, 20 mM KH_2PO_4, 8.5 mM NaCl, 1 g $^{15}NH_4Cl$, 4 g [^{13}C] glucose, 0.2 g [^{13}C, ^{15}N] CELTONE rich medium powder, 1 mM $MgSO_4$, 100 μM $CaCl_2$, 16 nM riboflavin, trace elements and full vitamin) at a starting OD_{600} value of 0.1. Induction of expression of trFBD was carried out when the OD_{600} value reach 0.7 – 0.8 with 0.4 mM isopropyl β-D-1-thiogalactopyranoside (IPTG). The cell culture was then incubated at 30 °C for 10 – 12 hours with a shaking speed of 180 rpm. Afterwards, the cells were harvested at 4 °C and the cell pellet was re-suspended into 50 mM Tris-acetate buffer (pH 6.7 at room temperature) containing 30 μg/mL chicken egg lysozyme on ice for 30 min. The lysate was centrifuged and the pellet was re-suspended into 100 mM Tris-acetate

buffer (pH 6.7 at room temperature) containing Complete-Mini protease tablets on ice for sonication. Ultracentrifugation was then performed and the supernatant containing trFBD was collected and loaded to DEAE Sepharose column equilibrated with loading buffer (50 mM Tris-acetate, 0.1 mM EDTA, 0.2 mM DTT, 10 % glycerol, 1 μM FMN, pH 6.7 at room temperature). The column was first washed with 0.2 M NaCl in loading buffer and then gradient elution was performed in the range of 0.2 – 0.3 M NaCl in loading buffer. The U-^{15}N-labeled trFBD was expressed with unlabeled glucose and [^{15}N] CELTONE rich medium powder. For expression of unlabeled trFBD, the adapted cells were inoculated to 1 L LB medium at a starting OD_{600} value of 0.03 and induced at OD_{600} = 2. The purified trFBD appeared as a single band on the SDS-polyacrylamide gel. The concentration of the oxidized trFBD was determined using the extinction coefficients 12.2 $mM^{-1}cm^{-1}$ at 454 nm.[36]

Full-length wild-type rabbit cyt P450 2B4 (cyt P450 2B4) and U-^{15}N labeled full-length wild-type rabbit cyt b_5 were expressed and purified individually as described previously [20,37–39].

5.3.3 Solution NMR experiments

All solution NMR experiments were carried out at 298 K in NMR buffer (40 mM potassium phosphate, 10% D_2O, pH 7.4). All NMR data was processed by Topspin 2.1 (Bruker) and analyzed in Sparky[40].

5.3.3.1 Sequence specific assignment

Sequence specific assignment of ^{1}HN, ^{15}N, ^{13}Cα, ^{13}Cβ and ^{13}CO backbone resonances of trFBD was achieved using a set of TROSY-based 3D HNCO, HNCA, HNCACB and CBCA(CO)NH experiments on U-^{13}C, ^{15}N-trFBD.[41,42] Two-dimensional ^{1}H/^{15}N TROSY-HSQC spectra were periodically acquired to check the stability of the protein sample in between the 3D experiments. All of these experiments were performed on a Bruker 900 MHz NMR spectrometer equipped with a 5 mm triple-resonance TXI cryo-probe.

5.3.3.2 Interaction between trFBD and cyt P450 2B4

Mapping of the binding interface on trFBD for interaction with cyt P450 2B4 was achieved by a combination of (1) titration of unlabeled cyt P450 2B4 into U-^{15}N-trFBD; (2) solvent PRE

experiments using PRE agent Gd(DTPA)BMA. NMR titration experiments were performed at 298 K on a Bruker Avance II 600 MHz Spectrometer equipped with a cryoprobe. For the titration experiments, spectra were first recorded with 0.1 mM free ^{15}N-trFBD in NMR buffer, followed by a titration of unlabeled cyt P450 2B4 at molar ratios (trFBD : cyt P450 2B4) of 1:0, 1:0.3, 1:0.6, and 1:1. The solvent PRE experiment was carried out by adding 1 mM Gd(DTPA)BMA to a sample containing ^{15}N-trFBD and unlabeled cyt P450 2B4 at the molar ratio of 1:0.3. NMR experiments were performed before and after addition of Gd(DTPA)BMA.

To investigate the effect of substrates on trFBD – cyt P450 2B4 binding, subtrates BHT, methoxyflurane and benzphetamine were added to the 1:1 ^{15}N-trFBD : cyt P450 2B4 NMR sample at a protein : substrate molar ratio of 1:3 respectively. NMR experiments were performed before and after addition of the substrates.

All NMR experiments were recorded using two-dimensional (2D) ^{1}H/^{15}N TROSY HSQC spectra with 32 scans and 256 t1 increments. The weighted amide chemical shift perturbation ($\Delta\delta_{avg}$) was calculated using the equation below:

$$\Delta\delta_{avg} = \sqrt{(\Delta\delta N \times \frac{F_2\ SW}{F_1\ SW})^2 + \Delta\delta H^2}$$

where $\Delta\delta N$ and $\Delta\delta H$ are the changes in the amide nitrogen and hydrogen chemical shifts respectively, while $F_1\ SW$ and $F_2\ SW$ represent the spectral width in the first and second dimension respectively, all parameters are in ppm [43,44].

5.3.3.3 Substrate modulation on the interaction between cyt b_5 and cyt P450 2B4

To investigate the effects of a range of different substrates on the interaction between cyt b_5 and cyt P450 2B4, similar approaches were applied as detailed in Chapter 4. Briefly, each substrate, including methoxyflurane, benzphetamine and cyclohexane, was added to a 1:1 ^{15}N-cyt b_5 : unlabeled cyt P450 2B4 complex sample, followed by titration of sodium chloride at concentrations of 100, 250 and 400 mM NaCl. 2D ^{1}H/^{15}N TROSY HSQC spectra with 64 scans and 256 t1 increments.

5.3.3.4 Substrate modulation on competitive binding between cyt b_5 and trFBD in the trFBD-cyt P450 2B4-cyt b_5 tertiary protein system

2D $^{1}H/^{15}N$ TROSY HSQC was first recorded on ^{15}N-trFBD with one molar equivalence unlabeled cyt P450 2B4 in the absence or presence of three molar equivalence substrate methoxyflurane or benzphetamine. Then one molar equivalence of unlabeled cyt b_5 was added to the sample, followed by acquisition of 2D $^{1}H/^{15}N$ TROSY HSQC with 32 scans and 256 t1 increments.

5.3.4 Cyt P450 2B4 – trFBD complex structure calculation

HADDOCK 2.2[45,46] program was used to calculate a model of the trFBD-cyt P450 complex based on defined ambiguous restraints. Crystal structures of trFBD (PDB code 1AMO) and cyt P450 2B4 (PDB code 1SUO) were used as starting structures. Ligand and topology files were generated from the PRODRG server.[47] 1000 structures were generated in the rigid body docking step, followed by simulated annealing of 200 lowest-energy structures from the last step and finally the 50 best structures were selected for solvent refinement in an 8.0 Å shell of TIP3P water molecules. The resulting 50 final structures were analyzed and grouped into clusters based on the backbone r.m.s.d. values. Molecular models of the complexes were viewed and graphed using PYMOL.[48]

5.4 Results and Discussion

5.4.1 Backbone sequence assignment of trFBD

With a set of standard 3D backbone resonance assignment experiments, 93.4% of all trFBD residues have been assigned on the 2D $^{1}H/^{15}N$ TROSY HSQC (Figure 5.1). The sequential assignment was achieved via 3D walk through the sequence of trFBD, *e.g.* the pulse sequence of HNCACB experiment links the $^{13}C\alpha$, $^{13}C\beta$ magnetization of the current residue with those of the previous residue, HNCA links the $^{13}C\alpha$ magnetization of the current residue with that of the previous residue double confirming the results from the HNCACB experiments (Figure 5.2). Besides the 6 proline residues which do not show up on a 2D $^{1}H/^{15}N$ TROSY HSQC due to lack of amide proton, residues I57, Q58, T59, D144, F201 and F230 could not be assigned due to their

flexibility and fast exchange of amide proton with solvent. Ambiguous assignments were made for residues R78 and A169, A95 and L122, L98 and V188 because they overlap heavily on HSQC. Minor conformers are found for residues either in flexible loop regions due to their somewhat unrestricted motion of some residues near Phe, Tyr or Trp due to ring-current effects.

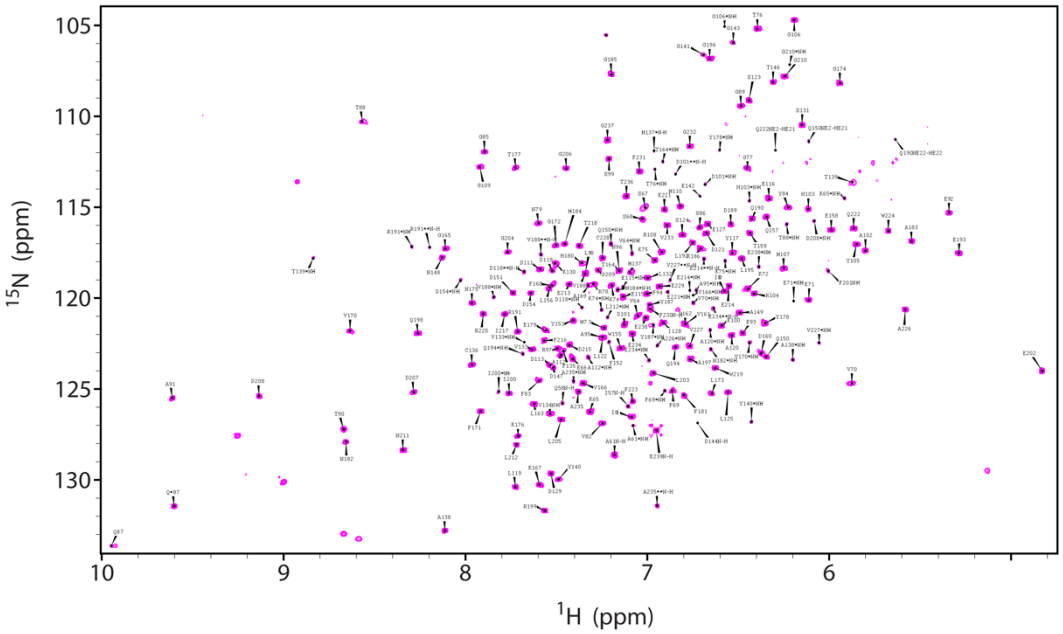

Figure 5.1 Assignment of trFBD backbone resonances on 2D ^{1}H/^{15}N TROSY HSQC.

5.4.2 Interaction between trFBD and cyt P450 2B4 – a complex structural model for trFBD-cyt P450 2B4

In order to better understand complex formation between trFBD and cyt P450, a series of ^{15}N/^{1}H TROSY HSQC NMR spectra were recorded to monitor ^{15}N-trFBD – unlabeled-cyt P450 2B4 interaction. The addition of cyt P450 2B4 to a solution of trFBD leads to significant increase in line-width (Figure 5.3) and moderate chemical shift perturbation ($\Delta\delta_{avg} \leq 0.1$ ppm) for amide resonances of trFBD. The small and wide-spread chemical shift perturbations (CSP) could be occurring for two reasons: first, intermediate chemical exchange between free- and bound-trFBD, which would also explain the overall broadening of trFBD resonances [49,38]; second, the formation of an ensemble of dynamic "encounter complexes" causes the "averaging out" of the chemical shift changes, thus leading to small CSP values [50–54]. At 1:1 molar ratio between the two proteins, nearly half of the resonances fall into noise level, (Figure 5.4) which makes it unreliable to

determine the binding interface at this titration point. Therefore, results from titration points at 1:0.3 and 1:0.6 molar ratio of trFBD to cyt P450 2B4 were utilized for mapping residues potentially involved in interaction with cyt P450. Residues with relative peak heights of more than one standard deviation below the average value are considered to be significantly affected upon interaction with cyt P450 2B4. As presented in Figure 5.5, in which the relative trFBD resonance peak heights are plotted against trFBD residue number at 1:0.3 and 1:0.6 molar ratio with cyt P450 2B4, residues located on the loop region holding the FMN cofactors are mapped out as significantly perturbed upon interaction with cyt P450 2B4 for both molar ratios and therefore are considered to be most likely involved in interaction with cyt P450 among all other trFBD residues. These residues include S86, Q87, T88, E92, which either are directly in contact with cyt P450 2B4 or have changed dynamics indirectly induced by residues in directly contact with cyt P450 2B4.

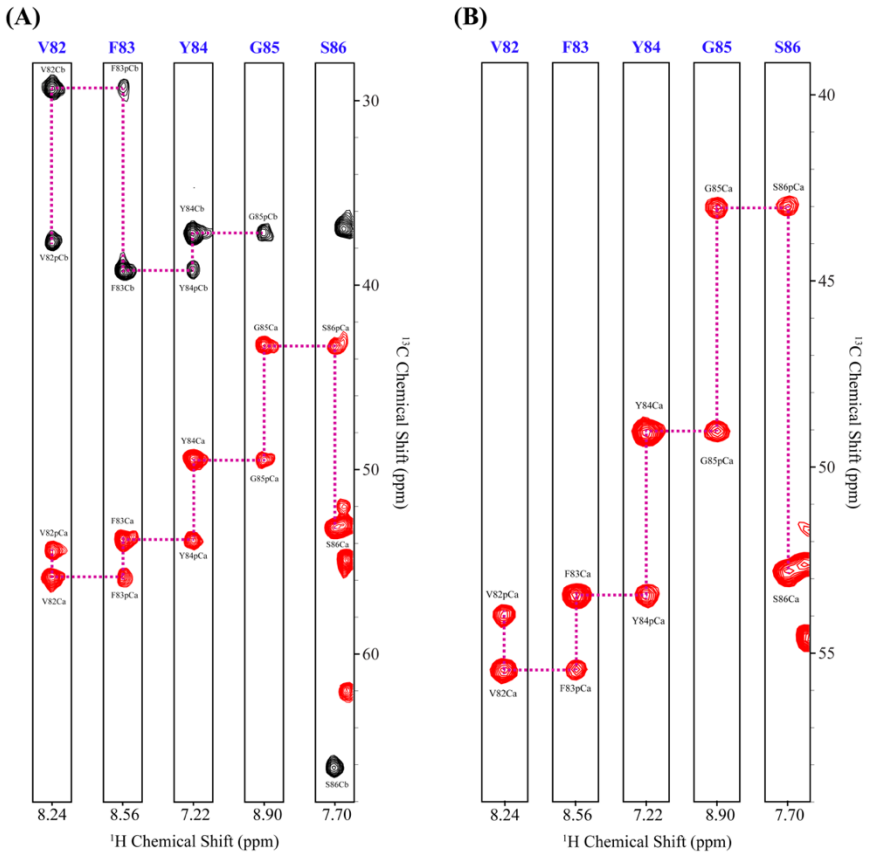

Figure 5.2 Strips of HNCACB (left) and HNCA (right) used to make sequential assignment of trFBD backbone resonances.

Complimentary solvent PRE experiments were performed in order to better identify residues in contact with cyt P450 2B4. The solvent PRE agent Gd(DTPA)BMA induces fast T2

relaxation of residues exposed to solvent leading to line broadening effect of these residues. Therefore, trFBD residues that are solvent exposed on the structure but are in direct contact with cyt P450 2B4 should show minimal line-broadening effect when trFBD forms complex with cyt P450 2B4. The solvent PRE agent was added to a sample containing 1:0.3 molar ratio of 15N-trFBD and cyt P450 2B4, and the resonance intensities of trFBD residues were compared before and after addition of Gd(DTPA)BMA. (Figure 5.6) Residues with high solvent accessibility on the structure of trFBD showing minimal perturbation in line width include: K176, T177, H180, D208, N211. These residues are also located on the loop region surrounding the solvent exposed edge of the FMN cofactor.

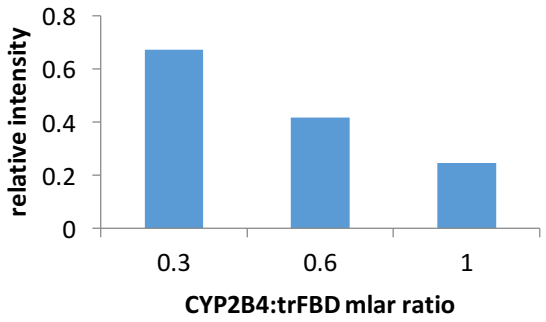

Figure 5.3 Relative average resonance intensities of ^{15}N-trFBD residues at each titration point of cyt P450 2B4.

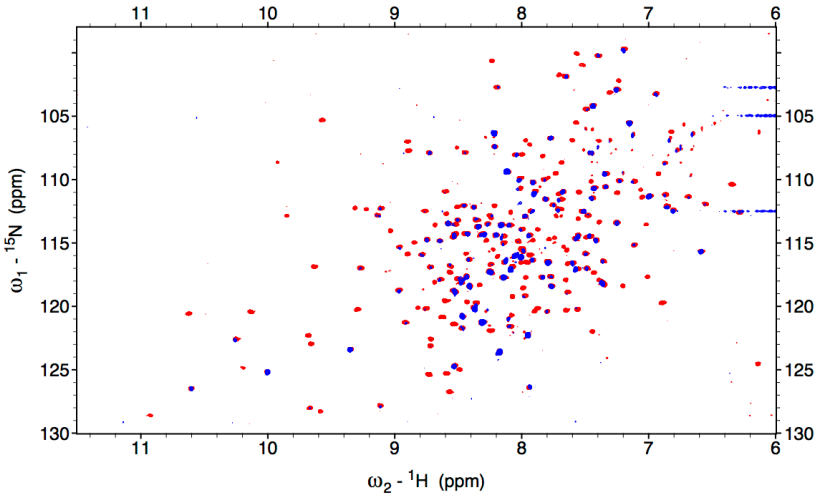

Figure 5.4 Overlay of the HSQC spectrum of 1:1 complex of ^{15}NtrFBD-cyt P450 2B4 (blue) to that of ^{15}NtrFBD alone.

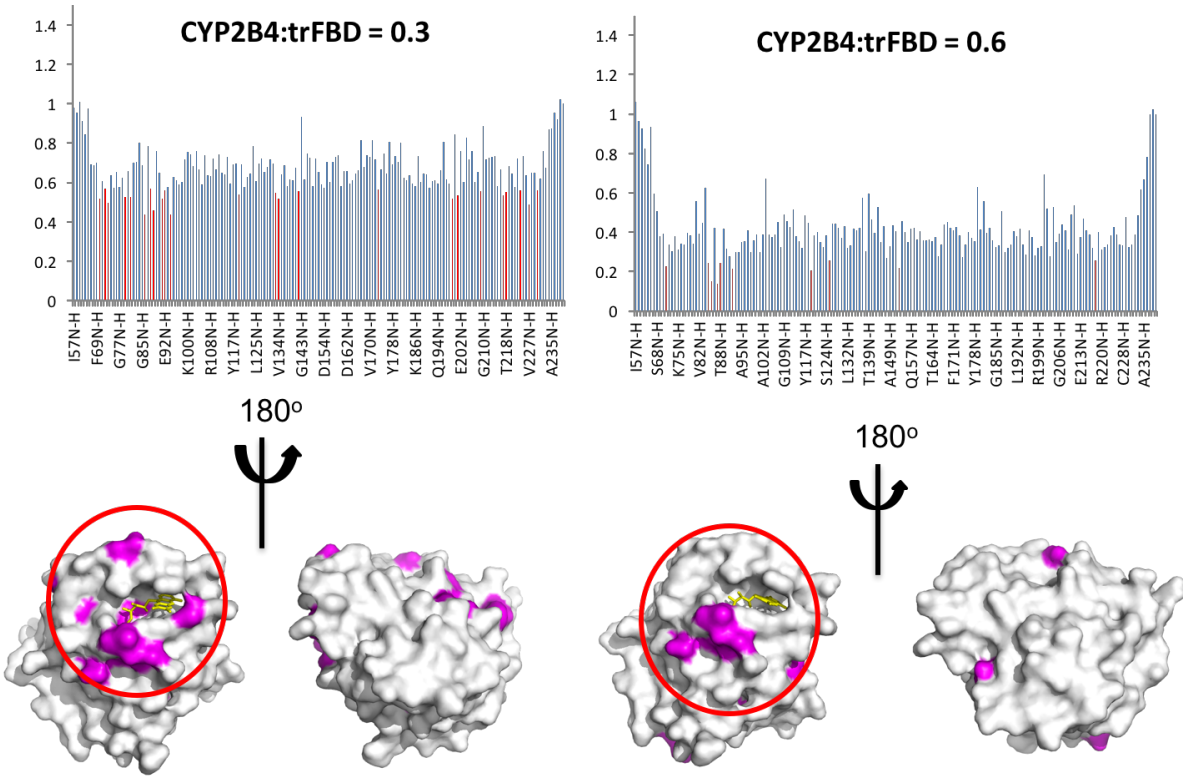

Figure 5.5 Differential line broadening of trFBD resonances upon addition of cyt P450 2B4 at molar ratios of 1:0.3 and 1:0.6.

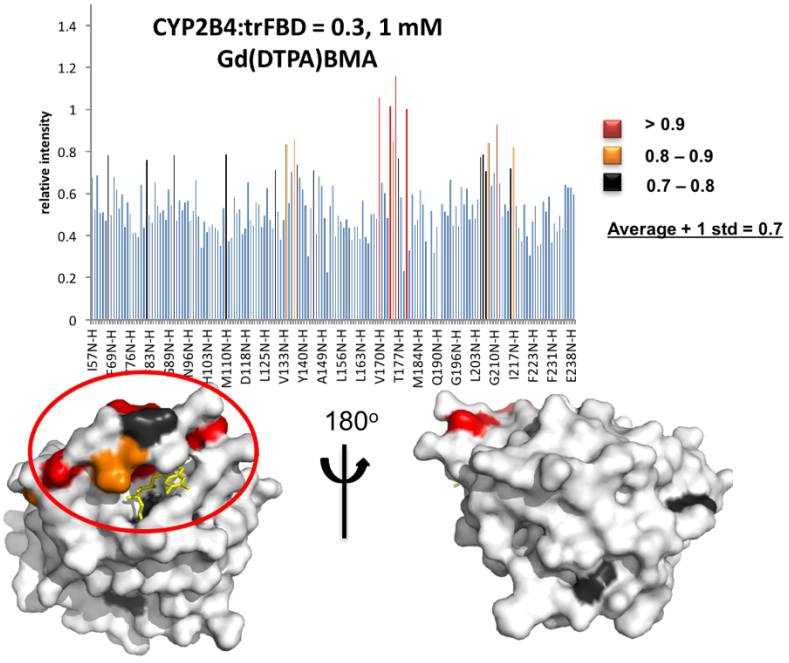

Figure 5.6 Mapping of the binding interface on trFBD from the results of solvent PRE experiments.

In order to generate a complex structure for trFBD-cyt P450 2B4 based on these experimental data, a docking program HADDOCK (High Ambiguity Driven biomolecular DOCKing) was utilized which performs rigid body docking, followed by molecular dynamics simulations allowing flexibility of the side chains of amino acids which improves the complementarity of the binding interface and better defines electrostatic interactions between the two proteins.[45,46] The protein structures used in the docking process are crystal structures of the FMN binding domain part of CPR (PDB 1AMO) and cyt P450 2B4 (PDB 1SUO). The residues mapped out from both differential line broadening analysis and solvent PRE results were used as active ambiguous restraints for trFBD. Residues next to the active ambiguous restraints and also solvent accessible were used as passive restraints. The active ambiguous restraints of cyt P450 2B4 were obtained from a previous mutagenesis study indicating these residues affect binding between CPR and cyt P450 2B4 dramatically.[20] The restraints were carefully selected after the first run of the docking and those that showed violations in more than half of the final 50 structures were removed from the restraint table. The final restraints used for docking the complex structure are listed in Table 5.1.

Table 5.1 Active and passive restraints for trFBD and cyt P450 2B4 used for docking the complex structure by HADDOCK.

	1st molecule (A) - trFBD	2nd molecule (B) – CYP2B4
Active	S86, Q87, T88, E92, K176, T177, H180, D208, N211	Arg-122, Arg-126, Arg-133, Phe-135, Met-137, Lys-139, Arg-422, Lys-433, Arg-443
Passive	G89, T90, Y178, E179, N182, A183, L205, D209, G210, T218	

The docking simulations revealed a major cluster of an ensemble of 34 complex structures in the final 50 lowest-energy structures, which gives an r.m.s.d value of 2.54 Å compared to the lowest-energy structure. As shown in Figure 5.7A, the FMN cofactor and the heme are nearly perpendicular to each other. The shortest edge-to-edge distance between the FMN and the heme is

11.8 Å, well within the 14.0 Å limit predicted for efficient electron transfer.[55] An electron transfer pathway was then predicted based on the complex structure using the program HARLEM.[56] As presented in Figure 5.7B, residues Met132 and Arg133 of cyt P450 2B4 are predicted to be involved in shuttling the electron from the FMN to the heme. Mutation of Arg133 was reported to result in the greatest reduction in binding affinity with CPR out of nine positively charged residue mutations.[20] Residues on the binding interface of trFBD are mostly located on the loops holding the FMN cofactor, including residues Gln-87, Thr-88, Thr-90, Glu-93, Asp-113, Glu-115, Glu-116, Tyr-140, Gly-141, Asp-147, Asn-148, Gln-150, Asn-175, Thr-177, Tyr-178, Glu-179, Asp-208, Asn-211, Glu-213, Glu-214. These residues are mostly negatively charged or polar with no charge. Residues on the binding interface of cyt P450 2B4 are mostly positively charged or hydrophobic, including Arg-126, Leu-129, Ala-130, Arg-133, Asp-134, Phe-135-Lys-139, Ser-141, Glu-143, Glu-144 spanning the most important C helix, C-D loop and D helix, Leu-340, Arg-343 and Ala-344 on J-K loop, Asp-415, Ala-416, Asn-417, Ala-419, Leu-420, Arg-422, Lys-433 and Leu-437 on K-L loop and Gly-440, Glu-439, and Arg-443 on helix L. Salt bridges are observed between Asp-113, Glu-115, Asp-147, Asp-208 and Glu-214 from FBD and Arg-126, Arg-133, Arg-343, Arg-422 from cyt P450. Residues Asp-113 and Glu-115 are conserved through all mammalian and yeast CPRs and have been reported to play important roles in binding cyt P450.[20,23,57,58] Mutation of Asp-208 has been found to result in drastic decrease of cyt P450 activities.[21,22] Hydrogen bonds were observed between Thr-177, Tyr-178 and FMN from FBD and Glu-134, Met-137, Lys-139 and Arg-133 from cyt P450.

In order to investigate the effect of substrates on the interaction between trFBD and cyt P450 2B4, substrates BHT, benzphetamine and methoxyflurane were added to a ^{15}N-trFBD : cyt P450 2B4 = 1:1 NMR sample respectively and 2D ^{1}H/^{15}N TROSY HSQC spectra were compared before and after addition of the substrates. (Figure 5.8) For all three substrates, chemical shift perturbation was very small and thus negligible. All of them led to very slight enhancement in line-broadening of the resonances of trFBD, among which BHT gives to most enhancement while benzphetamine and methoxyflurane are very similar to each other. (Figure 5.9) In general, substrates do not affect trFBD-cyt P450 2B4 interaction much, implying that complex formation between the two redox partners are not modulated by substrates within the scope of the current study.

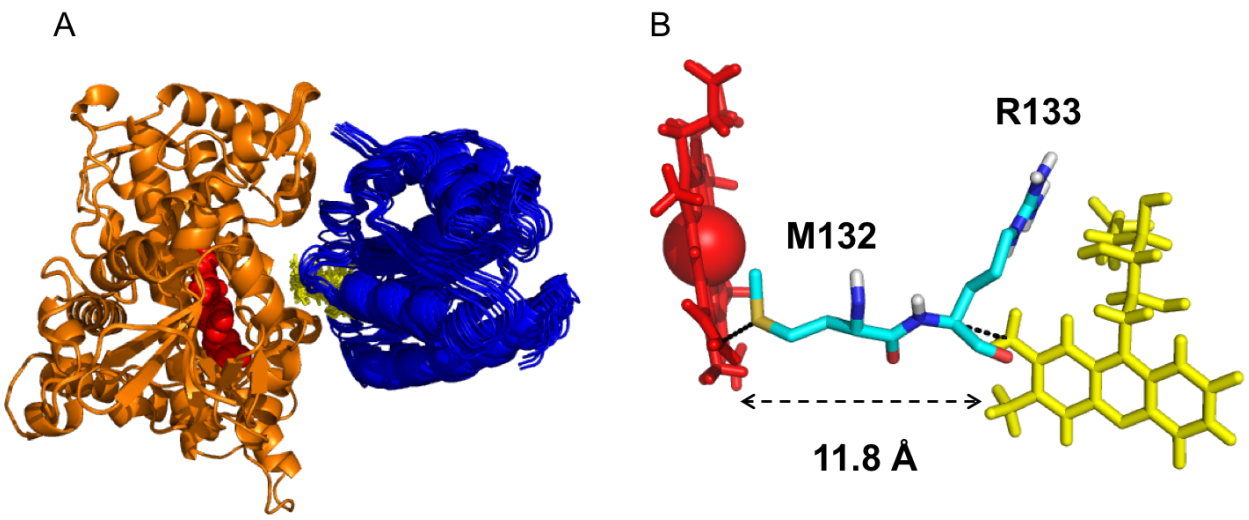

Figure 5.7 Structural model of the cyt P450 2B4-trFBD complex. (A) Overlap of the lowest-energy complex structures from the major cluster, in which cyt P450 2B4 is colored in orange, trFBD in blue, the heme in red spheres and FMN in yellow sticks. (B) The electron transfer pathway predicted by HARLEM based on the complex structures in (A).

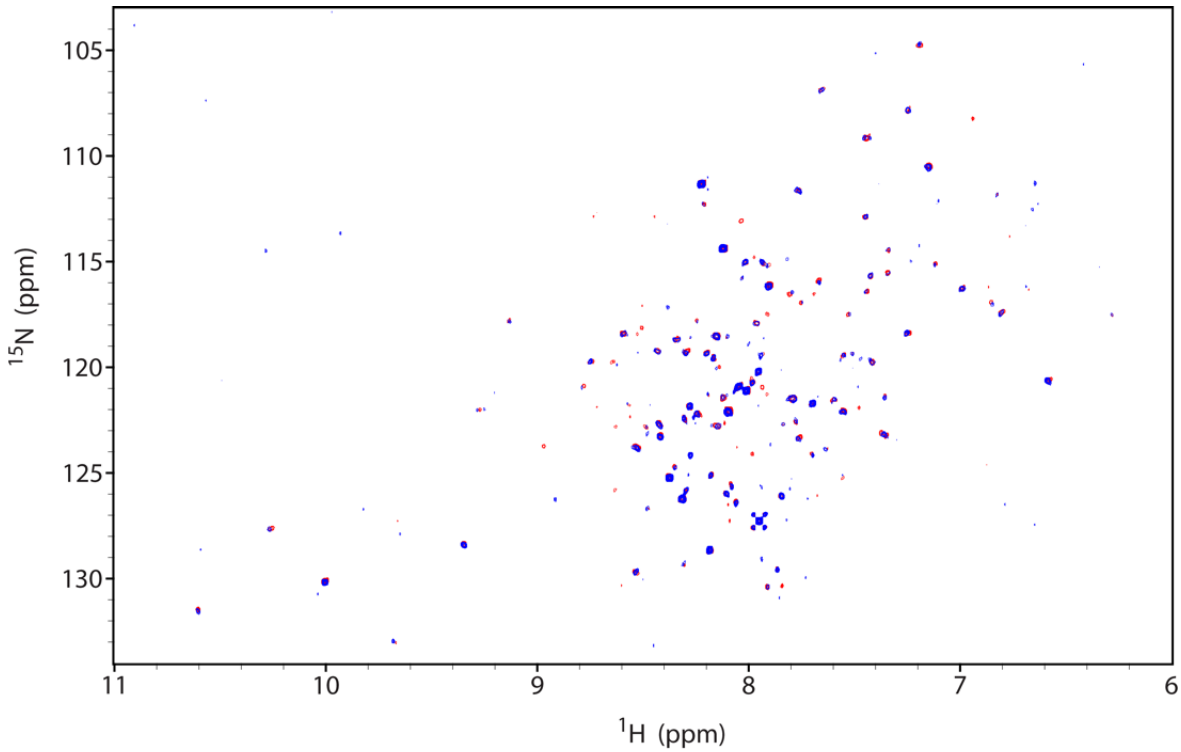

Figure 5.8 Overlay of the HSQC spectrum of 1:1 complex of 15NtrFBD-cyt P450 2B4 with (blue) and without (red) the substrate BHT.

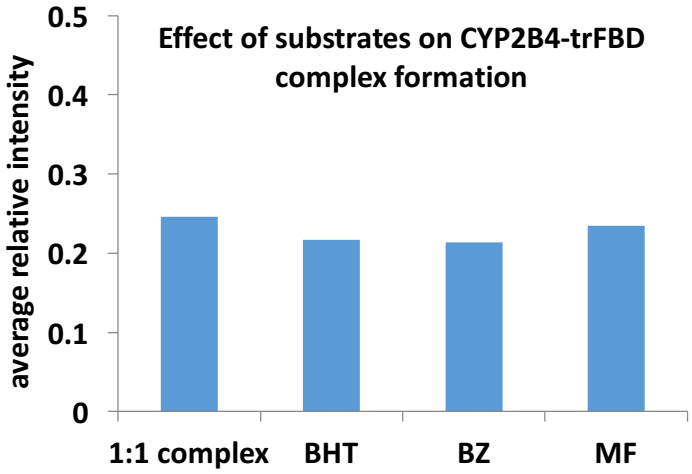

Figure 5.9 Comparison of the average relative intensity of trFBD in complex with cyt P450 2B4 in the absence and presence of different substrates.

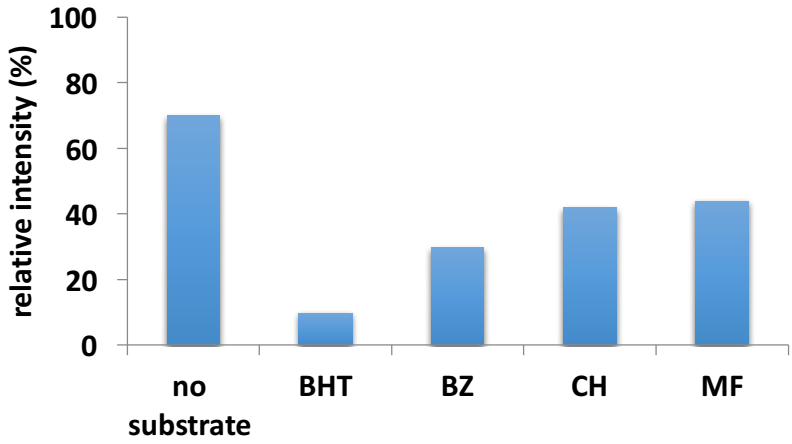

Figure 5.10 Comparison of the average relative intensity of cyt b_5 in complex with cyt P450 2B4 in the absence and presence of different substrates.

5.4.3 Substrate modulation on cyt b_5-cyt P450 2B4 interaction and competitive binding between cyt b_5 and trFBD in a trFBD-cyt P450-cyt b_5 tertiary protein system

In Chapter 4, an approach is introduced to study the effect of the substrate BHT on the interaction between cyt b_5 and cyt P450 2B4. In order to study the effect of a broader range of substrates on cyt b_5 – cyt P450 2B4 complex formation, similar method was applied with addition of each substrate in to a 1:1 ^{15}N-cyt b_5 – cyt P450 2B4 complex sample and titration with NaCl. In general, all substrates led to more extensive line-broadening of cyt b_5 resonances. Among all

substrates studied – BHT, benzphetamin, cyclohexane, methoxyflurane – BHT enhances protein-protein interaction the most, followed by benzphetamine. Cyclohexane and methoxyflurane led to similar enhancement in complex formation. (Figure 5.10) Residues with relative intensity more than one standard deviation below average were considered as significantly perturbed in binding cyt P450 and most likely to be on the binding interface. Residues H44, F63, E64, D65, T70, D71 of cyt b_5 were mapped on the binding interface in the presence of benzphetamine; H44, D65, V66, T70, D71 were mapped out in the presence of cyclohexane; I17, F40, R52, E64, D65, L75 for methoxyflurane. (Figure 11) All of them showed overlap region on the front face of cyt b_5 surrounding the solvent exposed heme edge, especially the on lower cleft, which agrees with what was observed in the absence of substrates. Salt titration experiments indicated that the most specific bindig occurs in the presence of BHT, followed by benzphetaming, and methoxyflurane gives the least specific binding. (Figure 12)

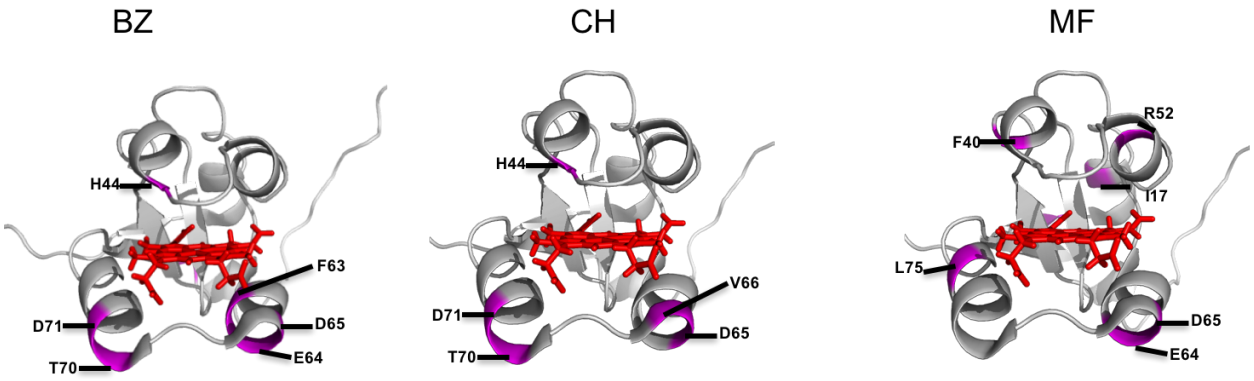

Figure 5.11 Mapping of the binding interface of cyt b_5 in complex with cyt P450 2B4 in different substrates: benzphetamine (left), cyclohexane (middle), methoxyflurane (right).

It has been reported that cyt b_5 stimulates cyt P450 activity to a much higher extent for methoxyflurane than benzphetamine, which is in negative correlation to the interaction strength observed between cyt b_5 and cyt P450 in out study. The reason probably lies in a competitive binding mechanism where cyt b_5 and CPR competes with each other for an overlapping but non-identical binding interface on cyt P450. Since substrates enhance the interaction between cyt b_5 and cyt P450 a lot, while not minimally affect the interaction between trFBD and cyt P450, the first electron transfer step that can only be fulfiled by trFBD might be inhibited due to cyt b_5 occupying cyt P450. In order to test our hypothesis, we added cyt b_5 into a solution containing

15N-trFBD and cyt P450 2B4 in the presence and absence of substrates BHT, benzphetamine and methoxyflurane respectively. Upon addition of cyt b_5, most of the resonances that were broadened out due to interaction with cyt P450 showed increase in intensity dramatically, as shown in Figure 5.13 using BHT as an example. The relative average intensities of trFBD resonances in the absence and presence of different substrates are compared in Figure 5.14, which shows that in the presence of benzphetamine the trFBD is almost 100% in the free trFBD state instead of the bound state, while in the presence of methoxyflurane trFBD still remains partially bound to cyt P450. This finding supports our aforementioned hypothesis for a competitive binding mechasim which is regulated by different substrates.

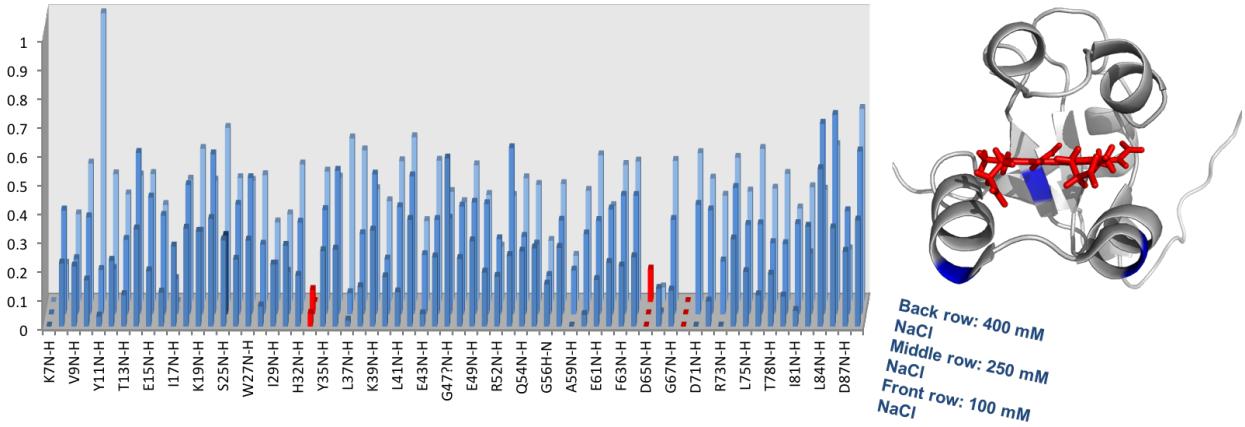

Figure 5.12 Salt titration shows specific binding between cyt b_5 and cyt P450 2B4 in the presence of benzphetamine.

5.5 Conclusion

In summary, we have generated a complex structure for trFBD-cyt P450 using HADDOCK based on both NMR restraints and previous mutagenesis data. An electron transfer pathway has been predicted based on this complex structure indicating that Met132 and R133 are involved in transferring electrons from FMN to the heme of cyt P450 2B4. The interaction between trFBD and cyt P450 2B4 are not influenced much by different substrates. In contrast, interaction between cyt b5 and cyt P450 2B4 are drastically enhanced to different extents depending on different substrates. A competitive binding mechanism is discovered when all three proteins are present in the system, which has been found to be regulated by different substrates as well. This research provides insights on the structural basis into complex formation between trFBD and cyt P450, as well as

the basic mechanism of how the three proteins coordinate with each other for electron transfer processes.

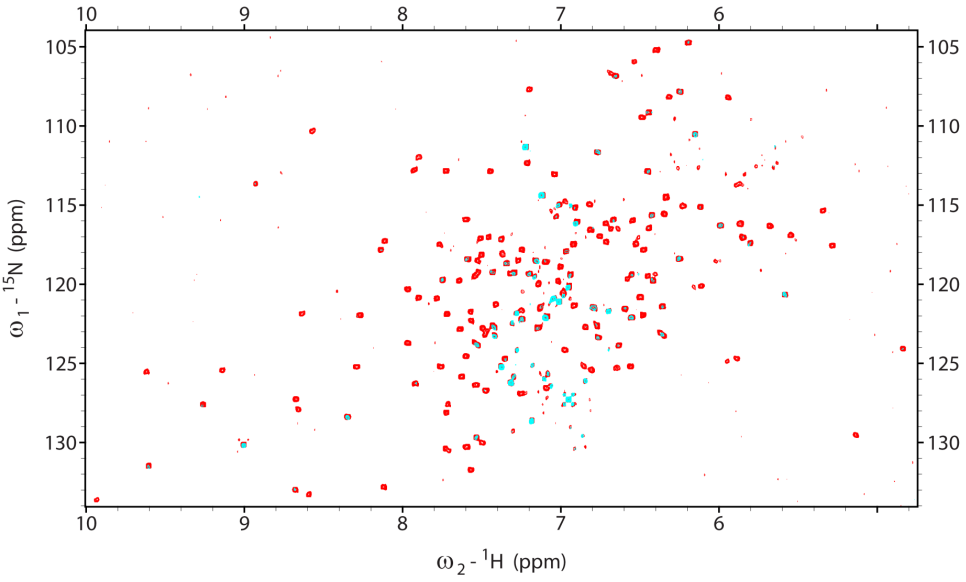

Figure 5.13 Overlay of the HSQC spectrum of 1:1:3 complex of ^{15}NtrFBD-cyt P450 2B4-BHT in the absence (cyan) and presence of one molar equivalence of cyt b_5 (red).

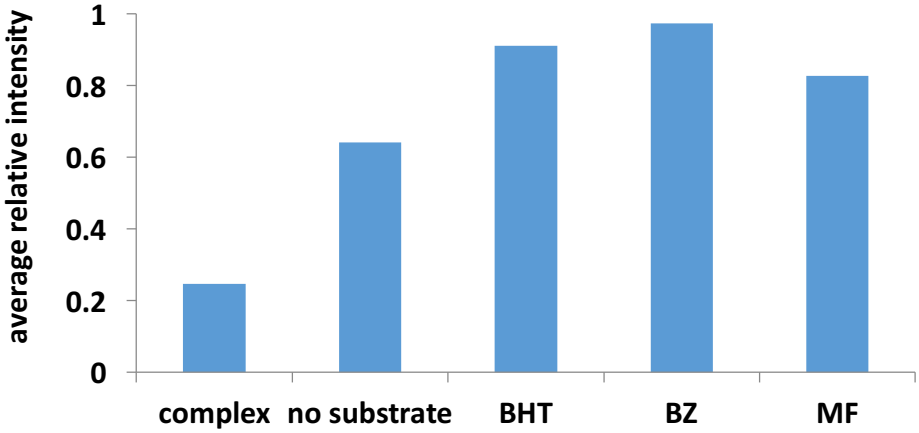

Figure 5.14 Comparison of the average relative intensity of trFBD in complex with substrate-bound cyt P450 2B4 after addition of cyt b_5.

5.6 References

1. Guengerich, F. P. Cytochromes P450, drugs, and diseases. *Mol. Interv.* **3,** 194–204 (2003).
2. Guengerich, F. P. Cytochrome P450s and other enzymes in drug metabolism and toxicity.

AAPS J. **8,** E101–11 (2006).

3. Guengerich, F. P. Cytochrome p450 and chemical toxicology. *Chem. Res. Toxicol.* **21,** 70–83 (2008).
4. Guengerich, F. P., Wu, Z.-L. & Bartleson, C. J. Function of human cytochrome P450s: characterization of the orphans. *Biochem. Biophys. Res. Commun.* **338,** 465–9 (2005).
5. Dürr, U. H. N., Waskell, L. & Ramamoorthy, A. The cytochromes P450 and b5 and their reductases--promising targets for structural studies by advanced solid-state NMR spectroscopy. *Biochim. Biophys. Acta* **1768,** 3235–59 (2007).
6. Im, S.-C. & Waskell, L. The interaction of microsomal cytochrome P450 2B4 with its redox partners, cytochrome P450 reductase and cytochrome b(5). *Arch. Biochem. Biophys.* **507,** 144–53 (2011).
7. Zhang, H., Hamdane, D., Im, S.-C. & Waskell, L. Cytochrome b5 inhibits electron transfer from NADPH-cytochrome P450 reductase to ferric cytochrome P450 2B4. *J. Biol. Chem.* **283,** 5217–25 (2008).
8. Yang, Y. *et al.* Structural and functional characterization of a cytochrome P450 2B4 F429H mutant with an axial thiolate-histidine hydrogen bond. *Biochemistry* **53,** 5080–91 (2014).
9. Wang, M. *et al.* Three-dimensional structure of NADPH-cytochrome P450 reductase: prototype for FMN- and FAD-containing enzymes. *Proc. Natl. Acad. Sci. U. S. A.* **94,** 8411–6 (1997).
10. Page, C. C., Moser, C. C., Chen, X. & Dutton, P. L. Natural engineering principles of electron tunnelling in biological oxidation-reduction. *Nature* **402,** 47–52 (1999).
11. Bhattacharyya, A. K., Lipka, J. J., Waskell, L. & Tollin, G. Laser flash photolysis studies of the reduction kinetics of NADPH:cytochrome P-450 reductase. *Biochemistry* **30,** 759–765 (1991).
12. Gutierrez, A. *et al.* Interflavin electron transfer in human cytochrome P450 reductase is enhanced by coenzyme binding. Relaxation kinetic studies with coenzyme analogues. *Eur. J. Biochem.* **270,** 2612–2621 (2003).
13. Gutierrez, A., Paine, M., Wolf, C. R., Scrutton, N. S. & Roberts, G. C. K. Relaxation kinetics of cytochrome P450 reductase: internal electron transfer is limited by conformational change and regulated by coenzyme binding. *Biochemistry* **41,** 4626–37 (2002).

14. Frances, O. *et al.* A Well-balanced preexisting equilibrium governs electron flux efficiency of a multidomain diflavin reductase. *Biophys. J.* **108,** 1527–1536 (2015).
15. Haque, M. M. *et al.* Distinct conformational behaviors of four mammalian dual-flavin reductases (cytochrome P450 reductase, methionine synthase reductase, neuronal nitric oxide synthase, endothelial nitric oxide synthase) determine their unique catalytic profiles. *FEBS J.* **281,** 5325–5340 (2014).
16. Huang, W. C., Ellis, J., Moody, P. C. E., Raven, E. L. & Roberts, G. C. K. Redox-linked domain movements in the catalytic cycle of cytochrome P450 reductase. *Structure* **21,** 1581–1589 (2013).
17. Vincent, B. *et al.* The Closed and Compact Domain Organization of the 70-kDa Human Cytochrome P450 Reductase in Its Oxidized State As Revealed by NMR. *J. Mol. Biol.* **420,** 296–309 (2012).
18. Laursen, T., Jensen, K. & Møller, B. L. Conformational changes of the NADPH-dependent cytochrome P450 reductase in the course of electron transfer to cytochromes P450. *Biochim. Biophys. Acta* **1814,** 132–8 (2011).
19. Ellis, J. *et al.* Domain motion in cytochrome P450 reductase. Conformational equilibria revealed by NMR and small-angle x-ray scattering. *J. Biol. Chem.* **284,** 36628–36637 (2009).
20. Bridges, A. *et al.* Identification of the binding site on cytochrome P450 2B4 for cytochrome b5 and cytochrome P450 reductase. *J Biol Chem* **273,** 17036–17049 (1998).
21. Zhao, Q. *et al.* Crystal structure of the FMN-binding domain of human cytochrome P450 reductase at 1.93 A resolution. *Protein Sci.* **8,** 298–306 (1999).
22. Shen, A. L. & Kasper, C. B. Role of acidic residues in the interaction of NADPH-cytochrome P450 oxidoreductase with cytochrome P450 and cytochrome c. *J. Biol. Chem.* **270,** 27475–80 (1995).
23. Jang, H.-H. *et al.* Beta sheet 2-alpha helix C loop of cytochrome P450 reductase serves as a docking site for redox partners. *Biochim. Biophys. Acta* **1804,** 1285–93 (2010).
24. Kenaan, C., Zhang, H., Shea, E. V & Hollenberg, P. F. Uncovering the role of hydrophobic residues in cytochrome P450-cytochrome P450 reductase interactions. *Biochemistry* **50,** 3957–67 (2011).
25. Bridges, a *et al.* Identification of the binding site on cytochrome P450 2B4 for cytochrome

b5 and cytochrome P450 reductase. *J. Biol. Chem.* **273,** 17036–49 (1998).

26. Voznesensky, a I. & Schenkman, J. B. The cytochrome P450 2B4-NADPH cytochrome P450 reductase electron transfer complex is not formed by charge-pairing. *J. Biol. Chem.* **267,** 14669–14676 (1992).
27. Shen, S. & Strobel, H. W. Role of lysine and arginine residues of cytochrome P450 in the interaction between cytochrome P4502B1 and NADPH-cytochrome P450 reductase. *Arch. Biochem. Biophys.* **304,** 257–65 (1993).
28. Nikfarjam, L., Izumi, S., Yamazaki, T. & Kominami, S. The interaction of cytochrome P450 17alpha with NADPH-cytochrome P450 reductase, investigated using chemical modification and MALDI-TOF mass spectrometry. *Biochim. Biophys. Acta* **1764,** 1126–31 (2006).
29. Eyer, C. S. & Backes, W. L. Relationship between the rate of reductase-cytochrome P450 complex formation and the rate of first electron transfer. *Arch. Biochem. Biophys.* **293,** 231–40 (1992).
30. Zhang, H., Im, S.-C. & Waskell, L. Cytochrome b5 increases the rate of product formation by cytochrome P450 2B4 and competes with cytochrome P450 reductase for a binding site on cytochrome P450 2B4. *J. Biol. Chem.* **282,** 29766–76 (2007).
31. Voznesensky, A. I. & Schenkman, J. B. Quantitative analyses of electrostatic interactions between NADPH-cytochrome P450 reductase and cytochrome P450 enzymes. *J. Biol. Chem.* **269,** 15724–31 (1994).
32. Shimada, T., Mernaugh, R. L. & Guengerich, F. P. Interactions of mammalian cytochrome P450, NADPH-cytochrome P450 reductase, and cytochrome b(5) enzymes. *Arch. Biochem. Biophys.* **435,** 207–16 (2005).
33. Finn, R. D. *et al.* Defining the in Vivo Role for cytochrome b5 in cytochrome P450 function through the conditional hepatic deletion of microsomal cytochrome b5. *J. Biol. Chem.* **283,** 31385–93 (2008).
34. Zhang, H., Myshkin, E. & Waskell, L. Role of cytochrome b5 in catalysis by cytochrome P450 2B4. *Biochem. Biophys. Res. Commun.* **338,** 499–506 (2005).
35. McLaughlin, L. A., Ronseaux, S., Finn, R. D., Henderson, C. J. & Roland Wolf, C. Deletion of microsomal cytochrome b5 profoundly affects hepatic and extrahepatic drug metabolism. *Mol. Pharmacol.* **78,** 269–78 (2010).

36. Gutierrez, A., Lian, L. Y., Wolf, C. R., Scrutton, N. S. & Roberts, G. C. Stopped-flow kinetic studies of flavin reduction in human cytochrome P450 reductase and its component domains. *Biochemistry* **40,** 1964–75 (2001).
37. Dürr, U. H. N., Yamamoto, K., Im, S.-C., Waskell, L. & Ramamoorthy, A. Solid-state NMR reveals structural and dynamical properties of a membrane-anchored electron-carrier protein, cytochrome b5. *J. Am. Chem. Soc.* **129,** 6670–1 (2007).
38. Ahuja, S. *et al.* A model of the membrane-bound cytochrome b5-cytochrome P450 complex from NMR and mutagenesis data. *J. Biol. Chem.* **288,** 22080–95 (2013).
39. Saribas, A. S., Gruenke, L. & Waskell, L. Overexpression and purification of the membrane-bound cytochrome P450 2B4. *Protein Expr Purif* **21,** 303–309 (2001).
40. Kneller, D. G. & Kuntz, I. D. UCSF Sparky-an NMR display, annotation, and assignment tool. *J. Cell. Biochem.* **53,** 254–254 (1993).
41. Salzmann, M., Wider, G., Pervushin, K. & Wuthrich, K. Improved sensitivity and coherence selection for [15N,1H]-TROSY elements in triple resonance experiments. *J Biomol NMR* **15,** 181–184 (1999).
42. Kay, L. E., Ikura, M., Tschudin, R. & Bax, A. 3-Dimensional Triple-Resonance Nmr-Spectroscopy of Isotopically Enriched Proteins. *J. Magn. Reson.* **89,** 496–514 (1990).
43. Williamson, R. A., Carr, M. D., Frenkiel, T. A., Feeney, J. & Freedman, R. B. Mapping the binding site for matrix metalloproteinase on the N-terminal domain of the tissue inhibitor of metalloproteinases-2 by NMR chemical shift perturbation. *Biochemistry* **36,** 13882–9 (1997).
44. Williamson, M. P. Using chemical shift perturbation to characterise ligand binding. *Prog. Nucl. Magn. Reson. Spectrosc.* **73,** 1–16 (2013).
45. Dominguez, C., Boelens, R. & Bonvin, A. M. HADDOCK: a protein-protein docking approach based on biochemical or biophysical information. *J Am Chem Soc* **125,** 1731–1737 (2003).
46. van Zundert, G. C. P. *et al.* The HADDOCK2.2 Web Server: User-Friendly Integrative Modeling of Biomolecular Complexes. *J. Mol. Biol.* **428,** 720–725 (2015).
47. Schüttelkopf, A. W. & van Aalten, D. M. F. PRODRG: a tool for high-throughput crystallography of protein-ligand complexes. *Acta Crystallogr. D. Biol. Crystallogr.* **60,** 1355–1363 (2004).

48. DeLano, W. L. The PyMOL Molecular Graphics System, Version 1.5.0.4 Schrödinger, LLC. (2010). at <http://www.pymol.org/citing>
49. Estrada, D. F., Laurence, J. S. & Scott, E. E. Substrate-modulated cytochrome P450 17A1 and cytochrome b5 interactions revealed by NMR. *J. Biol. Chem.* **288,** 17008–18 (2013).
50. Prudêncio, M. & Ubbink, M. Transient complexes of redox proteins: structural and dynamic details from NMR studies. *J. Mol. Recognit.* **17,** 524–39 (2004).
51. Volkov, A. N., Ferrari, D., Worrall, J. A. R., Bonvin, A. M. J. J. & Ubbink, M. The orientations of cytochrome c in the highly dynamic complex with cytochrome b5 visualized by NMR and docking using HADDOCK. *Protein Sci.* **14,** 799–811 (2005).
52. Tang, C., Iwahara, J. & Clore, G. M. Visualization of transient encounter complexes in protein-protein association. *Nature* **444,** 383–6 (2006).
53. Volkov, A. N., Ubbink, M. & van Nuland, N. A. J. Mapping the encounter state of a transient protein complex by PRE NMR spectroscopy. *J. Biomol. NMR* **48,** 225–36 (2010).
54. Suh, J.-Y., Tang, C. & Clore, G. M. Role of electrostatic interactions in transient encounter complexes in protein-protein association investigated by paramagnetic relaxation enhancement. *J. Am. Chem. Soc.* **129,** 12954–5 (2007).
55. Page, C. C., Moser, C. C. & Dutton, P. L. Mechanism for electron transfer within and between proteins. *Curr. Opin. Chem. Biol.* **7,** 551–6 (2003).
56. Kurnikov, I. V. HARLEM Molecular Modeling Package. version 1.0, Department of Chemistry, University of Pittsburgh, Pittsburg, PA (2000).
57. Nadler, S. G. & Strobel, H. W. Role of electrostatic interactions in the reaction of NADPH-cytochrome P-450 reductase with cytochromes P-450. *Arch. Biochem. Biophys.* **261,** 418–29 (1988).
58. Nadler, S. G. & Strobel, H. W. Identification and characterization of an NADPH-cytochrome P450 reductase derived peptide involved in binding to cytochrome P450. *Arch. Biochem. Biophys.* **290,** 277–84 (1991).

CHAPTER 6

Conclusions and Future Directions*

6.1 Conclusions

The goal of this thesis is to understand the electron transfer mechanism between cytochrome P450 and its redox partners – cytochrome b_5 and cytochrome P450 reductase – on a structural basis at the atomic resolution using mainly NMR technology in combination with other biochemical and biophysical tools. In this dissertation, I explored the effect of different membrane mimetics on the interaction interface and binding affinity between cytochrome P450 and cytochrome b_5, based on which new membrane mimetics were designed to improve stability of both individual proteins and protein-protein complexes for better future studies. The role of substrates in complex formation between cytochrome P450 and cytochrome b_5 were investigated. It is found that substrates enhance protein-protein binding affinity through promotion of short-range specific interactions between the two proteins, which is likely to be the result of the structural plasticity of cytochrome P450 2B4. The interaction between cytochrome P450 and the FMN binding domain (FBD) of cytochrome P450 reductase was studied using solution NMR techniques detecting the uniformly ^{15}N-labeled FBD, for which resonance assignment was achieved through a set of standard triple-resonance three-dimensional solution NMR experiments. A complex structural model was generated for cytochrome P450-FBD using the docking program HADDOCK, based on which the electron transfer pathway was predicted using HARLEM involving residues Met 132 and Arg 133 on cytochrome P450. A competitive binding mechanism between cytochrome b_5 and FBD for an overlapping but non-identical binding interface of cytochrome P450 was discovered and was found to be regulated by different substrates to different extents depending on the effect of substrates on each individual redox partner complexes respectively.

* This thesis research was supported by funds from the National Institutes of Health (NIH to A.R.).

In Chapter 2, we investigated the interaction between full-length wild-type cytochrome P450 2B4 and full-length wild-type cytochrome b_5 in the following conditions: non-lipid solution, detergent micelles, and isotropic bicelles in which lipids form the planar region as a bilayer and detergents form the edge. The isotropic bicelles are found to enhance binding between cytochrome P450 and cytochrome b_5 as compared to the other two conditions, emphasizing on the important roles that membrane bilayers play in membrane bound redox complex formation. Detergent micelles are found to impair the secondary structural integrity of cytochrome P450 and convert it into the inactive P420 form, which coincides with the above findings in their effect on cytochrome P450 binding its redox partners. We also investigated the interaction between full-length wild-type cytochrome b_5 and the truncated cytochrome P450 in the presence and absence of lipid bilayers which were found to similarly enhance binding between these two proteins. It is likely that lipid bilayers facilitate cytochrome P450-cytochrome b_5 in the following ways: 1. The transmembrane domains of the two proteins anchor them to the membrane, bringing both proteins into close proximity with respect to each other, reducing searching dimensionality and increasing the probability of encounter complex formation; 2. The interaction between the globular domain of cytochrome P450 and lipid bilayer poses the protein into certain orientations that favor its interaction with its redox partners for more efficient electron transfer.

Since it is found in Chapter 2 that detergents are destructive for the structure and function of cytochrome P450, given that bicelles still contain detergents at the edge of the disc, we designed a peptide-based nanodisc that completely eliminates application of detergents in Chapter 3. This nanodisc contains lipid bilayer in its planar region, and what's forming the rim region is not detergents but several 22-amino acid long peptides. Preparation of both empty nanodiscs and nanodiscs containing proteins does not require assistant from detergents, unlike the conventional MSP base nanodiscs. With this nanodisc, we were able to dissociate the aggregates of cytochrome b_5 as well as cytochrome P450 in solution and achieve high homogeneity of the size of the discs both empty and containing proteins. Although it has been a big challenge in the nanodisc field to reconstitute membrane bound protein complexes since the protein partners are always positioned into opposite sides of the discs making it impossible for them to interact with each other, we were able to successfully incorporate the productive cytochrome P450-cytochrome b_5 complex into our nanodisc with the observation of effective interactions between the two proteins from 2D TROSY NMR experiments. The methodology established by this study paves the way for reconstitution of

membrane protein complexes. More work regarding investigation on cytochrome P450 interaction with its redox partners is ongoing in our lab following up this project.

In Chapter 4, we investigated the role that substrates play in cytochrome P450-cytochrome b_5 complex formation. The results showed a drastic enhancement in the binding between the two redox partners. The mechanism of the effect of substrates was investigated based on the distinct responses encounter complexes dominated with long-range electrostatic interactions and stereospecific complexes dominated with short-range specific interactions with respect to ionic strength alteration using solution NMR techniques. Substrates were found to promote specific binding between cytochrome P450 and cytochrome b_5, which likely results from structural rearrangement of cytochrome P450 for accommodation of different substrates. Residues most likely involved in stereospecific binding with cytochrome P450 and therefore important for electron transfer include D65, V66, T70, D71 and A72.

In Chapter 5, the interaction between FBD and cytochrome P450 was investigated both in the presence and absence of different substrates. In addition, the interplay of all three redox partners were explored. A "fingerprint" – assignment of backbone resonances – was produced for FBD with the application of the following 3D NMR experiments: HNCACB, CBCA(CO)NH, HNCO and HNCA. The binding hot-spots were then mapped out on FBD based on both differential line-broadening NMR analysis and solvent paramagnetic relaxation enhancement (PRE) NMR experiments. Utilizing HADDOCK, with AIRs generated from NMR data, we were able to calculate the complex structural model for FBD-cytochrome P450. An electron transfer pathway involving Met132 and Arg133 was predicted based on the structure model. Substrates were found either not affect or slightly enhance binding between FBD and cytochrome P450, in contrast to cytochrome P450-cytochrome b_5 whose affinity was dramatically increased in the presence of substrates. Cytochrome b_5 was found to displace FBD for binding cytochrome P450 to different extents in the presence and absence of different substrates, unravelling a competitive binding mechanism between cytochrome b_5 and FBD for cytochrome P450. The complex structural models for both complexes also revealed an overlapping but non-identical binding interface of cytochrome b_5 and FBD on the surface of cytochrome P450, in agreement with the experimental data. Our results in this study provides better and more in-depth understanding for both complex formation between FBD and cytochrome P450 on the structural basis and the mechanism of all three redox partners interact with one another in the same system that better

resembles the native environment.

6.2 Future directions

6.2.1 Residue specific information from cytochrome P450

In order to fully understand the electron transfer mechanism on the structural basis, experimental evidence needs to be collected not only for cytochrome b_5 and FBD but also for cytochrome P450. However, given the size of cytochrome P450 – 58 kDa – and its tendency to aggregate due to its amphipathic nature, achievement of residue specific information using NMR technology is extremely challenging.

In the current dissertation, a novel membrane mimetic – peptide-based nanodisc – has been designed in Chapter 3, which is capable of dissociating the protein aggregates of cytochrome b_5 as well as cytochrome P450 into either smaller aggregates or monomers. The size of these nanodiscs could be easily controlled through variation of the molar ratio between the peptide and lipids. Reduction in overall size of nanodiscs containing cytochrome P450 will greatly improve signal-to-noise ratio and resolution on an NMR spectrum, aiding resonance assignment, structure calculation and residue specific information collection. Improvement in sample stability at room temperature will also render it possible for high dimensional NMR experiments to be carried out.

Although the overall size of cytochrome P450 embedded in lipid bilayers could be drastically brought down through application of the peptide-based nanodiscs, it is still above 100 kDa given the molecular weight of a single cytochrome P450 of around 58 kDa. This overall size is still quite challenging for solution NMR experiments on a uniformly ^{13}C, ^{15}N-labeled protein even with partial or full deuteration due to significant dipolar coupling that does not average out with the slow tumbling rate which contributes to an increased relaxation rate resulting in resonances broadened out on the NMR spectra. Therefore, we will employ a range of different labeling strategies, including selective amino acid labelling and selective ^{13}C-methyl labelling, which are both complimentary to each other and also to the information obtained from the uniformly labeled sample. NMR on selectively labeled samples, *e.g.* ^{15}N-Ala cytochrome P450, has proven to provide an overall simplified spectrum and results in improved spectrum resolution.[1] Methyl groups are important probes for protein structure and dynamics since they are located throughout a well folded protein including the areas deeply buried inside. Their resonances give

strong signals and are well dispersed over the entire spectrum. Methyl TROSY on selective ^{13}C-methyl labeled proteins has been proven to be particularly useful for large protein systems due to the fast tumbling rate of methyl groups and triply intensified signals by the attached ^{1}H.[2]

Another recently developed NMR technology – ^{15}N detected TROSY – utilizes the advantage of the slow transverse relaxation of ^{15}N for data acquisition, which improves signal-to-noise ratio and spectral resolution at magnetic fields higher than 600 MHz.[3] With the application of this technique, proteins could be uniformly ^{15}N-labeled without the need for deuteration due to reduced/diluted dipolar coupling between ^{1}H spins, which largely increases protein yield and, for most proteins, stability. In addition, incomplete amide proton back-exchange could be avoided, which also contributes to stronger signal-to-noise ratio. Three- and/or four-dimensional NMR experiments based on ^{15}N detected TROSY, in combination with non-uniform sampling (NUS), could be applied to uniformly ^{15}N-labeled cytochrome P450 for fast resonance assignment, dynamics characterization, and structure determination, setting up the foundation for further investigation on the electron transfer process between cytochrome P450 and redox partners.

6.2.2 Investigation of domain motion on cytochrome P450 reductase

In our previous work, we have found that the opening-closing motion of the wild-type cytochrome P450 reductase is related to its redox state: at two-electron-reduced state, cytochrome P450 reductase opens up, exposing the FMN cofactor in the FMN binding domain to the environment, making it available for direct contact with cytochrome P450, enabling electron transfer to occur; at one-electron-reduced state, however, no electron transfer is observed and therefore it is speculated that the conformation of cytochrome P450 reductase is largely in the closed state.[4] Although a lot of hypotheses have been made in the literature regarding the domain motion of cytochrome P450 reductase and its correlation with both the intra-protein electron transfer and the inter-protein electron transfer processes, direct experimental evidence is still lacking.[5–11]

In order to provide a better understanding on the conformational dynamics of cytochrome P450 reductase as well as its gating factors and relationship with cytochrome P450 electron transfer, we will utilize NMR dynamics experiments, including Car-Purcell-Meiboom-Gill (CPMG) relaxation dispersion, chemical exchange saturation transfer (CEST), ZZ-exchange, *etc.* depending on the time-scale of the domain motion, on either uniformly ^{15}N-labeled cytochrome

P450 reductase with deuteration for normal ^{1}H-detection, or without deuteration using ^{15}N-detection, or selectively amino acid or ^{13}C-methyl labeled cytochrome P450 reductase, or that with a paramagnetic relaxation enhancement (PRE) probe on either domain of the protein, which will provide information on the time-scale of the motion, and the relative population of each state (open or close) under a range of different conditions including in the presence and absence of potential gating factors, or cytochrome P450, at different redox states, *etc.* Segmental labelling could also be applied for dilution of the NMR spectrum to achieve better resolution, in which only one domain (*e.g.* the FMN binding domain) is uniformly ^{15}N-labeled while the rest of the protein is unlabeled and therefore non-detectable by NMR. This approach could be achieved through separately expressing and purifying the labeled domain and the unlabeled domain respectively, followed by chemical ligation using a sortase corresponding to the mutation performed prior to protein expression. NMR on segmentally labeled cytochrome P450 reductase could provide better signal-to-noise ratio and spectral resolution, with high quality information achieved on the conformational dynamics of the protein.

6.3 References

1. Ahuja, S. *et al.* A model of the membrane-bound cytochrome b5-cytochrome P450 complex from NMR and mutagenesis data. *J. Biol. Chem.* **288,** 22080–95 (2013).
2. Ollerenshaw, J. E., Tugarinov, V. & Kay, L. E. MAGNETIC RESONANCE IN CHEMISTRY Methyl TROSY: explanation and experimental verification. *Magn. Reson. Chem* **41,** 843–852 (2003).
3. Takeuchi, K., Arthanari, H., Shimada, I. & Wagner, G. Nitrogen detected TROSY at high field yields high resolution and sensitivity for protein NMR. *J. Biomol. NMR* **63,** 323–31 (2015).
4. Huang, R., Zhang, M., Rwere, F., Waskell, L. & Ramamoorthy, A. Kinetic and Structural Characterization of the Interaction between the FMN Binding Domain of Cytochrome P450 Reductase and Cytochrome c. *J. Biol. Chem.* **290,** 4843–55 (2015).
5. Ellis, J. *et al.* Domain motion in cytochrome P450 reductase. Conformational equilibria revealed by NMR and small-angle x-ray scattering. *J. Biol. Chem.* **284,** 36628–36637 (2009).
6. Laursen, T., Jensen, K. & Møller, B. L. Conformational changes of the NADPH-dependent

cytochrome P450 reductase in the course of electron transfer to cytochromes P450. *Biochim. Biophys. Acta* **1814,** 132–8 (2011).

7. Aigrain, L., Pompon, D. & Truan, G. Role of the interface between the FMN and FAD domains in the control of redox potential and electronic transfer of NADPH-cytochrome P450 reductase. *Biochem. J.* **435,** 197–206 (2011).
8. Vincent, B. *et al.* The Closed and Compact Domain Organization of the 70-kDa Human Cytochrome P450 Reductase in Its Oxidized State As Revealed by NMR. *J. Mol. Biol.* **420,** 296–309 (2012).
9. Huang, W. C., Ellis, J., Moody, P. C. E., Raven, E. L. & Roberts, G. C. K. Redox-linked domain movements in the catalytic cycle of cytochrome P450 reductase. *Structure* **21,** 1581–1589 (2013).
10. Frances, O. *et al.* A Well-balanced preexisting equilibrium governs electron flux efficiency of a multidomain diflavin reductase. *Biophys. J.* **108,** 1527–1536 (2015).
11. Haque, M. M. *et al.* Distinct conformational behaviors of four mammalian dual-flavin reductases (cytochrome P450 reductase, methionine synthase reductase, neuronal nitric oxide synthase, endothelial nitric oxide synthase) determine their unique catalytic profiles. *FEBS J.* **281,** 5325–5340 (2014).